



universität  
wien

# DISSERTATION

Titel der Dissertation

Shape and Image Matching with Nonconvex  
Regularization

Verfasser

José Alberto Iglesias Martínez

angestrebter akademischer Grad

Doktor der Naturwissenschaften (Dr. rer. nat.)

Wien, 2015

Studienkennzahl lt. Studienblatt: A 796 605 405

Dissertationsgebiet lt. Studienblatt: Mathematik

Betreuer: Univ.-Prof. Dipl.-Ing. Dr. Otmar Scherzer

Mitbetreuer: Prof. Dr. Martin Rumpf



# Abstract

## Shape and Image Matching with Nonconvex Regularization

by José Alberto Iglesias Martínez

In different imaging scenarios, such as medical and biological applications, the alignment of two or more images of similar objects is of crucial importance. Two such problems are treated in this work, from the point of view of continuous variational models which are then discretized for numerical computations. A common feature of the models presented is the use of nonconvex regularization, in addition to the natural nonconvexity of registration problems.

The first is surface matching, in which the data is given as two different surfaces. In this framework, we consider surfaces embedded in some computational domain and represented by their signed distance functions. Our approach is to consider shell energies penalizing expansion, compression and bending of the first surface, which are simplified using the level set scenario and the geometry of the second surface. For this problem, two models are proposed. The first is a direct approach which effectively encodes the geometry of the situation, while the second formulation is further refined to allow proving weak lower semicontinuity and existence of minimizers, along with efficient numerical computations on adaptive grids.

The second is the estimation of optical flow along a full sequence of images. For it, a novel time regularization along the trajectories of the flow is proposed. It penalizes the convective acceleration of the resulting vector field, instead of the naive time derivative of the Eulerian velocity field. The resulting problem can then be approximated in a semi-implicit fashion by a sequence of linear ones. Numerical results show a marked improvement with respect to just using the time derivative.





## Acknowledgements

As in any document of this type, there are a lot of people to say ‘thank you’ to.

First, to my thesis advisor, Otmar Scherzer, for his patience and always believing in what I was doing, even when it didn’t look like it was going very well, and for giving me a lot of leeway to do things my way.

To all the members of the Computational Science Center in Vienna, who create a very good working (and non-working!) atmosphere of which it was a pleasure to take part of.

To Martin Rumpf and the members of his group in Bonn, who introduced me to many of the concepts necessary to the completion of this work and very patiently helped me navigate a sea of code libraries that looked very foreign at first, thus enabling all the numerical computations realized here.

To the reviewers of this thesis, Jan Modersitzki and Adrian Nachman, who truly have had to deal with it. I am also very grateful to the latter for many interesting discussions and the possibility of a wonderful visit to the Fields Institute in Toronto just before the work for this thesis started.

To everyone in Madrid and beyond (you know who you are). Thanks for always helping me challenge my perception, and may you do the same for years to come.

And last but not least, to my mother, who often cared far more than I did myself.

### **Funding:**

The work presented here was supported by the Austrian Science Fund (FWF) through the National Research Network ‘Geometry+Simulation’ (NFN S117) and Doctoral Program ‘Dissipation and Dispersion in Nonlinear PDEs’ (W1245). Furthermore, the Hausdorff Center for Mathematics funded several visits to the University of Bonn.



# Contents

<b>Abstract</b>	<b>iii</b>
<b>Acknowledgements</b>	<b>v</b>
<b>Contents</b>	<b>vii</b>
<b>Preamble</b>	<b>ix</b>
<b>List of notation</b>	<b>xi</b>
<b>1 Introduction and Background</b>	<b>1</b>
1.1 Problems considered	1
1.1.1 Shape matching	1
1.1.2 Optical flow	1
1.2 Analysis tools employed	3
1.2.1 Direct method in the calculus of variations	3
1.2.2 Vectorial problems. Quasiconvexity, rank-one convexity, polyconvexity, and compensated compactness	3
1.2.3 Gamma-convergence	5
1.3 Related concepts from continuum mechanics	6
1.3.1 Nonlinear elasticity	6
1.3.2 Plate and shell theories	7
1.3.3 Convective acceleration	10
1.4 Computational methods	10
1.4.1 Multiscale descent for registration problems	10
1.4.2 FEM and adaptivity	11
References	11
<b>2 A Thin Shell Approach to the Registration of Implicit Surfaces</b>	<b>15</b>
2.1 Introduction and motivation	15
2.2 Related work	16
2.3 A thin shell matching model	17
2.4 Level set framework	19
2.5 Discretization and minimization	21
2.6 Results	23
2.7 Conclusions and future work	26
References	27
<b>3 Implicit Surface Matching with a Lower Semicontinuous Shell Energy</b>	<b>31</b>
3.1 Introduction	31
3.2 Deformation and matching of level set surfaces	35

3.2.1	Tangential derivative and area and length distortion . . . . .	35
3.2.2	Surface bending and curvature mismatch . . . . .	37
3.3	Energy functional . . . . .	38
3.3.1	Tangential distortion energy . . . . .	38
3.3.2	Bending energy . . . . .	40
3.3.3	Mismatch penalty and volumetric regularization energies . . . . .	42
3.3.4	Total energy . . . . .	42
3.4	Existence of optimal matching deformations . . . . .	43
3.4.1	Oscillations and lack of rank-one convexity for the naive approach . . . . .	52
3.5	Finite element discretization based on adaptive octrees . . . . .	55
3.6	Numerical results . . . . .	58
	References . . . . .	61
<b>4</b>	<b>Convective Regularization for Optical Flow</b>	<b>67</b>
4.1	Introduction . . . . .	67
4.2	Model . . . . .	70
4.2.1	Convective acceleration . . . . .	70
4.2.2	Convective regularization . . . . .	72
4.2.3	Data term and contrast invariance. . . . .	75
4.3	Numerical solution . . . . .	77
4.4	Experiments . . . . .	78
4.5	Conclusion . . . . .	79
	References . . . . .	81
<b>A</b>	<b>First Variation of Level Set Shell Energies</b>	<b>83</b>
A.1	Functionals of Chapter 2 . . . . .	84
A.1.1	Membrane energy . . . . .	84
A.1.2	Bending energy . . . . .	85
A.2	Functionals of Chapter 3 . . . . .	85
A.2.1	Membrane energy . . . . .	85
A.2.2	Bending energy . . . . .	87
<b>B</b>	<b>Deutsche Kurzfassung</b>	<b>89</b>
<b>C</b>	<b>Curriculum Vitae</b>	<b>91</b>

# Preamble

This dissertation introduces several methods for the family of problems known as registration or matching. These attempt to retrieve an unknown deformation relating two or more given observations. We focus on two particular instances, the matching of two given surfaces and optical flow in the space-time domain.

Throughout, the emphasis is on continuous modeling and variational approaches, the resulting match being a vector field defined either on the image domain for the case of optical flow, or on a computational domain containing the shapes, minimizing an appropriate integral functional on it. The nature of the registration problem with large deformations naturally leads to nonconvex data terms. In our case, the models include regularization terms which are also nonconvex, but in turn reflect desirable properties of the resulting deformations. Since in many cases the nonconvexity of the data term already has to be treated, the use of nonconvex regularization does not necessarily incur additional computational costs.

In Chapter 2 we present a first model for the matching of implicit surfaces considered as thin shells. The use of the level set framework allows to use quantities related to the second surface to simplify the modelling, even when a soft matching constraint is used. This in turn allows for a model containing only first-order derivatives that can be discretized with first-order finite elements and minimized in a cascadic multiscale fashion.

However, the model in Chapter 2 results in an energy functional which is not lower semicontinuous. This may result in nonexistence of solutions, a large amount of nonuniqueness, or (of special importance when finding numerical solutions) highly-oscillatory minimizing sequences. This is remedied in the model introduced in Chapter 3, which is based on determinants of minors along changing directions that depend on the deformed configuration. This construction allows to model resistance to surface distortion and curvature matching, while allowing to prove weak lower semicontinuity of the functional. Additionally, simulations are performed on adaptive grids refined around the surfaces, thereby greatly reducing the number of nonessential degrees of freedom in the computation.

In Chapter 4, a model for optical flow in the space-time domain is presented. Optical flow is the name given to the problem of extracting a vector field from the apparent motion in a sequence of images. It is a naturally ill-posed problem, since motion along object edges can not be detected, and hence requires regularization. Here, the Eulerian convective acceleration of the vector field is proposed as a regularity measure, to be included in the variational approach. An iterative numerical method for its solution is presented, and numerical examples demonstrate the superiority of our method with respect to the commonly-used plain time derivative of the vector field.

This is a cumulative dissertation. The status of the different parts is as follows.

- The material in Chapter 2 has been published as [Igl+13]. The non-alphabetical naming convention reflects the proportion of contributions to the paper.

- Chapter 3 is a slightly enlarged version of an article submitted for publication to the journal *Foundations of Computational Mathematics* in September 2015. It is a collaboration with my thesis advisor Otmar Scherzer (CSC, Uni. Wien and RICAM, Austrian Academy of Sciences) and co-advisor Martin Rumpf (INS, Uni. Bonn). It has been submitted as an article with alphabetically ordered authors, and as such, credit should be distributed equally.
- The content of Chapter 4 has been accepted for publication (subject to minor revisions) as a book chapter in the *Radon Series in Computational and Applied Mathematics*. It is a collaboration with Clemens Kirisits (RICAM, Austrian Academy of Sciences). It has been submitted as an article with alphabetically ordered authors, and as such, credit should be distributed equally.

## References

- [Igl+13] J.A. Iglesias, B. Berkels, M. Rumpf, and O. Scherzer. “A Thin Shell Approach to the Registration of Implicit Surfaces”. In: *Proceedings of the Vision, Modeling, and Visualization Workshop 2013*. Eurographics Association, 2013, pp. 89–96.

# List of notation

## Chapter 2

$d$   
 $\Omega$   
 $\phi : \Omega \rightarrow \mathbb{R}^d$   
 $\nabla, D$   
 $\mathbb{1}$   
 $\mathcal{M}_i \subset \mathbb{R}^d$   
 $\mathbf{d}_i : \Omega \rightarrow \mathbb{R}$   
 $\mathcal{M}_i^c = \{x \in \Omega \mid \mathbf{d}_i(x) = c\}$   
 $N_i = \nabla \mathbf{d}_i$   
 $T_x \mathcal{M}_i^{\mathbf{d}_i(x)} = N_i(x)^\perp$   
 $\mathcal{S}_i = D^2 \mathbf{d}_i$   
 $S_{rel}[\phi]$   
 $H_i = \text{tr}(\mathcal{S}_i)$   
 $\eta_\sigma \in C_0^\infty(\mathbb{R})$   
 $\sigma$   
 $\delta$   
 $P = \text{Id} - \nabla \mathbf{d}_1 \otimes \nabla \mathbf{d}_1$   
 $D_{\text{tg}} \phi = D\phi P$   
 $A[\phi] = D\phi^T D\phi$   
 $A_{\text{tg}}[\phi] = D_{\text{tg}} \phi^T D_{\text{tg}} \phi$   
 $v \otimes w \in \mathbb{R}^{d \times d}$   
 $W_{\text{mem}}$   
 $\lambda, \mu$   
 $W_{\text{bend}}$   
 $W_{\text{sh}}$   
 $\mathcal{E}_{\text{sh}}$   
 $\xi$   
 $W_{\text{vol}}, \mathcal{E}_{\text{vol}}$   
 $\tilde{\lambda}, \tilde{\mu}$   
 $\mathcal{E}_{\text{matching}}$   
 $\mathcal{E} = \mathcal{E}_{\text{matching}} + \mathcal{E}_{\text{sh}} + \mathcal{E}_{\text{vol}}$   
 $\epsilon$   
 $h$

Dimension of ambient space,  $d = 2, 3$ .  
 Computational domain,  $\Omega = [0, 1]^d$  in numerics.  
 Unknown deformation.  
 Gradient of scalar function and Jacobian of vector function.  
 Identity matrix.  
 Surfaces to be matched,  $i = 1, 2$ .  
 Signed distance function to  $\mathcal{M}_i$ .  
 Offset surfaces.  
 Unit normal vector to offset surfaces.  
 Tangent space at  $x$  to the corresponding offset surface.  
 Hessian  $\mathbf{d}_i$ , contains shape operator of offset surface.  
 Relative shape operator comparing  $\mathcal{S}_1$  and the pullback of  $\mathcal{S}_2$ .  
 Mean curvature of offset surface.  
 Narrow band function supported on  $[-\sigma, \sigma]$ .  
 Half-width of the narrow band  $\text{supp}(\eta_\sigma \circ \mathbf{d}_1)$ .  
 Shell width parameter (distinct from  $\sigma$ ).  
 Projection onto tangent space of offsets of  $\mathcal{M}_1$ .  
 Tangentially-projected derivative of the deformation.  
 Classical Cauchy-Green strain tensor.  
 Tangential Cauchy-Green strain tensor.  
 Tensor product of  $v, w \in \mathbb{R}^3$ .  
 Tangential energy density, to be applied to  $A_{\text{tg}}[\phi]$ .  
 Lamé parameters used in  $W_{\text{mem}}$ .  
 Bending energy density, to be used on  $S_{\text{rel}}[\phi]$ .  
 Complete shell energy density.  
 Complete shell energy.  
 Volume energy weighting parameter.  
 Volume regularization density and energy.  
 Lamé parameters used in  $W_{\text{vol}}$ .  
 Penalty for constraint  $\phi(\mathcal{M}_1) = \mathcal{M}_2$ .  
 Final energy functional.  
 Inverse of penalization weight appearing in  $\mathcal{E}_{\text{matching}}$ .  
 Spacing of computational grid.

## Chapter 3

$n$   
 $\Omega$   
 $\phi : \Omega \rightarrow \mathbb{R}^n$

Dimension of ambient space,  $d = 2, 3$ .  
 Computational domain,  $\Omega = [0, 1]^n$  in numerics.  
 Unknown deformation.

$\nabla, \mathcal{D}$	Gradient of scalar function and Jacobian of vector function.
$\mathbb{1}$	Identity matrix.
$\mathcal{M}_i \subset \mathbb{R}^d$	Surfaces to be matched, $i = 1, 2$ .
$\mathbf{d}_i : \Omega \rightarrow \mathbb{R}$	Signed distance function to $\mathcal{M}_i$ .
$\mathcal{M}_i^c = \{x \in \Omega \mid \mathbf{d}_i(x) = c\}$	Offset surfaces.
$\mathbf{n}_i = \nabla \mathbf{d}_i$	Unit normal vector to offset surfaces.
$T_x \mathcal{M}_i^{\mathbf{d}_i(x)} = \mathbf{n}_i(x)^\perp$	Tangent space at $x$ to the corresponding offset surface.
$\mathcal{S}_i = \mathcal{D}^2 \mathbf{d}_i$	Hessian $\mathbf{d}_i$ , contains shape operator of offset surface.
$\mathcal{S}_i^{ext} = \mathbf{P}_i \mathcal{D}^2 \mathbf{d}_i \mathbf{P}_i + \mathbf{n}_i \otimes \mathbf{n}_i$	Extended shape operator that avoids degeneracy.
$\eta_\sigma \in C_0^\infty(\mathbb{R})$	Narrow band function supported on $[-\sigma, \sigma]$ .
$\sigma$	Half-width of the narrow band $\text{supp}(\eta_\sigma \circ \mathbf{d}_1)$ .
$\delta$	Shell width parameter (distinct from $\sigma$ ).
$v \otimes w \in \mathbb{R}^{d \times d}$	Tensor product of $v, w \in \mathbb{R}^3$ .
$\text{PSD}(n), \text{O}(n), \text{SO}(n)$	Positive semidefinite, rotation and proper rotation matrices.
$\mathbf{P}(e) = \mathbb{1} - e \otimes e$	Projection matrix onto subspace $e^\perp$ .
$\mathbf{Q}(e) \in \text{SO}(n)$	Rotation matrix such that $\mathbf{Q}(e) = (0, \dots, 1)^T$ .
$\mathbf{P}_i = \mathbb{1} - \nabla \mathbf{d}_i \otimes \nabla \mathbf{d}_i$	Projection onto tangent space of offsets of $\mathcal{M}_i$ .
$\mathcal{D}_{\text{tg}} \phi(x) = \mathbf{P}_2(\phi(x)) \mathcal{D} \phi(x) \mathbf{P}_1(x)$	Tangential derivative of the deformation.
$W$	Tangential energy density.
$\lambda, \mu$	Lamé parameters used in $W$ .
$\mathcal{C} : \mathbb{R}^{n \times n} \rightarrow \text{PSD}(n)$	Regularization function for matrices.
$W_{\text{vol}}, E_{\text{vol}}$	Volume regularization density and energy.
$p, q, s, \alpha_p, \beta_q, \gamma_s$	Parameters of $W_{\text{vol}}$ .
$E_{\text{match}}$	Penalty for constraint $\phi(\mathcal{M}_1) = \mathcal{M}_2$ .
$E_{\text{mem}}$	Membrane energy.
$E_{\text{bend}}$	Bending energy.
$\Lambda(A, B, C), A, B, C \in \mathbb{R}^{n \times n}$	Pullback matching construction used in $E_{\text{bend}}$ .
$E$	Complete energy functional.
$\nu$	Inverse of penalization weight appearing in $E_{\text{match}}$ .
$\tilde{\mathcal{D}}_{\text{tg}}, \tilde{E}_{\text{mem}}$	Tangential derivative and membrane energy of Chapter 2.
$\ell$	Maximum level of grid.
$h = 2^{-\ell}$	Minimal spacing of computational grid.

## Chapter 4

$\gamma(t; x)$	Trajectory description of underlying flows.
$v$	Generic flow velocity vector for examples.
$u$	Unknown optical flow velocity vector.
$\Omega \subset \mathbb{R}^2$	Space domain.
$E = (0, T) \times \Omega$	Space-time domain.
$f_t$	Partial time derivative of $f : E \rightarrow \mathbb{R}^n$ .
$D_u f = f_t + \nabla f \cdot u$	Convective derivative of $g$ along flow with velocity $f$ .
$\bar{u} = (1 \ u^1 u^2)^T$	Space-time velocity vector.
$\bar{\nabla} f = (f_t \ \nabla f)$	Space-time gradient of $f$ .
$D_u u = u_t + \nabla u u = \bar{\nabla} u \bar{u}$	Convective acceleration of flow described by $u$ .
$\kappa_\gamma$	Curvature of $\gamma : (0, T) \rightarrow \Omega$ .
$\lambda \in L^\infty(E)$	Data term weight for approximate contrast invariance.



$\mathcal{E}(u)$	Proposed energy functional.
$\alpha, \beta$	Parameters of convective and isotropic regularization.
$\mathcal{G}(u, w)$	Splitting of $\mathcal{E}$ considered for numerics.
$\mathcal{H}(u)$	Energy for optical flow with isotropic regularization.



# Introduction and Background

## 1.1 Problems considered

### 1.1.1 Shape matching

In shape matching, one is given two curves or surfaces which are in a suitable sense similar to each other, and the task is to produce a deformation taking every point of one shape to a corresponding point in the other, in a way that is in some sense natural. Typically, these shapes are extracted from some imaging procedure, and since the the only available data are the geometric objects, it is necessary to formulate a criterion for the selection of a particular deformation. In Chapters 2 and 3 we argue that considering the surfaces as thin elastic shells, with deformations minimizing the corresponding energy, is one effective such criterion. Indeed, the use of membrane and bending energies reflects desirable properties like low tangential distortion (the deformation should be nearly isometric whenever possible) and small changes in curvature. An additional advantage is that if knowledge about the elastic material properties of the objects being imaged is available, it can be easily incorporated in such a framework.

Our motivation for studying such a problem is twofold. On the one hand, there are direct practical applications for automatically-found correspondences between imaged objects in the fields of computer graphics and computer vision. On the other, a matching model can be used as a stepping stone into more advanced methods of shape analysis, which have a number of promising applications in areas like computational anatomy [Mil04]. The idea of discrete geodesic calculus as defined in [RW15] is to provide a meaningful relation between matching models (including those using nonlinear elasticity ideas) and shape spaces, in which one may interpolate between shapes and even perform a variety of statistical operations [Fle+04]. The key idea is to replace the energy of the path, in the sense of Riemannian geometry, with the sums of the matching energies along the path. That is, infinitesimally the matching energy corresponds to squared Riemannian length. An advantage of this method is that by giving physical meaning and more structure to the approximating discrete problems, a far smaller number of time points, and consequently higher resolution shapes, may be used.

### 1.1.2 Optical flow

Image registration is the problem of matching two images whose intensity values (or some other feature) are assumed to be similar, but whose domain has undergone a geometric transformation, which is the unknown of the problem. That is, if  $I_1, I_2$  are the given images and  $\phi$  is the unknown map, one assumes

$$I_2(\phi(x)) \approx I_1(x).$$

which when considered as an equation receives the name “brightness constancy assumption”. Here, once again, one needs to formulate selection criteria to single out particular deformations among those satisfying the above constraint.

A related applied problem is that of optical flow, that is, finding the apparent motion between two or more video frames. Typically, since one is considering different frames of the same sequence, in optical flow the displacements between frames can be assumed to be small. In consequence, the above condition can be linearized around the identity  $\phi(x) = x + \epsilon u(x)$ , arriving at

$$(I_2 - I_1)(x) \approx -\nabla I_2(x) \cdot u(x).$$

Note that this condition only provides information about  $u$  across the edges of objects present in the image, that is, in the direction of  $\nabla I_2(x)$ . This is not surprising, since motion of a non-textured object along its edge can not be detected. One can think, for example, of a white circle rotating against a dark background. Even worse, there might be points where  $\nabla I_2(x) = 0$  but  $(I_2 - I_1)(x) \neq 0$ , in which case the brightness constancy assumption can never be satisfied. The availability of only partial information and ensuing nonuniqueness and instability motivates the use of variational approaches containing regularization. A common starting point is combining a quadratic penalty for the linear condition above with a Dirichlet energy term that ensures well-posedness of the resulting problem, resulting in the Horn-Schunck functional [HS81]

$$\int_{\Omega} |I_2(x) - I_1(x) - \nabla I_2(x) \cdot u(x)| + |\nabla u(x)|^2 dx, \quad (1.1.1)$$

whose optimality conditions can be easily and efficiently solved numerically.

A logical step in the hope of obtaining better results is considering the problem of optical flow estimation over a whole sequence of images which are all considered to be coupled, in contrast with the two-frame problem considered above. In this case, the image sequence can be modeled as depending on an additional continuous time variable, so that correspondingly the fidelity term reads

$$\int_0^T \int_{\Omega} |\partial_t I(t, x) - \nabla I(t, x) \cdot u(t, x)| dx dt.$$

As for the regularization term, a natural generalization [WS01b] is of the form

$$\int_0^T \int_{\Omega} (\partial_t u(t, x))^2 + |\nabla u(t, x)|^2 dx dt.$$

In comparison to (1.1.1), a time derivative appears. From the modeling perspective, it is desirable to penalize temporal inconsistencies of the flow. Mathematically, it is required to ensure that the resulting Euler-Lagrange equation is elliptic. However, the time derivative  $\partial_t u$  has no natural meaning in terms of the trajectories of the flow. We try to remedy this problem in Chapter 4 through the introduction of a novel regularization term.

## 1.2 Analysis tools employed

### 1.2.1 Direct method in the calculus of variations

A very successful strategy for proving existence of solutions of variational problems is the use of topological tools in a global fashion, to find minimizers as limits of readily available almost-minimizers. The starting point is the choice of a minimizing sequence, that is, a sequence  $x_k$  such that  $\lim E[x_k] = \inf_x E[x]$ . Then, a topology needs to be chosen, under which the energy manages to have the two properties:

- Coercivity, stating that sequences whose energy is bounded should be contained in some compact set for the chosen topology, so that a limit to the  $x_k$  can be extracted.
- Lower semicontinuity of the energy with respect to the given topology, so that the limit is the desired minimizer.

Indeed, if both of these properties are present, we may extract a limit  $x_0$  for a subsequence of the  $x_k$ , and in turn lower semicontinuity implies

$$E[x_0] \leq \liminf E[x_k] = \inf_x E[x],$$

so that  $x_0$  is a minimizer of  $E$ . However, these two properties “work against each other”, in the sense that choosing a stronger topology will make lower semicontinuity easier to attain, but may destroy coercivity. Conversely, weak topologies are convenient for coercivity, but may prevent lower semicontinuity.

In our case, we use the weak topology of reflexive Sobolev spaces, in which coercivity is obtained by comparison with the norm and an application of the Banach-Alaoglu theorem, thereby displacing the main difficulty to the lower semicontinuity. To obtain it, one needs to look more closely at the particular nature of the problem. In the case of an integral functional depending on derivatives of candidate functions  $u : \mathbb{R}^n \supset \Omega \rightarrow \mathbb{R}^N$  with Jacobian matrix  $\mathcal{D}u(x) \in \mathbb{R}^{N \times n}$ ,

$$E[\phi] = \int_{\Omega} W(x, u(x), \mathcal{D}u(x)) \, dx,$$

some convexity condition is required of the density  $W$ . If  $n = 1$  or  $N = 1$  and under very mild technical assumptions, convexity of  $W(y, \xi, \cdot)$  for fixed  $y, \xi$  is necessary and sufficient for weak lower semicontinuity [Dac08]. In the genuinely vectorial case  $n > 1, N > 1$  weaker convexity conditions, which we briefly review in the next subsection, are in many cases either necessary or sufficient.

### 1.2.2 Vectorial problems. Quasiconvexity, rank-one convexity, polyconvexity, and compensated compactness

A density  $W : \mathbb{R}^{N \times n}$  is said to be quasiconvex when

$$W(A) \leq \frac{1}{|U|} \int_U W(A + D\varphi(x)) \, dx, \text{ for all } U \subset\subset \Omega \text{ open, } \varphi \in C_0^\infty(U, \mathbb{R}^N),$$

with  $|U|$  the Lebesgue measure of  $U$ . Quasiconvexity is an integral condition that can not be reduced to a pointwise criterion [Kri99], making it extremely hard to check for directly. However, unlike other conditions which are easier to handle, it is not only sufficient for the lower semicontinuity of vectorial problems under appropriate technical assumptions, but also in many cases a necessary condition, as first discovered by Morrey [Mor66]. One limitation of lower semicontinuity theorems for quasiconvex functionals is that upper bounds on the integrands are required. Typically, a condition of the form  $W(A) \leq C(|A|^p + 1)$  is required for weak lower semicontinuity in  $W^{1,p}(\Omega; \mathbb{R}^n)$ . This is quite natural, since one needs to recover conditions on integrals on the whole domain from a local assumption.

Another useful condition is convexity along rank-one matrices of the density  $W$ . The requirement is that the function  $t \rightarrow W(A + t(b \otimes c))$  is convex for any  $A \in \mathbb{R}^{N \times n}$ ,  $b \in \mathbb{R}^N$  and  $c \in \mathbb{R}^n$ , where  $b \otimes c = bc^T$  denotes the tensor product. It is implied by quasiconvexity, as may be checked by using plane wave test functions of the type  $\varphi(x) = b\eta(x) \sin(k(c \cdot x))$ , with  $\eta$  a bump function supported on  $U$  and  $k \gg 1$ . As such, it is a useful condition to prove that a certain energy is not weakly lower semicontinuous. We make use of this definition in a counterexample in Chapter 3.

We now turn our attention to a subset of quasiconvex functions more amenable to immediate application. As an example, let  $u \in W^{1,2}(\omega; \mathbb{R}^2)$  with  $\omega \subset \mathbb{R}^2$ . Owing to the fact that we may write

$$\operatorname{div}(u^1 \partial_2 u^2, -u^1 \partial_1 u^2) = \partial_1 u^1 \partial_2 u^2 - \partial_1 u^2 \partial_2 u^1 + u^1 \partial_1 \partial_2 u^2 - u^1 \partial_2 \partial_1 u^2 = \det \mathcal{D}u,$$

and observing that the components of the vector field above are products of one strongly convergent and one weakly convergent sequence, we get that the Jacobian determinant is a weakly continuous function from  $W^{1,2}$  to  $L^1$ , that is

$$\det \mathcal{D}u_k \rightharpoonup \det \mathcal{D}u \text{ in } L^1(\Omega) \text{ whenever } \mathcal{D}u_k \rightharpoonup \mathcal{D}u \text{ in } L^2(\Omega).$$

By induction and expansion along a row or column a similar divergence structure can be inferred for higher-dimensional determinants, so analogous results can be proved in the appropriate spaces [Dac08]. An energy density  $W$  is termed polyconvex when it can be written as a jointly convex function of the matrix argument, its determinant, and the determinants of minors. The combination of a weakly continuous construction with a convex function preserves lower semicontinuity, making the direct method still applicable.

In addition to being easier to handle, polyconvexity has the advantage of no longer requiring upper bounds on the integrands in order to prove lower semicontinuity theorems. In fact, this is the case in the model introduced in Chapter 3, with a density  $W$  for which it is not necessarily true that  $W \circ \mathcal{D}\phi \in L^1(\Omega)$  for all  $\phi \in W^{1,p}(\Omega; \mathbb{R}^3)$ , although the corresponding functional is weakly lower semicontinuous and possesses minimizers in the latter space.

As may be seen through the sequence  $u_k^2$  with  $u_k = \cos(2\pi k x) \in L^2(0, 1)$ , the product of weakly converging sequences does not necessarily converge to the product of the corresponding limits. However, there are situations in which products of weakly converging sequences do converge to the right limit, as in the Jacobian determinant above.

It is natural to ask, then, in which situations a similar phenomenon can be expected. The systematic study of these situations is the theory of compensated compactness, first developed by Murat and Tartar [Tar79; Mur78]. It tells us (very roughly) that a product of weakly converging

functions does converge to the expected limit, in situations where each of the members of the sequence satisfies an adequate differential constraint whose form works together with that of the product in consideration to prevent interference between the different factors. A typical result consists in considering a sequence of weakly convergent vector fields  $U_k \rightharpoonup U_\infty$  in  $L^2_{loc}(\Omega; \mathbb{R}^N)$  (with  $\Omega \subset \mathbb{R}^n$ ) satisfying the first order partial differential equation

$$\sum_{i=1}^n \sum_{j=1}^N \frac{\partial (A_{i,j} U_k^j)}{\partial x_i} = 0, \quad (1.2.1)$$

and a weakly convergent quadratic form of components of  $U_k$ ,

$$Q(U_k) = \sum_{j,l=1}^N q_{j,l} U_k^j U_k^l \xrightarrow{*} \nu \text{ in } \mathcal{M}(\Omega),$$

where  $\mathcal{M}(\Omega)$  denotes the space of scalar Radon measures. Then  $\nu = Q(U_\infty)$  provided that for all  $\xi \in \mathbb{S}^{n-1}$  and  $\lambda \in \Lambda_\xi$  we have  $Q(\lambda) = 0$ , where

$$\Lambda_\xi = \left\{ \lambda \in \mathbb{R}^N \mid \sum_{i=1}^n \sum_{j=1}^N \xi_i A_{i,j} \lambda = 0 \right\}.$$

This kind of analysis can be understood as “plane wave analysis at infinite frequencies”. The cones  $\Lambda_\xi$  represent the directions in phase space that are not controlled by the equation (1.2.1), so they are required to be directions in which the quadratic form  $Q$  applied to our weakly convergent sequence has to degenerate. As an example, for the two-dimensional Jacobian determinant we would have  $n = 2$ ,  $N = 4$ ,  $U_k = (\partial_1 u_k^1, \partial_2 u_k^1, \partial_1 u_k^2, \partial_2 u_k^2)$  and the differential constraint corresponds to mixed partials commuting.

The theory of H-Measures [Tar90] extends this kind of results to variable coefficients  $A_{i,j}, q_{j,l} \in C^0(\Omega)$ . Such a situation appears in the model proposed in Chapter 3, which is formulated in terms of determinants of minors of the Jacobian, but the directions along which these minors are taken depend on the position and on the deformed configuration at that position. However, under the assumption of continuous coefficients, we recover weak continuity of the corresponding determinants. This weak continuity result again leads to weak lower semicontinuity of the associated functionals.

### 1.2.3 Gamma-convergence

In many situations one is led to consider a sequence of functionals that are supposed to approximate a harder problem, thereby having to consider a limiting procedure such that minimizers or critical points converge. A particularly productive formalization is the setting of  $\Gamma$ -convergence. It is indeed the natural (albeit nonlinear) notion of convergence for approximating variational problems by simpler ones that may be solved through the direct method. It depends on a choice of topology in the underlying space, and in particular ensures that the resulting limit functional is lower semicontinuous with respect to this topology. Formally, it consists of the following two conditions for a sequence  $f_k$  converging to  $f$ , usually called the  $\liminf$  and  $\limsup$  inequalities, respectively.

- For each  $x \in X$ , and any sequence  $x_k \rightarrow x$  we have  $f(x) \leq \liminf_k f(x_k)$ .
- For each  $x \in X$ , there is a sequence  $x_k \rightarrow x$  such that  $f(x) \geq \limsup_k f(x_k)$ .

It follows from these definitions that the limit functional  $f$  is automatically lower semicontinuous with the chosen topology [Bra02, Proposition 1.28]. In the spirit of the direct method, what remains in order to prove convergence of minimizers (which is what we are after) is some sort of coercivity condition. A (quite weak) such condition is mild equi-coercivity of the  $f_k$ , stating that there exists some compact set  $K$  such that  $\inf_{x \in K} f_k(x) = \inf_{x \in X} f_k(x)$  for all  $k$ . In this situation, the compactness of  $K$  (which does not depend on  $k$ ) can be used to obtain convergence of minimizers [Bra02, Theorem 1.21]. When using weak-\* topologies in which the Banach-Alaoglu theorem is applicable, uniform norm bounds along the sequence of functionals ensure equi-coerciveness.

In this work,  $\Gamma$ -convergence will only make a brief appearance when exploring the penalization limit of shape matching in Chapter 3, in which the shapes and their offsets are eventually forced to correspond exactly.

## 1.3 Related concepts from continuum mechanics

### 1.3.1 Nonlinear elasticity

In the setting of so-called hyperelastic materials, equilibrium configurations appear as critical points of a functional depending on the infinitesimal strain, namely

$$\int_{\Omega} W(D\phi) - F \cdot \phi \, dx, \quad (1.3.1)$$

where  $\phi : \Omega \rightarrow \mathbb{R}^3$  is a deformation of the reference configuration of an elastic body occupying the domain  $\Omega$ ,  $W$  is the so-called stored energy function and  $F : \Omega \rightarrow \mathbb{R}^3$  is some volumetric applied force.

The most important feature of this approach is the availability of assumptions on the energy density  $W$  which are simultaneously physically realistic, and allow for the use of the direct method to prove the existence of minimizers with no size restrictions on the applied force  $F$ . This is in contrast to the solution of the equations for an equilibrium directly using some infinite-dimensional implicit function theorem, in which bounds on appropriate norms of  $F$  have to be assumed.

When we say physically realistic in a nonlinear setting, significant difficulties arise. A reasonable assumption is that the model is frame-invariant, that is, it does not depend on the choice of orthonormal basis chosen to represent the deformed configuration. In terms of the energy, this means that we should have  $W(QA) = W(A)$  for any  $Q \in \text{SO}(3)$ , where  $\text{SO}(3)$  is the group of proper rotations on  $\mathbb{R}^3$ . But, combined with the natural requirement that the identity should not be penalized (i.e., it has zero energy), we infer that  $\text{SO}(3) \subset \arg \min W$ . But if  $W$  were convex, this would mean that  $0 \in \text{co SO}(3) \subset \arg \min W$ , where  $\text{co}$  denotes the convex envelope. And this implies that constant deformations mapping the whole of  $\Omega$  to a fixed point would also have zero energy.



Luckily, as we have seen in the previous section, convexity of the integrand is not necessary for the direct method to apply. Indeed, polyconvex stored energy functions allow for frame indifference, and can even ensure that the obtained deformations are invertible (non-interpenetration of matter, in physical terms) through growth conditions ensuring that  $W(A) \rightarrow +\infty$  fast enough as  $\det A \rightarrow 0$  [Bal81]. Numerous families of materials have been successfully included in this framework, like Ogden's materials [Ogd72] describing nonlinear regimes of rubber and biological tissue. Such stored energy functions are the main building block for the model of Chapter 2.

Additionally, it is possible to engineer stored energy functions such that the linearized problem corresponding to a critical point of the energy matches standard representations of parameters of linear elasticity. This corresponds to the condition for the Hessian of  $W$

$$\mathcal{D}^2 W(\mathbb{1})(A, A) = 2\mu|e|^2 + \lambda \operatorname{tr}(e)^2, \quad (1.3.2)$$

where  $\mathbb{1}$  is the identity matrix,  $e$  corresponds to the symmetrized gradient  $e = (A + A^T)/2$  and  $\lambda, \mu$  are the commonly used Lamé parameters, which are sufficient to parametrize any isotropic linearly elastic material [Cia78]. Polyconvex energies that ensure non-interpenetration of matter and satisfy (1.3.2) were introduced in [CG82]. A similar density, but which is continuous on  $\mathbb{R}^{3 \times 3}$ , is used in Chapter 3. Observe that it is natural for the linearization to depend only on the symmetric part of the derivative, since the tangent space to  $\operatorname{SO}(3)$  at the identity matrix is precisely the set of antisymmetric matrices.

### 1.3.2 Plate and shell theories

Often it is required to describe the elastic behavior of an object which is much smaller in one direction than in the others. One such case is that of plates, whose resting configuration is assumed to be flat, that is, they can be written as  $\Omega = \omega \times (-\frac{\delta}{2}, \frac{\delta}{2})$  with  $\omega \subset \mathbb{R}^2$ , middle surface  $\omega \times \{0\} \subset \mathbb{R}^3$  and width  $\delta > 0$ . A more general configuration is that of shells, whose resting configuration is curved, that is, they may be written as a tubular neighborhood of a surface  $\mathcal{M} \subset \mathbb{R}^3$ , so that  $\Omega = \{x \in \mathbb{R}^3 \mid \operatorname{dist}(x, \mathcal{M}) < \delta/2\}$ , where  $\operatorname{dist}(x, \mathcal{M}) = \inf_y |x - y|$ . In these cases, one wants a description of the elastic behavior of these structure, formulated only on  $\omega$  or  $\mathcal{M}$  respectively, thereby obtaining a two-dimensional problem.

To accomplish such a dimension reduction, there are two main routes. The first is a phenomenological one: make some a priori assumptions on the nature of the resulting deformation, and incorporate them into an ad-hoc variational or PDE model. The problem here is that different sets of reasonable assumptions lead to different models and different behavior of solutions [Cia00]. One particular set of models arises from the nonlinear Kirchhoff assumption, stating that the normal fibers to the middle surface remain normal after the deformation, and do not suffer any stretching.

The other, more recent, alternative is to try to derive the two-dimensional model as a limit of volumetric models whose depth tends to zero. However, since the limit of the volumetric energies is always zero, for this approach to produce meaningful results, it is necessary to assume that the energies converge at a certain asymptotic rate, that is, one looks at (in the case of plates) the

$\Gamma$ -limit as  $\delta \rightarrow 0$  of

$$E_\delta[\phi] = \frac{1}{\delta^\beta} \int_{\omega \times (-\frac{\delta}{2}, \frac{\delta}{2})} W(\mathcal{D}\phi) \, dx = \frac{1}{\delta^{\beta-1}} \int_{\omega \times (-\frac{1}{2}, \frac{1}{2})} W(|\partial_1 \phi| |\partial_2 \phi| (1/\delta) |\partial_3 \phi|) \, dx,$$

where  $a|b|c \in \mathbb{R}^{3 \times 3}$  denotes the matrix given columnwise by  $a, b, c \in \mathbb{R}^3$ . Therefore, part of the investigation is displaced to the question of which boundary conditions produce the desired energy scaling when applied to the original volumetric models, so that the computed limit reflects the correct physical behavior.

For the exponent  $\beta = 1$  (constant energy per unit area on the surface  $\omega$ ), the corresponding  $L^p$   $\Gamma$ -limits were computed in [LDR95a] and [LDR96]. In the case of plates, the resulting functional can be written as

$$E[\phi] = \begin{cases} \int_{\omega} QW_0(\mathcal{D}\phi) \, dx, & \text{if } \partial_{x_3}\phi = 0 \\ +\infty & \text{otherwise,} \end{cases}$$

where  $Q$  denotes the quasiconvex envelope, and  $W_0(A) = \inf_{\zeta \in \mathbb{R}^3} W(A^1 |A^2| \zeta)$ , with  $A^i$  the  $i$ -th column of  $A$ . In this expression, two features are immediately evident. The first is the appearance of a minimization over director vectors  $\zeta$ , signifying that along minimizing sequences, material fibers will eventually be oriented in the the most energetically advantageous direction.

The second is the appearance of a quasiconvex envelope [Dac08, Section 6.3]. For an energy density  $W$  of the type usually appearing in nonlinear elasticity, with a single well in  $\text{SO}(3)$  and with built-in orientation preservation, the appearance of this quasiconvex envelope has the effect of nullifying compressional resistance of the material for the obtained limit. Compression resistance of an elastic shell in fact leads to oscillatory behavior, as in particular explored in Chapters 2 and 3, and also matching the everyday experience of crumpling appearing when applying a compressional force to a piece of paper. Therefore, the appearance of a quasiconvexification and lack of oscillations in minimizing sequences should be taken as an artifact of the limiting procedure, rather than a feature of the physical system that one is trying to model. Indeed, as already noted an energy obtained by  $\Gamma$ -convergence is lower semicontinuous in the chosen topology.

In our shape matching models we make use of similar membrane terms in our energies, which penalize tangential distortion. In Chapter 2 a term that does penalize compression, but is in exchange not lower semicontinuous, is used. In contrast, the term used in Chapter 3 recovers lower semicontinuity by measuring and penalizing distortion only along the level sets corresponding to the target surface. In this way, a functional which penalizes both expansion and compression of the deformation (measured along the surfaces in question) but does not encourage oscillatory behavior is obtained. The idea is that making the functional “forget” the normal direction to the target surface prevents it from compensating compression with oscillations. This construction is of course only possible in a shape matching scenario, in which the target surface is given as data, since otherwise this normal direction is not available.

For the exponent  $\beta = 3$ , the limit was obtained in [FJM02; Fri+03] and corresponds to the Kirchhoff bending regime. In the limit problem, only isometric deformations of  $\omega$  are allowed, and differences of curvature are penalized. Heuristically, the exponent can also be justified through the nonlinear Kirchhoff-Love assumption postulating that the fibers normal to the middle surface remain normal and are not stretched or compressed through the deformation. To see this,

one can think of a plate as a collection of massless rods joined by springs attached at points which are equidistant to the middle surface (see Figure 1.1). From Hooke's law, the stored energy on each of these springs is proportional  $|\Delta\ell|^2$ , where  $\Delta\ell$  is the difference between the resting and stretched lengths, analogous to the continuous displacement. On the other hand, the curvature of the resulting middle surface is proportional to the angle between fibers, so that if  $\delta \ll 1$  we have that  $\Delta\ell$  is proportional to the height  $y$  over the middle surface. Finally, integration over  $y$  on the interval  $(-\delta/2, \delta/2)$  brings us to the conclusion that the resulting energy is of order  $\delta^3$ .

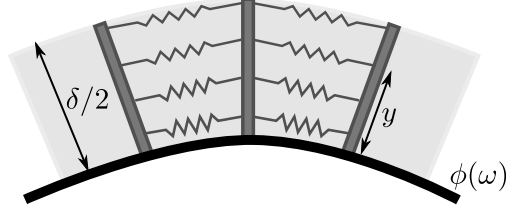


FIGURE 1.1: Rough sketch of the energy scaling of bending.

In the case of plates the resulting functional [FJM02] under the assumption that the Hessian of  $W$  satisfies (1.3.2) is the energy

$$\frac{1}{24} \int_{\omega} 2\mu |\mathbb{I}|^2 + \frac{\lambda\mu}{\mu + \lambda/2} (\text{tr } \mathbb{I})^2,$$

which penalizes the size of the second fundamental form  $\mathbb{I}$  of the deformed surface with respect to the parametrization given by the deformation. Observe this is a singular perturbation problem, since second derivatives of  $\phi$  are present in the limit but were absent in the original functionals. The whole procedure depends crucially on the powerful rigidity estimates proved in [FJM02], stating that for any  $W^{1,2}$  function  $\psi : \Omega \rightarrow \mathbb{R}^n$  we have

$$\|\mathcal{D}\psi - R\|_{L^2(\Omega)} \leq C \|\text{dist}(\mathcal{D}\psi, \text{SO}(3))\|_{L^2(\Omega)},$$

where  $R$  is an element of  $\text{SO}(3)$  determined by  $\psi$  and the constant  $C$  depends only on the domain  $\Omega$ .

The case of shells requires taking into account the curvature that was already present in the surface before the deformation. As it turns out, the correct way to measure this increase of curvature is through the relative shape operator [Fri+03], defined for a surface  $\mathcal{M}$  and a smooth parametrization of it  $r : \omega \rightarrow \mathcal{M}$  as

$$\mathcal{D}\phi^T(r(x))\mathcal{S}_{\phi(\mathcal{M})}(\phi(r(x)))\mathcal{D}\phi(r(x)) - \mathcal{S}_{\mathcal{M}}(r(x))$$

for  $x \in \omega$  and a deformation  $\phi : \mathcal{M} \rightarrow \mathbb{R}^3$ . Here  $\mathcal{S}_{\mathcal{M}}, \mathcal{S}_{\phi(\mathcal{M})}$  are the matrix representations of the Weingarten operators of  $\mathcal{M}$  and  $\phi(\mathcal{M})$  arising from the parametrizations  $r$  and  $(\phi \circ r)$ . The appearance such an expression is not unexpected, since in it the shape operator of the deformed surface  $\phi(\mathcal{M})$  is pulled back through  $\phi$  as a 2-tensor and compared linearly with the original one. This fits with the geometric nature of the shape operator and, furthermore, implies that energies derived from this expression do not depend on the choice of parametrization  $r$ .

In Chapter 2 the non-vanishing of the relative shape operator is penalized, but substituting the shape operator of the deformed surface with that of the target surface, thereby obtaining

a functional with only first order derivatives. In Chapter 3 this condition is further simplified through regularization of the shape operators and a kind of tangential factorization, in order to be able to obtain a lower semicontinuous functional.

### 1.3.3 Convective acceleration

Convective acceleration arises in the Eulerian description of fluid mechanics. Eulerian coordinates can be thought to be fixed at particular points of space, in the usual manner. This means that at a given space position, different material particles will be found at different times. In contrast, Lagrangian coordinates follow the material, so that the same coordinates at different times correspond to the same material particles.

Its expression  $\partial_t u + \nabla u \cdot u$ , where  $u$  is the mentioned Eulerian velocity field (see Chapter 4 for a derivation) contains a nonlinear term reflecting the fact that the fluid itself is moving, a fact that needs to be taken into account when computing its acceleration.

The starting observation for Chapter 4 is that, even though time derivatives have been used in the regularization terms of variational models for optical flow, usually only the time derivative with respect to the fixed Eulerian frame  $\partial_t u$  is used, which does not have any meaning in terms of the flow itself. Instead, we propose to use the convective acceleration as a regularity measure, and then attempt to minimize it via a semi-implicit iterative scheme.

## 1.4 Computational methods

### 1.4.1 Multiscale descent for registration problems

Unlike in optical flow problems, when performing image registration without linearization of the matching condition, the data terms involved present a dramatic lack of convexity. As an example, consider the expression

$$\int_{\Omega} |I_2(\phi(x)) - I_1(x)|^2 dx.$$

Taking second derivatives of the integrand with respect to the unknown  $\phi$ , we obtain that it is convex at a point, if and only if the image  $I_2$  is. However, the data obtained from any real-world imaging system is often not only of very low regularity, but also noisy and possibly containing artifacts manifesting as oscillations.

A common approach to try to mitigate this fundamental nonconvexity without just limiting oneself to linearized data terms is to implement a multiscale descent. First, one discretizes the relevant data, obtaining a discrete energy, as opposed to first obtaining optimality conditions which are then discretized and solved. Next, the problem is severely undersampled to obtain a formulation on a very coarse grid, and solved as if it were a convex minimization problem. Then the solution of the coarse problem is extended into a finer grid through an interpolation procedure, in the hope that one has obtained a good initial guess for the minimization problem on the higher-detailed data. The last two steps are then repeated until the maximal resolution is reached or the detail of the obtained deformation is deemed sufficient. A prime example of application of such methods to registration problems is [Mod04].

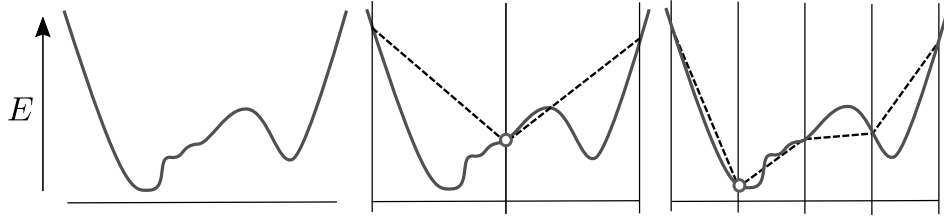


FIGURE 1.2: Idea of multiscale descent. The sampling points are indicated by vertical lines, and the corresponding discrete energy is dashed. In this example, even though neither the original energy nor the one in the second discretization step are convex, a good approximation for the minimum is quickly found.

In Chapters 2 and 3, approaches of this type are used to treat the minimization of the proposed models. These contain penalization terms for the constraint  $\phi(\mathcal{M}_1) = \mathcal{M}_2$ , where  $\mathcal{M}_1$  and  $\mathcal{M}_2$  are given surfaces, and whose convexity again depends directly on the data. Additionally, the nonlinear elasticity terms used are also inevitably nonconvex due to their geometric nature.

## 1.4.2 FEM and adaptivity

Finite element methods are Galerkin approaches to the solution of partial differential equations, in which the underlying functional space in which the equation is well-posed are replaced by a chain of finite-dimensional approximations of it. A central feature is that the form of the problem often does not change when restricted to smaller spaces. One typically looks at the weak formulation of a PDE problem, which arises as a critical point condition for an associated energy. All of the discretizations employed in this work are of this type.

This line of thinking fits nicely with the ideas sketched in the previous subsection. Indeed, instead of using simpler interpolation schemes, one can consider a chain of finite element spaces on which the minimization problem is considered, together with adequate projections. In this case, the unknowns of the corresponding discrete problem are the coefficients of the minimizer in an appropriate basis.

A common topic in FEM research is the use of spaces in which the computational mesh is subdivided only in particular places of interest, instead of everywhere. This gives rise to the theory of adaptivity in FEM, in which convergence guarantees for the sequence of approximate solutions are sought, when the mesh is refined according to properties of the last obtained solution. In Chapter 3 we use FEM on nonuniform meshes refined around the surfaces of interest, which are embedded in a higher-dimensional domain on which the energy functional is formulated. Here the adaptive approach is of great help, since regular discretizations would lead to a very high number of degrees of freedom.

## References

- [Bal81] J. M. Ball. “Global invertibility of Sobolev functions and the interpenetration of matter”. *Proc. Roy. Soc. Edinburgh Sect. A* 88 (1981), pp. 315–328.

- [Bra02] A. Braides.  *$\Gamma$ -convergence for beginners*. Vol. 22. Oxford Lecture Series in Mathematics and its Applications. Oxford: Oxford University Press, 2002. xii+218.
- [CG82] P.G. Ciarlet and G. Geymonat. “Sur les lois de comportement en élasticité non linéaire compressible”. *CR Acad. Sci. Paris Sér. II* 295 (1982), pp. 423–426.
- [Cia00] P. G. Ciarlet. *Mathematical elasticity, volume III: Theory of shells*. Amsterdam: North-Holland, 2000.
- [Cia78] P. G. Ciarlet. *The Finite Element Method for Elliptic Problems*. Amsterdam: North-Holland, 1978.
- [Dac08] B. Dacorogna. *Direct methods in the calculus of variations*. 2nd ed. Vol. 78. Applied Mathematical Sciences. New York: Springer, 2008. xii+619.
- [FJM02] G. Friesecke, R.D. James, and S. Müller. “A theorem on geometric rigidity and the derivation of nonlinear plate theory from three-dimensional elasticity”. *Comm. Pure Appl. Math.* 55.11 (2002), pp. 1461–1506.
- [Fle+04] P. T. Fletcher, C. Lu, S. M. Pizer, and S. Joshi. “Principal geodesic analysis for the study of nonlinear statistics of shape”. *IEEE Trans. Med. Imag.* 23.8 (2004), pp. 995–1005.
- [Fri+03] G. Friesecke, R.D. James, M.G. Mora, and S. Müller. “Derivation of nonlinear bending theory for shells from three-dimensional nonlinear elasticity by Gamma-convergence”. *C. R. Acad. Sci. Paris Sér I Math.* 336.8 (2003), pp. 697–702.
- [HS81] B. K. P. Horn and B. G. Schunck. “Determining optical flow”. *Artificial Intelligence* 17 (1981), pp. 185–203.
- [Kri99] J. Kristensen. “On the non-locality of quasiconvexity”. *Ann. Inst. H. Poincaré Anal. Non Linéaire* 16.1 (1999), pp. 1–13.
- [LDR95a] H. Le Dret and A. Raoult. “The nonlinear membrane model as variational limit of nonlinear three-dimensional elasticity”. *J. Math. Pures Appl.* 74 (1995), pp. 549–578.
- [LDR96] H. Le Dret and A. Raoult. “The membrane shell model in nonlinear elasticity: A variational asymptotic derivation”. *J. Nonlinear Sci.* 6 (1 1996), pp. 59–84.
- [Mil04] M. I. Miller. “Computational anatomy: shape, growth, and atrophy comparison via diffeomorphisms”. *NeuroImage* 23, Supplement 1.0 (2004), S19 –S33.
- [Mod04] J. Modersitzki. *Numerical Methods for Image Registration*. OUP Oxford, 2004.
- [Mor66] C. B. Morrey. *Multiple Integrals in the Calculus of Variations*. Vol. 130. Die Grundlehren der Mathematischen Wissenschaften. New York: Springer Verlag, 1966.
- [Mur78] F. Murat. “Compacité par compensation”. *Ann. Sc. Norm. Super. Pisa Cl. Sci.* 4.5 (1978), pp. 489–507.

- 
- [Ogd72] R. W. Ogden. “Large Deformation Isotropic Elasticity - On the Correlation of Theory and Experiment for Incompressible Rubberlike Solids”. *Proc. R. Soc. A* 326.1567 (1972), pp. 565–584.
- [RW15] M. Rumpf and B. Wirth. “Variational time discretization of geodesic calculus”. *IMA J. Numer. Anal.* 35.3 (2015), pp. 1011–1046.
- [Tar79] L. Tartar. “Compensated compactness and applications to partial differential equations”. In: *Nonlinear analysis and mechanics: Heriot-Watt Symposium, Vol. IV*. Vol. 39. Res. Notes in Math. Boston, Mass.: Pitman, 1979, pp. 136–212.
- [Tar90] L. Tartar. “H-measures, a new approach for studying homogenisation, oscillations and concentration effects in partial differential equations”. *Proc. Roy. Soc. Edinburgh Sect. A* 115 (3-4 1990), pp. 193–230.
- [WS01b] J. Weickert and Ch. Schnörr. “Variational optic flow computation with a spatio-temporal smoothness constraint”. *J. Math. Imaging Vision* 14 (3 2001), pp. 245–255.





# A Thin Shell Approach to the Registration of Implicit Surfaces

## Abstract

Frequently, one aims at the co-registration of geometries described implicitly by images as level sets. This paper proposes a novel shape sensitive approach for the matching of such implicit surfaces. Motivated by physical models of elastic shells a variational approach is proposed, which distinguishes two different types of energy contributions: a membrane energy measuring the rate of tangential distortion when deforming the reference surface into the template surface, and a bending energy reflecting the required amount of bending. The variational model is formulated via a narrow band approach. The built in tangential distortion energy leads to a suitable equidistribution of deformed length and area elements, under the optimal matching deformation, whereas the minimization of the bending energy fosters a proper matching of shape features such as crests, valleys or bumps. In the implementation, a spatial discretization via finite elements, a nonlinear conjugate gradient scheme with a Sobolev metric, and a cascadic multilevel optimization strategy are used. The features of the proposed method are discussed via applications both for synthetic and realistic examples.

## 2.1 Introduction and motivation

We address the problem of matching closed surfaces or curves, which are given as the zero level sets of functions defined in a volume or a planar domain. In vision many geometric objects are actually extracted from images as level sets. Furthermore, formulating geometric problems in terms of level sets often simplifies their numerical implementation, since regular grids can be used. As a consequence, we look for deformations of the whole computational domain which closely match a template surface to a reference surface, are invertible both on the surfaces and globally, and match geometric features (e.g. curvatures) of the surfaces while having low tangential distortion. For the mathematical modeling, we think of the reference surface as a layer of an elastic material (for example, rubber) embedded in a block of another much softer isotropic elastic material (foam, say), subject to a matching force that forces it onto the template surface.

With this in mind we derive a variational formulation motivated from the standard mathematical theories of nonlinear elasticity. However, our model is different from them in some aspects, to better exploit the specific advantages of our matching scenario, not present in physical situations. We will point out both the similarities and differences as we introduce and motivate the different parts of our energy.

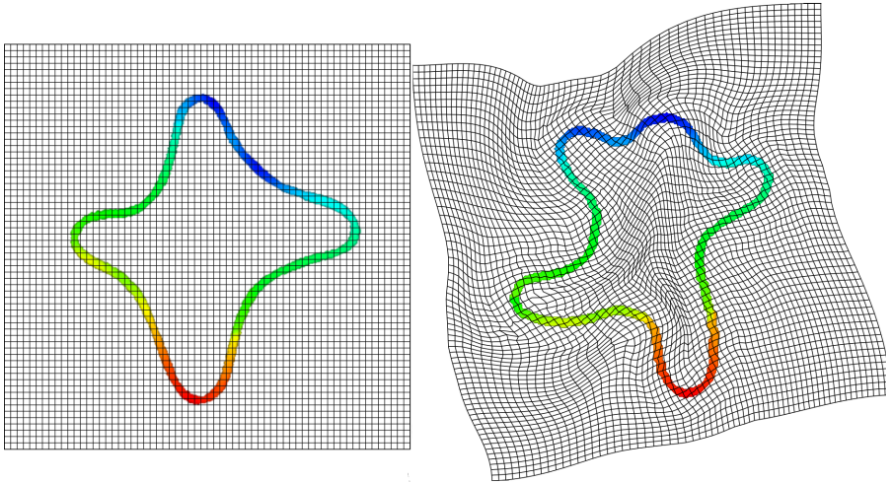


FIGURE 2.1: Result obtained with our method, when used for curves in a 2D domain. We look for a global and invertible deformation, which closely matches two input shapes, in a way that balances being as isometric as possible on the shapes, and matching their curvatures. On the left the reference shape is shown on the undeformed grid, whereas on the right the deformed reference shape matching the given template shape is rendered together with the deformed mesh. Undeformed and deformed points are colored identically.

## 2.2 Related work

In recent years, theories of nonlinear elasticity have found use in many problems of computer vision and graphics. Some applications are deformation of meshes [Cha+10], shape averages and geodesics between shapes [RW09; Wir+11], and registration of medical images [BMR13]. In the last work, the efficient discretization and numerical solution of hyperelastic regularization energies is studied. The chosen approach is a cascadic minimization scheme involving a Gauss-Newton method on each level.

Linear elasticity is also used for image registration [Mod04] and shape modeling [Fuc+09], but the advantage of nonlinear models is that they allow for intuitive deformations when the displacements are large.

In this paper, the focus is on nonlinear elastic matching of thin shells. A finite element method for the discretization of bending energies of thin shell type biological interfaces has been studied in [BNP10]. Their approach uses quadratic isoparametric finite elements to handle the interface on which an elastic energy of Helfrich type is approximated. In [Sri+09], face matching based on a matching of corresponding level set curves on the facial surfaces is investigated. To match pairs of curves an optimal deformation between them is computed using an elastic shape analysis of curves. Compared to our approach, this model does not take into account dissipation along deformation paths caused by a bending of the curves. The paper [BPW12] discusses a new concept for the treatment of higher order variational problems on surfaces described as jump sets of functions of bounded variation type. This approach in particular enables the analytical rigorous treatment of elastic energies on such surfaces. The matching of surfaces with elastic energies has recently been studied in [Win+11]. Their energy splits into a membrane energy depending on the

Cauchy-Green strain tensor and a bending energy, comparing only the mean curvatures on the surfaces. The matching problem is phrased in terms of a binary linear program in the product space of sets of surface patches. A relaxation approach is used to render it computationally feasible. An approach related to ours is presented in [Lit+05], where nonlinear elastic energies are proposed for matching of open, parametrized surface patches. Here, we propose a method for closed surfaces that does not require a parametrization.

A method for matching and blending represented by level sets has been presented in [MR12]. A level set evolution generates an interpolating family of curves, where the associated propagation speed of the level sets depends on differences of level set curvatures. In this class of approaches, geometric evolution problems are formulated, whereas here we focus on variational models for matching deformations. Registration of implicit surfaces was considered in [LL08], but only through volumetric terms, in contrast to our tangential distortion and bending terms.

Let us mention that our approach is inspired by the works [DZ94; DZ95] in which partial differential equations for shell models are derived in terms of distance functions. Shape warping based on the framework of [DZ94] from a less physical perspective has been discussed in [CFK04].

## 2.3 A thin shell matching model

Our model for the shape sensitive matching of surfaces is based on physical models for the elastic deformation of a thin shell [Cia00]. Thereby, a shell  $\mathcal{M}$  is considered as the  $d - 1$  dimensional mid-surface of a layer of material of thickness  $\delta \ll 1$  in  $\mathbb{R}^d$ .

To match two shell surfaces  $\mathcal{M}_1$  and  $\mathcal{M}_2$  via a deformation  $\phi$ , we take into account the elastic energy of a deformation  $\phi : \mathcal{M}_1 \rightarrow \mathbb{R}^3$  under the constraint  $\phi(\mathcal{M}_1) = \mathcal{M}_2$ . The energy can be decomposed into a membrane energy (penalizing stretching and compression strain) and a bending energy (penalizing strain caused by bending). Under this constraint the energy actually depends only on the Jacobian of the deformation  $\phi$  and not on second derivatives of  $\phi$ , since curvatures for the bending term can be evaluated on  $\mathcal{M}_2$ .

**Membrane energy.** The rate of tangential distortion at each point is described by the tangential Cauchy-Green strain tensor (cf. Figure 2.2)

$$A_{\text{tg}}[\phi] = D_{\text{tg}}\phi^T D_{\text{tg}}\phi.$$

Here, the tangential Jacobian of the deformation is defined by  $D_{\text{tg}}\phi = D\phi^{ext}P$  for an extension  $\phi^{ext}$  of  $\phi$  onto a neighborhood of  $\mathcal{M}_1$ ,  $P = \mathbb{1} - N_1 \otimes N_1$  being the projection onto the tangent space of  $\mathcal{M}_1$  with normal  $N_1$ . Then, the associated membrane energy is given by

$$\mathcal{E}_{\text{mem}}[\phi] = \delta \int_{\mathcal{M}_1} W_{\text{mem}}(A_{\text{tg}}[\phi]) \, da, \quad (2.3.1)$$

where we choose as the requisite energy density

$$W_{\text{mem}}(A) = \frac{\mu}{2} \text{tr } A + \frac{\lambda - 2\mu}{8} \det A + \frac{2\mu + \lambda}{8} (\det A)^{-1}. \quad (2.3.2)$$

Here,  $\lambda$  and  $\mu$  are the Lamé constants of a St. Venant–Kirchhoff material [Cia88] with  $\text{tr } A$  and  $\det A$  denoting the trace and the determinant of  $A$  considered as an endomorphism on the tangent bundle of  $\mathcal{M}_1$ . Notice that  $\det A$  describes area distortion, while  $\text{tr } A$  measures length distortion. The polyconvex function  $W_{\text{mem}}$  is rigid body motion invariant, and it can be verified, using the invariance, that the identity is its only minimizer. Furthermore, the second order Taylor expansion at the identity reveals the classical quadratic energy of linearized, isotropic elasticity.

A simplification of the functional in (2.3.1) corresponds to the known  $\Gamma$ -limit of volume elasticity models for vanishing thickness parameter  $\delta$  [LDR96]. This limit does not account for compression resistance [FJM06]. In our case, the energy density (2.3.2) does reflect compression resistance through the term involving  $(\det A)^{-1}$ , which also avoids self interpenetration, thus giving a more precise physical model.

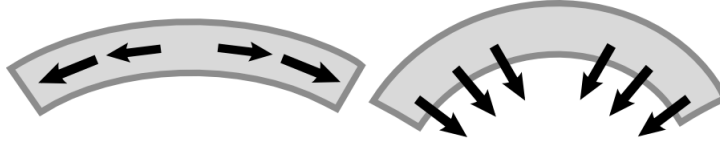


FIGURE 2.2: A sketch of the two different modes of deformation of a thin shell: tangential distortion (left) and bending (right)

**Bending energy.** The bending energy measures the local rate of bending described by the change of curvature under the deformation (cf. Figure 2.2). The shape operator of  $\mathcal{M}_i$  is defined as the tangential Jacobian  $D_{\text{tg}} N_i$  of the normal  $N_i$ . From the fact that  $0 = \partial_k \|N_i\|^2 = 2\partial_k N_i \cdot N_i$ , one deduces that  $(D_{\text{tg}} N_i)(x)$  is an endomorphism of the tangent space  $T_x \mathcal{M}_i$ . Aiming at a comparison of  $D_{\text{tg}} N_1$  at some point  $x \in \mathcal{M}_1$  and  $D_{\text{tg}} N_2$  at the deformed position  $\phi(x)$ , we have to use a corresponding pullback under the deformation  $\phi$  and with it define the relative shape operator

$$S_{\text{rel}}[\phi](x) := D_{\text{tg}} \phi^T (D_{\text{tg}} N_2)(\phi(x)) D_{\text{tg}} \phi - (D_{\text{tg}} N_1)(x).$$

If  $\phi$  is an isometric deformation of the shell  $\mathcal{M}_1$ , i.e.  $A_{\text{tg}}[\phi](x) = \mathbb{1}_{T_x \mathcal{M}_1}$ , then we recover the definition of the relative shape operator used in the rigorous analysis in Friesecke et al. [Fri+03]. In this case, the leading order term of the bending energy as the  $\Gamma$ -limit of 3D elasticity is *cubic* in the thickness  $\delta$  and given by

$$\mathcal{E}_{\text{bend}}[\phi] = \delta^3 \int_{\mathcal{M}_1} W_{\text{bend}}(S_{\text{rel}}[\phi]) \, da. \quad (2.3.3)$$

Although other choices are conceivable, we consider  $W_{\text{bend}}(S) = \|S\|_F^2$ , where  $\|S(x)\|_F$  denotes the Frobenius norm of the corresponding linear operator  $S(x) : T_x \mathcal{M} \rightarrow T_x \mathcal{M}$ . Notice that different from bending energies considered in graphics elsewhere,  $S_{\text{rel}}[\phi]$  takes into account the full change of the shape operators on  $\mathcal{M}_1$  and  $\mathcal{M}_2$ , not only the change of their traces (i.e. mean curvatures), so that changes of bending *directions* get accounted for appropriately.

**Deformation energy.** Combining membrane (2.3.1) and bending (2.3.3) contributions, we obtain the total elastic shell energy

$$\mathcal{E}_{\text{sh}}[\phi] = \alpha_{\text{bend}} \mathcal{E}_{\text{bend}}[\phi] + \alpha_{\text{mem}} \mathcal{E}_{\text{mem}}[\phi]. \quad (2.3.4)$$

A fundamental insight arising from the analysis of shell models [Cia00] and the recent advances in a rigorous limit theory [LDR96; Fri+03] is that pure membrane terms and pure bending terms cannot coexist in the limit of zero thickness, since the scaling of these terms with respect to it is governed by a different power of the width of the shell  $\delta$ . However, because of their distinct properties, in shape matching applications it is beneficial to use both, in particular considering the bending energy of non-isometric deformations. This formulation is the basis for our level set method for surface matching discussed in the next section.

## 2.4 Level set framework

Now we derive the actual variational approach for the matching of implicit surfaces. To this end, we suppose that the geometries  $\mathcal{M}_1$  and  $\mathcal{M}_2$  are implicitly described hypersurfaces on a computational domain  $\Omega \subset \mathbb{R}^d$  (curves for  $d = 2$  and surfaces for  $d = 3$ ). Explicitly, we assume  $\mathcal{M}_i$  to be described by its signed distance function  $\mathbf{d}_i$ , which constitute our input data (cf. Figure 2.3). For closed surfaces our convention is that  $\mathbf{d}_i$  is positive outside  $\mathcal{M}_i$ . If the input is not a distance function but any other regular level set function, one can obtain a distance function via the application of the fast marching method [Set99]. For any  $c$ , we denote the  $c$ -offsets to these surfaces by  $\mathcal{M}_i^c = \{x \in \Omega \mid \mathbf{d}_i(x) = c\}$ . In what follows, we consider a deformation  $\phi : \Omega \mapsto \mathbb{R}^3$ , which approximately maps  $\mathcal{M}_1$  onto  $\mathcal{M}_2$ . Since the  $\mathbf{d}_i$  are distance

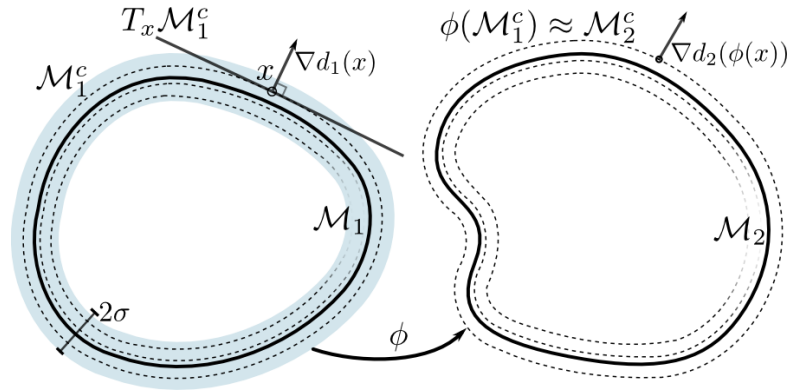


FIGURE 2.3: A sketch of the level set framework with the narrow band around the surface  $\mathcal{M}_1$  marked in light blue. The dashed lines on the left indicate different level sets of  $\mathbf{d}_1$  (left) and their deformed images (right).

functions, we have  $|\nabla \mathbf{d}_i| = 1$ , so that  $\nabla \mathbf{d}_i(x)$  is the unit normal to  $\mathcal{M}_i^{\mathbf{d}_i(x)}$  at a point  $x$ . Then, the tangent space to  $\mathcal{M}_i^{\mathbf{d}_i(x)}$  at  $x$ , denoted by  $T_x \mathcal{M}_i^{\mathbf{d}_i(x)}$ , consists of all vectors orthogonal to  $\nabla \mathbf{d}_i(x)$ . Projection matrices onto these tangent spaces can be computed by  $P_i(x) = \mathbb{1} - \nabla \mathbf{d}_i(x) \otimes \nabla \mathbf{d}_i(x)$ , which induce, on the whole domain, the tangential derivative  $D_{\text{tg}} \phi(x) = D\phi(x)P_1(x)$  of the deformation and the tangential Cauchy-Green strain tensor  $A_{\text{tg}}[\phi] = D_{\text{tg}} \phi^T D_{\text{tg}} \phi$  to each level set. Analogously, we can also compute the shape operators of  $\mathcal{M}_1^{\mathbf{d}_1(x)}$  at  $x$  and  $\mathcal{M}_2^{\mathbf{d}_2(\phi(x))}$  at

$\phi(x)$  through  $\mathcal{S}_1(x) = D^2 \mathbf{d}_1(x)$  and  $\mathcal{S}_2(x) = D^2 \mathbf{d}_2(\phi(x))$ . We can then use these level set expressions in the energies (2.3.1) and (2.3.3), to rewrite the components of the shell energies on a single level set in terms of the deformation and the two signed distance functions  $\mathbf{d}_1$  and  $\mathbf{d}_2$ . In what follows, we will combine this with a narrow band approach focusing on a small neighborhood of the actual surfaces of interest.

**Narrow band formulation of shell energies.** As is customary in level set methods [Set99], we introduce a narrow band around  $\mathcal{M}_1$ , whose deformation we want to capture (cf. Figure 2.3). This is done by a smooth and even cutoff function  $\eta_\sigma$  such that  $\eta_\sigma(0) = 1$  and  $\eta_\sigma(s) = 0$  if  $|s| > \sigma$ . The support of the composition  $\eta_\sigma \circ \mathbf{d}_1$  then identifies the narrow band.

To formulate a level set variational method, we measure the distortion created by the deformation  $\phi$  on each level set  $\mathcal{M}_1^c$  through the shell energy (2.3.4), obtaining  $\mathcal{E}_{\text{sh}}^c[\phi] = \int_{\mathcal{M}_1^c} W_{\text{sh}}[\phi] da$ . Here, the energy density  $W_{\text{sh}}[\phi]$  expressed in terms of  $\mathbf{d}_1$ ,  $\mathbf{d}_2$  and  $\phi$  is given by

$$W_{\text{sh}}[\phi] = \alpha_{\text{mem}} \delta W_{\text{mem}}(A_{\text{tg}}[\phi]) + \alpha_{\text{bend}} \delta^3 W_{\text{bend}}(S_{\text{rel}}[\phi]),$$

where  $A_{\text{tg}}[\phi] = D_{\text{tg}} \phi^T D_{\text{tg}} \phi$  is the tangential Cauchy-Green strain tensor, with  $D_{\text{tg}} \phi = D\phi(1 - \nabla \mathbf{d}_i \otimes \nabla \mathbf{d}_i)$  denoting the tangential derivative of the deformation, and  $S_{\text{rel}}[\phi] = D_{\text{tg}} \phi^T (D^2 \mathbf{d}_2 \circ \phi) D_{\text{tg}} \phi - D^2 \mathbf{d}_1$  is the relative shape operator expressed in terms of the distance functions and the deformation. Now, we weight this energy by  $\eta_\sigma(c)$  and use the coarea formula [EG92] (using once again that  $|\nabla \mathbf{d}_1| = 1$ ) to integrate the resulting weighted energy over all level sets of interest and obtain

$$\mathcal{E}_{\text{sh}}[\phi] = \int_{-\infty}^{+\infty} \mathcal{E}_{\text{sh}}^c[\phi] dc = \int_{\Omega} \eta_\sigma(\mathbf{d}_1) W_{\text{sh}}[\phi] dx. \quad (2.4.1)$$

In this manner we are able to define a global energy, defined as a volume integral over the computational domain, consistent with the surface energy defined on each of the offsets  $\mathcal{M}_1^c$  which fill up the narrow band.

**Handling the constraint.** In our shell model, we have assumed that  $\phi(\mathcal{M}_1^c) = \mathcal{M}_2^c$ . This allows us to formulate the bending energy in terms of the shape operators of the given surfaces  $\mathcal{M}_1^c$  and  $\mathcal{M}_2^c$  for  $|c| \leq \sigma$ . In practice, we use a quadratic penalty on the surface  $\mathcal{M}_1^c$  measuring the difference between the deformed distance function  $\mathbf{d}_2 \circ \phi$  and the desired distance value  $c$ , leading to the functional  $\frac{1}{\epsilon} \int_{\mathcal{M}_1^c} |\mathbf{d}_2 \circ \phi - c|^2 da$  for some small  $\epsilon > 0$ . Again using the coarea formula we obtain the global mismatch penalty

$$\mathcal{E}_{\text{mismatch}}[\phi] = \frac{1}{\epsilon} \int_{\Omega} \eta_\sigma(\mathbf{d}_1) |\mathbf{d}_2 \circ \phi - \mathbf{d}_1|^2 dx, \quad (2.4.2)$$

which amounts to the squared  $L^2$  distance of the pullback of  $\mathbf{d}_2$  under the deformation  $\phi$  and  $\mathbf{d}_1$ , weighted at each level set by  $\eta_\sigma$ .

**Volumetric hyperelastic regularization.** So far the resulting energy does not impose any restriction on the deformation outside the narrow band of thickness  $2\sigma$  around  $\mathcal{M}_1$ . Thus, to obtain a well-posed variational model on the whole computational domain, we have to take into

account some regularization functional outside the narrow band. To this end, we add an additional volumetric elastic energy evaluated on the deformation  $\phi$ . Following the usual paradigms of nonlinear elasticity, we choose

$$\mathcal{E}_{\text{vol}}[\phi] = \xi \int_{\Omega} W_{\text{vol}}(A[\phi]) \, dx \quad (2.4.3)$$

for  $\xi > 0$  small, where  $A[\phi] = D\phi^T D\phi$  is the usual Cauchy-Green strain tensor. The requisite energy density is given by

$$W_{\text{vol}}(A) = \frac{\tilde{\mu}}{2} \text{tr } A + \frac{\tilde{\lambda} - 2\tilde{\mu}}{8} \det A + \frac{2\tilde{\mu} + \tilde{\lambda}}{8} (\det A)^{-1} \quad (2.4.4)$$

for the Lamé constants  $\tilde{\lambda}$  and  $\tilde{\mu}$  of a St. Venant–Kirchhoff material. Notice that the difference with respect to the membrane energy (2.3.1) is the use of the three-dimensional strain tensor  $A$ , instead of  $A_{\text{tg}}$ . Physically, the resulting energy corresponds to a soft elastic material outside the narrow band in which the comparatively rigid surfaces inside the band are embedded. The addition of this term ensures that the obtained transformations are invertible on the whole domain, and this in turn implies that the deformed surfaces will not collapse and intersect themselves, a problem that can not be prevented with a tangential energy density alone.

We can alternatively consider the surfaces  $\mathcal{M}_1$  and  $\mathcal{M}_2$  as boundaries of volumetric objects, i.e. modeling elastic bodies those contours are themselves elastic shells, through

$$\mathcal{E}_{\text{vol}}[\phi] = \int_{\Omega} \left( \zeta + (1 - \zeta) \chi_{\{\mathbf{d}_1 < 0\}} \right) W_{\text{vol}}[\phi] \, dx. \quad (2.4.5)$$

**The registration energy.** Combining the above energy terms we obtain the total thin shell registration energy for implicit surfaces

$$\mathcal{E}_{\text{total}}[\phi] = \mathcal{E}_{\text{sh}}[\phi] + \mathcal{E}_{\text{mismatch}}[\phi] + \mathcal{E}_{\text{vol}}[\phi].$$

The numerical method for the minimization of this energy will be discussed in the following section.

## 2.5 Discretization and minimization

In the level set framework investigated here, we can use a straightforward space discretization to solve the problem numerically. Since the problem only includes first order derivatives of  $\phi$  in the energy, we take into account multi-linear finite elements for the spatial discretization of the involved energy and run an optimization method on the coefficients of the solution in this finite element basis.

**Computation of the curvatures.** However, we also need to compute curvatures from the distance functions  $\mathbf{d}_i$  given as data, i.e. we have to robustly compute a suitable approximation of  $D^2 \mathbf{d}_i$  to evaluate the shape operators. Furthermore, first derivatives of these functions have to be computed when the gradient of the energy is needed in the descent method. Our approach, similar



to the one used in [PR02], is to compute these derivative matrices by projection onto quadratic polynomials spanned in a local neighborhood of each point. In explicit, for each node  $x_k$  we consider the set of nodes  $x_j$  in the  $r$  neighborhood  $B_r(x_k)$  of  $x_k$  and compute the quadratic polynomial  $x \mapsto p_k(x)$  which minimizes

$$\sum_{x_j \in B_r(x_k)} \left( p_k(x_j) - \mathbf{d}_i^j \right)^2.$$

To solve this quadratic minimization problem, we have to solve a small linear system for every node  $x_k$ . The associated system matrix is independent of the node  $x_k$  on the regular grid lattice. Thus, we can precompute the  $LR$  decomposition of the matrix. Once the polynomial coefficients are computed, we replace the Hessian of  $\mathbf{d}_i$  at every node  $x_k$  in our matching model by the Hessian of the polynomial  $p_k$ .

**Cascadic multilevel descent.** Because we are solving a highly nonlinear and non convex registration problem, we apply the standard paradigm of a coarse-to-fine cascadic minimization. Let us suppose that a dyadic scale of a regular mesh is given, where the grid is divided by two on each level of the hierarchy. For the minimization at each level, we used a Fletcher-Reeves nonlinear conjugate gradient method (see [NW06], section 5.2), in which the gradients are computed with respect to a Sobolev metric by  $\text{grad}_{H^1} E[\phi] = (1 - \frac{\beta^2}{2} \Delta)^{-1} \text{grad}_{L^2} E[\phi]$ , where  $\text{grad}_{L^2} E[\phi]$  is the usual  $L^2$  gradient appearing in the Euler-Lagrange equation. This amounts to smoothing the descent directions by an approximation of a Gaussian with filter width  $\beta$ . As indicated in Algorithm 1, the smoothing is reduced gradually to be able to capture details of the deformation.

---

**Algorithm 1** Coarse-to-fine Sobolev descent

---

```

1:  $\phi \leftarrow \mathbb{1}$ 
2: for  $l \leftarrow l_{\min}$  to  $l_{\max}$  do
3:    $h \leftarrow 1/(2^l + 1)$ 
4:    $\beta \leftarrow \beta_{\max}$ 
5:   while  $\alpha > \beta_{\min}$  do
6:      $\phi \leftarrow \text{Sobolev-CG-descent}(\beta, \phi)$ 
7:      $\beta \leftarrow \beta/2$ 
8:   end while
9: end for
10: return  $\phi$ 

```

---

**Parameter choices.** Despite the many parameters present in the energy, the underlying physical intuition of the model allows to make judicious choices without much effort. We indicate some example ranges, which were used in all the applications presented. The material properties  $\alpha_{\text{mem}}, \alpha_{\text{bend}}$  of the shell in (2.3.4) were the ‘reference parameters’, and were taken to be  $\approx 1$ . One can choose then  $\lambda \approx 2, \mu \approx 0.25$ . In comparison  $\epsilon^{-1}$  in (2.4.2) should be large, and was taken to be  $\approx 10^3$ . The outside parameters should correspond to a comparably soft material, so picking  $\tilde{\lambda} = \lambda, \tilde{\mu} = \mu$  and  $\xi \approx 10^{-3}$  for (2.4.3) was sufficient. The bending energy (2.3.3) turned out to have enough influence to induce correct matchings with a shell width parameter



$\delta = 0.5$ . Additionally, we varied the parameters  $\epsilon$  and  $\delta$  when changing from a coarser to the next finer level by a factor 0.5, the above values being used on the coarsest grid level. This proved to be a very suitable strategy to ensure that  $\mathcal{M}_1$  and  $\mathcal{M}_2$  are appropriately matched at all scales, and that geometric details are actually resolved under the deformation on the finest grid level.

## 2.6 Results

We demonstrate the properties of our method with some numerical results. First, we depict some interesting qualitative properties of our models. Afterwards, we show some real applications for the matching of two dimensional surfaces.

**Redistribution of tangential distortion.** Here we aim to experimentally confirm that the membrane term (2.3.1) redistributes the tangential strain which necessarily occurs when shapes of different length or area are matched. This corresponds to the strict convexity of the integrand (2.3.2) in a neighborhood of the identity. For demonstrating this, we use the simple 2D shapes of Figure 2.4 and compare the matching of a circle with an ellipse, once solely using the volumetric elastic energy from (2.4.5) and once using our model energy (2.4.1) with membrane energy but without bending energy ( $\alpha_{mem} = 1$ ,  $\alpha_{bend} = 0$ ). The resulting tangential distortion measures are presented in Table 2.1. In Figure 2.4, we show the resulting matching for our model.

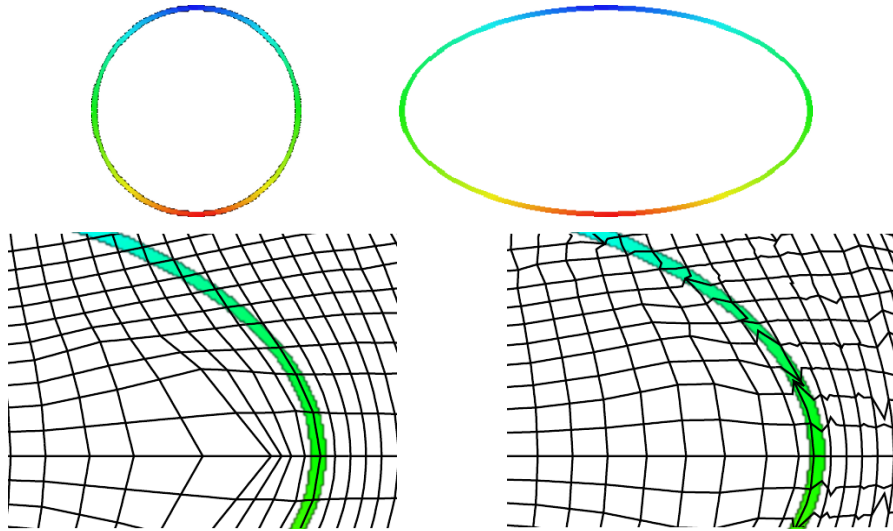


FIGURE 2.4: Matching problem to explore the redistribution of tangential strain induced by the membrane term. Upper row: Reference and template shapes (colors are the same at the undeformed position on the circle and the deformed position on the ellipse). Lower row: detail of the deformed grid, drawn over the template shape. On the left side, only the volumetric elastic energy has been used, whereas in the right side we have used our model without bending energy (Table 2.1). Observe the localized deformations in the tangential direction to ensure the equidistribution of tangential strain.

Level ( $h^{-1}$ )	$\mathcal{E}_{\text{vol}}$ only	$\mathcal{E}_{\text{sh}}$ with $\alpha_{\text{bend}} = 0$
5 (33)	0.8541	0.1758
6 (65)	0.7949	0.0875
7 (129)	0.8053	0.0440
8 (257)	0.7953	0.0234
9 (513)	0.7978	0.0143

TABLE 2.1: Standard deviation of the tangential strain on the narrow band  $2^{-\frac{1}{2}} \|D_{\text{tg}} \phi^T D_{\text{tg}} \phi \chi_{\{|\mathbf{d}_1| < h\}}\|_F$  around the reference curve. The ratio between length of the ellipse and length of the circle is  $\approx 2.38$ . When using only a volumetric elasticity term, the deformation is basically a stretching in horizontal direction with large variation of the tangential strain, whereas in our model the strain is asymptotically equidistributed with decreasing grid size.

**Crumpling when minimizing only the membrane energy.** One of the main limitations of using nonlinear membrane terms of the type (2.3.1), that strongly penalize compression, is that when trying to force a deformation from one shape to a thin neighborhood of a much smaller one, crumpling becomes unavoidable. Rather than a problem with our particular model, this is an issue with any realistic physical formulation, as crumpling occurs when crushing a sheet of paper, for example. If a very strong compression is required to match the reference to the template, oscillations are created to accommodate the excess of length. In this case, the continuous energy has no minimizer. We present a numerical example in which crumpling appeared in Figure 2.5. In

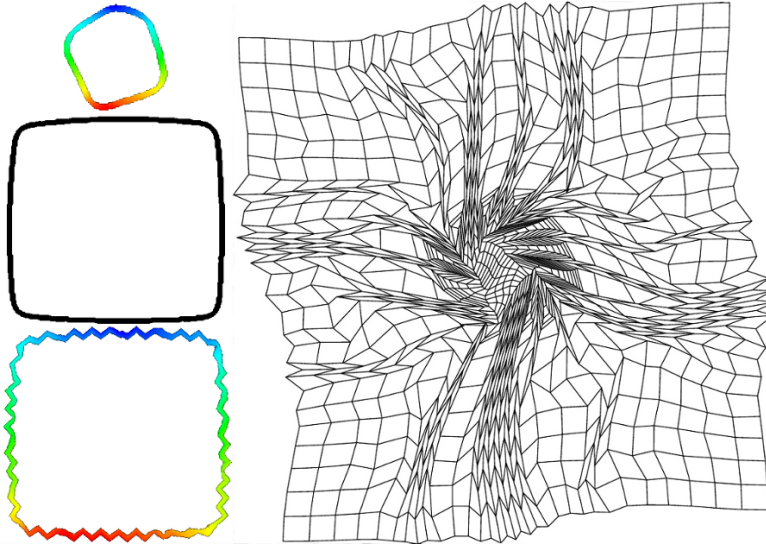


FIGURE 2.5: Numerical crumpling on a coarse grid ( $33^2$  points). Left column, top to bottom: Template curve, reference curve, and pullback of the template curve under the deformation  $\phi$ . Right: Grid deformed through  $\phi$ .

fact, in this case the penalty parameter  $\epsilon$  is not small enough to prevent the crumpling from being visible. This phenomenon was also observed in [Hee+12], for very small bending resistance.

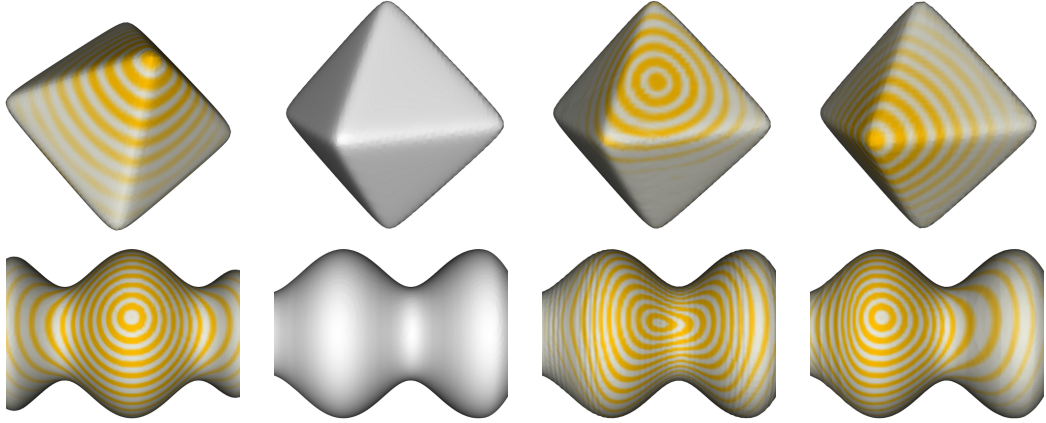


FIGURE 2.6: Upper row: Effect of the bending energy  $\mathcal{E}_{\text{bend}}$ . From left to right: Textured template shape, reference shape, deformed template (with a push forward of the template texture) based on a matching with  $\alpha_{\text{bend}} = 0$ , deformed template with  $\alpha_{\text{bend}} = 1$ . Lower row: Matching of constant mean curvature surfaces. From left to right: Textured template shape, reference shape, deformed template using the energy  $\mathcal{E}_{\text{bend}}^{\text{simple}}$ , deformed template using a direct comparison of the shape operators via  $\mathcal{E}_{\text{bend}}$ .

**Shape sensitive matching using the bending energy.** We present two examples to underline the importance of the curvature matching term in Figure 2.6. In the first example, we aim at matching two rotated versions of a rounded  $l^1$  ball. Without incorporating the curvature matching term  $E_{\text{bend}}$  ( $\alpha_{\text{bend}} = 0$ ), the corners are squashed in one position and grown in another via the deformation. When  $E_{\text{bend}}$  is activated, the method finds the right rotation, because the rounded edges have to be mapped onto each other to reduce the norm of the relative shape operator.

The second example shows the matching of two different sections of an unduloid. Unduloids are surfaces of constant mean curvature first derived by Delaunay [Del41]. We attempt this both with the proposed bending energy (2.3.3), and a simpler mean curvature comparison term of the form

$$\mathcal{E}_{\text{bend}}^{\text{simple}} = \int_{\Omega} \eta_{\sigma}(\mathbf{d}_1) |H_2 \circ \phi - H_1|^2 dx, \quad (2.6.1)$$

as in [Lit+05], where  $H_i$  is the mean curvature of the surface  $\mathcal{M}_i^{\mathbf{d}_i}$ . Clearly, taking into account just a comparison of mean curvatures with the above energy is not appropriate, whereas the proposed shape operator alignment (2.3.3) matches the surfaces correctly.

**Applications for shape matching.** As a further proof of concept, we investigate a couple of matching problems in the context of more complicated shapes in Figures 2.7, 2.8 and 2.9. In particular, we investigate the performance of the cascadic descent and depict matching results on different grid levels in Figures 2.7 and 2.9. In all these applications, we have used the full variational model presented above (in Figure 2.8 and 2.9 in comparison with the results for a pure volume matching energy).

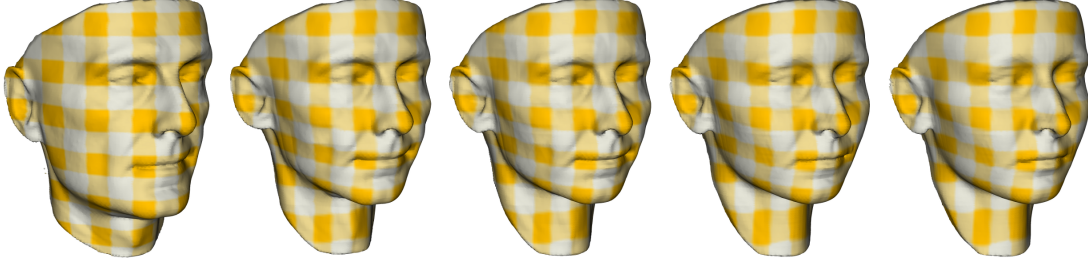


FIGURE 2.7: From left to right: Textured template shape, and resulting deformed template after different stages of the cascadic minimization scheme (on  $17^3$ ,  $33^3$ ,  $65^3$ ,  $129^3$  grids, respectively).

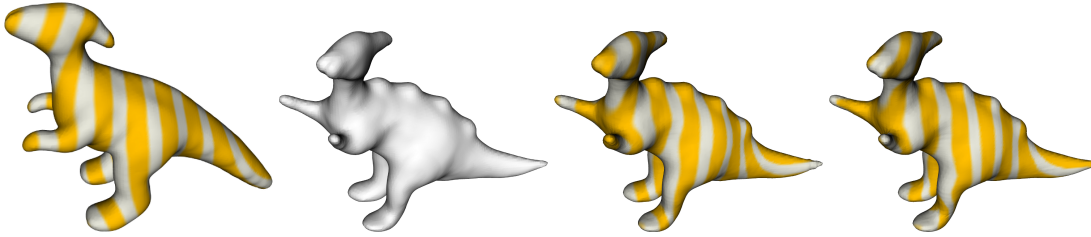


FIGURE 2.8: From left to right: textured template surface, reference input surface, matching results for the full model on a  $129^3$  grid (with a push forward of the texture), analogous result with only volume elastic regularization and no shell registration energy. Without the membrane and bending terms, several parts are incorrectly matched (front of the head, both pairs of legs).

## 2.7 Conclusions and future work

We have presented a variational method for the matching of implicit surfaces represented as level sets. The proposed energies penalize both stretching / compression and bending of the surfaces via physically realistic elastic energies. The level set approach allows a formulation with only first order derivatives, and computation on regular grids. We have demonstrated qualitative properties for a set of simple test cases and show the applicability of the chosen approach for more complex surfaces. In particular, we have shown correct matches in cases where simpler elastic approaches fail.

A future research direction is to define shape spaces of such implicit shells (cf. [Hee+12] for

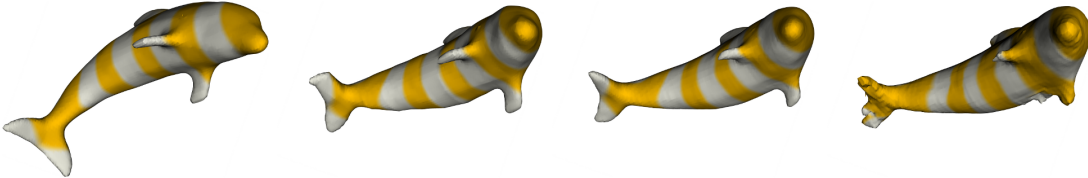


FIGURE 2.9: From left to right: Textured template shape, resulting deformed template after minimization on a grid with  $17^3$  nodes and on a grid with  $129^3$  nodes, respectively, when using the full proposed model. Right most image: matching results based on a purely elastic volume matching. In particular, we observe artifacts due to a lack of surface deformation energies.

the case of triangulated shell surfaces). Furthermore, a rigorous mathematical analysis of the model has to be developed, with criteria for the existence of minimizing deformations. Moreover, adaptive meshes would allow to treat much more detailed surfaces as they appear for instance in biological and medical applications.

## Acknowledgements

This research was supported by the Austrian Science Fund (FWF) through the National Research Network ‘Geometry+Simulation’ (NFN S117). The dinosaur and dolphin shapes were taken from the McGill 3D Shape Benchmark [Sid+08]. The scanned faces are part of the 3D Basel Face Model data [Pay+09].

## References

- [BMR13] M. Burger, J. Modersitzki, and L. Ruthotto. “A Hyperelastic Regularization Energy for Image Registration”. *SIAM J. Sci. Comput.* 35.1 (2013), B132–B148.
- [BNP10] A. Bonito, R. H. Nochetto, and M. S. Pauletti. “Parametric FEM for geometric biomembranes”. *J. Comput. Phys.* 229 (2010), pp. 3171–3188.
- [BPW12] K. Bredies, T. Pock, and B. Wirth. “Convex Relaxation of a Class of Vertex Penalizing Functionals”. *J. Math. Imaging Vis.* (2012), doi: 10.1007/s10851-012-0347-x.
- [CFK04] G. Charpiat, O. Faugeras, and R. Keriven. “Approximations of Shape Metrics and Application to Shape Warping and Empirical Shape Statistics”. *Found. Comp. Math.* 5 (2004), pp. 1–58.
- [Cha+10] I. Chao, U. Pinkall, P. Sanan, and P. Schröder. “A simple geometric model for elastic deformations”. *ACM Trans. Graph.* 29 (4 July 2010), 38:1–38:6.
- [Cia00] P. G. Ciarlet. *Mathematical elasticity, volume III: Theory of shells*. Amsterdam: North-Holland, 2000.
- [Cia88] P. G. Ciarlet. *Mathematical elasticity, volume I: Three-dimensional elasticity*. Vol. 20. Mathematics and its Applications. Amsterdam: North-Holland, 1988.
- [Del41] Ch. Delaunay. “Sur la surface de révolution dont la courbure moyenne est constante.” *fre. J. Math. Pures Appl.* (1841), pp. 309–314.
- [DZ94] M.C. Delfour and J.-P. Zolésio. “Shape analysis via oriented distance functions”. *J. Funct. Anal.* 123 (1994), pp. 129–201.
- [DZ95] M.C. Delfour and J.-P. Zolésio. “A boundary differential equation for thin shells”. *J. Differential Equations* 119.2 (1995), pp. 426–449.
- [EG92] L. C. Evans and R. F. Gariepy. *Measure theory and fine properties of functions*. Studies in Advanced Mathematics. Boca Raton, FL: CRC Press, 1992. viii+268.

- [FJM06] G. Friesecke, R. D. James, and S. Müller. “A Hierarchy of Plate Models Derived from Nonlinear Elasticity by Gamma-Convergence”. *Arch. Ration. Mech. Anal.* 180.2 (2006), pp. 183–236.
- [Fri+03] G. Friesecke, R.D. James, M.G. Mora, and S. Müller. “Derivation of nonlinear bending theory for shells from three-dimensional nonlinear elasticity by Gamma-convergence”. *C. R. Acad. Sci. Paris Sér I Math.* 336.8 (2003), pp. 697–702.
- [Fuc+09] M. Fuchs, B. Jüttler, O. Scherzer, and H. Yang. “Shape metrics based on elastic deformations”. *J. Math. Imaging Vis.* 35.1 (2009), pp. 86–102.
- [Hee+12] B. Heeren, M. Rumpf, M. Wardetzky, and B. Wirth. “Time-Discrete Geodesics in the Space of Shells”. *Computer Graphics Forum* 31.5 (2012), pp. 1755–1764.
- [LDR96] H. Le Dret and A. Raoult. “The membrane shell model in nonlinear elasticity: A variational asymptotic derivation”. *J. Nonlinear Sci.* 6 (1 1996), pp. 59–84.
- [Lit+05] N. Litke, M. Droske, M. Rumpf, and P. Schröder. “An Image Processing Approach to Surface Matching”. In: *Symposium on Geometry Processing*. Ed. by M. Desbrun and H. Pottmann. 2005, pp. 207–216.
- [LL08] T.-Y. Lee and S.-H. Lai. “3D non-rigid registration for MPU implicit surfaces”. In: *CVPR Workshop on Non-Rigid Shape Analysis and Deformable Image Alignment*. 2008.
- [Mod04] J. Modersitzki. *Numerical Methods for Image Registration*. OUP Oxford, 2004.
- [MR12] D. P. Mukherjee and N. Ray. “Contour interpolation using level-set analysis”. *Int. J. Img. Graph.* 12.1 (2012), p. 1250004.
- [NW06] J. Nocedal and S. Wright. *Numerical Optimization*. Second. Springer, 2006.
- [Pay+09] P. Paysan, R. Knothe, B. Amberg, S. Romdhani, and T. Vetter. “A 3D Face Model for Pose and Illumination Invariant Face Recognition”. In: *Proc. Advanced Video and Signal based Surveillance*. 2009.
- [PR02] T. Preusser and M. Rumpf. “A level set method for anisotropic geometric diffusion in 3D image processing”. *SIAM J. Appl. Math.* 62.5 (2002), pp. 1772–1793.
- [RW09] M. Rumpf and B. Wirth. “A nonlinear elastic shape averaging approach”. *SIAM J. Imaging Sci.* 2.3 (2009), pp. 800–833.
- [Set99] J. A. Sethian. *Level set methods and fast marching methods*. 2nd ed. Vol. 3. Cambridge Monographs on Applied and Computational Mathematics. Evolving interfaces in computational geometry, fluid mechanics, computer vision, and materials science. Cambridge: Cambridge University Press, 1999. xx+378.
- [Sid+08] K. Siddiqi, J. Zhang, D. Macrini, A. Shokoufandeh, S. Bouix, and S. Dickinson. “Retrieving articulated 3-D models using medial surfaces”. *Machine Vision and Applications* 19.4 (2008), pp. 261–275.

- 
- [Sri+09] A. Srivastava, C. Samir, S. H. Joshi, and M. Daoudi. “Elastic Shape Models for Face Analysis Using Curvilinear Coordinates”. *J. Math. Imaging. Vis.* 33 (2009), pp. 253–265.
- [Win+11] T. Windheuser, U. Schlickewei, F. R. Schmidt, and D. Cremers. “Geometrically consistent elastic matching of 3D shapes: A linear programming solution”. In: *International Conference on Computer Vision*. 2011, pp. 2134–2141.
- [Wir+11] B. Wirth, L. Bar, M. Rumpf, and G. Sapiro. “A Continuum Mechanical Approach to Geodesics in Shape Space”. *Int. J. Comput. Vis.* 93.3 (2011), pp. 293–318.





## Implicit Surface Matching with a Lower Semicontinuous Shell Energy

### Abstract

A shape sensitive, variational approach for the matching of surfaces considered as thin elastic shells is investigated. The elasticity functional to be minimized takes into account two different types of nonlinear energies: a membrane energy measuring the rate of tangential distortion when deforming the reference shell into the template shell, and a bending energy measuring the bending under the deformation in terms of the change of the shape operators from the undeformed into the deformed configuration. The variational method applies to surfaces described as level sets. It is mathematically well-posed and an existence proof of an optimal matching deformation is given. The variational model is implemented using a finite element discretization combined with a narrow band approach on an efficient hierarchical grid structure. For the optimization a regularized nonlinear conjugate gradient scheme and a cascadic multilevel strategy are used. The features of the proposed approach are studied for synthetic test cases and a collection of geometry processing applications.

### 3.1 Introduction

We present a variational model for the matching of surfaces implicitly represented as level sets. The approach is inspired by the mathematical theory of nonlinear elasticity of thin shells. The model consists in an energy functional, which is to be minimized among deformations of a computational domain in which two given surfaces are embedded. A minimizer of this functional is a deformation that closely maps one (reference) surface onto the other (template) surface. As the underlying model we consider the reference surface as a thin elastic shell, i.e., a layer of an elastic material embedded in a volume of another several orders of magnitude softer isotropic elastic material. Subject to matching forces the volume is deformed in such a way that the thin shell is mapped onto the template surface. The functional reflects desired phenomena like resistance to compression and expansion of the surface, resistance to bending, and rotational invariance, while solely involving the deformation and the Jacobian of the deformation. The model is formulated in terms of projected derivatives from the tangent space of the reference surface onto the expected tangent space of the template surface. Taking into account a suitable factorization of the natural pullback under a deformation of shape operators enables us to formulate a model with appropriate convexity properties. The actual surface matching constraint is handled through a penalty, allowing for efficient numerical computation.

Through arguments of compensated compactness, we are able to show weak lower semicontinuity of the energy and consequently existence of minimizing deformations. We present a numerical approach based on a multilinear finite element ansatz for the deformation implemented on adaptive octree grids. The resulting discrete energy is minimized in a multiscale fashion applying a regularized gradient descent.

In the conference article [Igl+13] (Chapter 2) a preliminary version of this approach was presented. For the functional in that paper lower semicontinuity could not be ensured for either the membrane or bending energies. This lack of lower semicontinuity manifests itself in applications, where compression of the surface is expected, and leads to undesired oscillations in almost-minimizing deformations, which we explore in the present work through explicit examples and computations. Additionally, to increase the efficiency the computational meshes are in the present paper adapted to the surfaces. Consequently the number of degrees of freedom scales asymptotically almost like that of a surface problem.

The main pillar of our modelling is the use of polyconvex energy densities, first introduced in [Bal77]. Energies of this type allow for geometric consistency properties like rotation invariance and the ability to measure area and volume changes. The core insight of this theory is that integrands consisting of convex functions of subdeterminants of the Jacobian give rise to integral functionals that are weakly lower semicontinuous in suitable Sobolev spaces. Indeed, this can be seen as an instance of compensated compactness [Mur87]. A generic polyconvex isotropic energy density of the type used in this work is

$$\alpha_p \|A\|^p + \beta_q \|\text{Cof } A\|^q + \Gamma(\det A), \quad (3.1.1)$$

for  $\text{Cof } A$  the cofactor matrix of  $A$ . Here, the coefficients and the function  $\Gamma$  are such that (3.1.1) attains its minimum for  $A \in \text{SO}(3)$ , indicating that rigid motions have minimal energy. Often in the modeling of nonlinear elasticity the condition

$$\lim_{\det A \rightarrow 0^+} \Gamma(A) = +\infty \quad (3.1.2)$$

is added, to reflect the non-interpenetration of matter [Bal81]. In our model we make use of densities both with and without this property.

**Related work.** Linear elasticity has been extensively used in computer vision and in graphics. Prominent applications are image registration [Mod04; KU03; RSW10; KFF06; KL10], optical flow extraction [KR05], and shape modeling [Fuc+09].

In recent years, theories of nonlinear elasticity have been applied in many computer vision and graphics applications such as mesh deformation [Cha+10], shape averaging [RW09], registration of medical images [BMR13]. The advantage of nonlinear models is that they allow for intuitive deformations when the displacements are large.

In this paper, we present a model for nonlinear elastic matching of thin shells. A finite element method for the discretization of bending energies of biological membranes has been introduced in [BNP10]. Their approach uses quadratic isoparametric finite elements to approximate the interface on which the gradient flow of an elastic energy of Helfrich type is considered. The papers [BPW13; BPW15] discuss accurate convex relaxation of higher order variational problems

on curves described as jump sets of functions of bounded variation. In particular, it enables the numerical treatment of elastic energies on such curves.

One challenge in polyhedral surface processing is to provide consistent notions of curvatures and second fundamental forms, i.e., notions that converge (in an appropriate topology or in a measure theoretic sense) to their smooth counterparts, given a smooth limit surface. One computationally popular model for discretizing the second fundamental form is Grinspun's et al. *discrete shells* model [Gri+03]. Another efficient, and robust method for nonlinear surface deformation and shape matching is PriMo [Bot+06]. This approach is based on replacing the triangles of a polyhedral surfaces by thin prisms. During a deformation, these prisms are required to stay rigid, while nonlinear elastic forces are acting between neighboring prisms to account for bending, twisting, and stretching of the surface. We refer to Botsch and Sorkine [BS08] for a discussion of pros and cons for various such methods.

The matching of surfaces with elastic energies has recently been studied in [Win+11]. Their energy contains a membrane energy depending on the Cauchy-Green strain tensor and a bending-type energy comparing the mean curvatures on the surfaces. The matching problem is formulated in terms of a binary linear program in the product space of sets of surface patches. For computations, a relaxation approach is used. A surface matching approach related to ours is presented in [Lit+05], where nonlinear elastic energies are used for matching parametrized surface patches. In comparison, our approach is non-parametric and allows surfaces of any topology.

In [Sri+09], face matching based on a matching of corresponding level set curves on the facial surfaces is investigated. To match pairs of curves an optimal deformation between them is computed using an elastic shape analysis of curves. Compared to our approach, this model does not take into account bending dissipation of the curves.

A method for matching and blending of curves represented by level sets has been presented in [MR12]. Thereby, a level set evolution generates an interpolating family of curves, where the associated propagation speed of the level sets depends on differences of level set curvatures. In this class of approaches, geometric evolution problems are formulated, whereas here we focus on variational models for matching deformations. Variational registration of implicit surfaces was also considered in [LL08], but only through volume elasticity, in contrast to our shell terms.

Our approach is inspired by the articles [DZ94; DZ95] in which surface PDE models are derived in terms of the signed distance function. Shape warping based on the framework of [DZ94] has been discussed from a geometric perspective in [CFK04].

**Outline.** The paper is organized as follows. In Section 2, we review the required preliminaries about distance functions and formulate the geometric non-distortion and matching conditions that inspire our model. In Section 3, we present the different contributions to our energy. Section 4 is devoted to proving the existence of minimizing deformations under suitable Dirichlet and Neumann boundary conditions. Furthermore, the strong convergence of solutions for vanishing matching penalty parameter is discussed and counterexamples showing the lack of lower semicontinuity of related simpler models are given. In Section 5 a numerical strategy for minimizing the energy on adaptive octree grids is presented. Finally, Section 6 contains a range of numerical examples demonstrating the behavior of solutions corresponding to our design criteria, and presents several potential applications.

**Some useful notation.** For later usage and the purpose of reference let us collect some useful notation, mostly introduced in detail in later sections:

- $|B|$  stands for the Lebesgue measure of  $B \subset \mathbb{R}^n$ , and  $\text{diam } B = \sup_{x,y \in B} |x - y|$  for its diameter.
- Generic matrices are denoted by  $A, B, M, N$ . We use  $\mathbb{1}$  for the identity matrix. The set of rotations is denoted by  $O(n)$  and  $SO(n)$  is the set of orientation-preserving rotations. The set of all symmetric and positive definite matrices is  $\text{SPD}(n)$ .
- Components of vectors are denoted with subindices. For  $v \in \mathbb{R}^n$ ,  $|v|$  denotes its Euclidean norm. The  $(n - 1)$ -dimensional sphere is  $\mathbb{S}^{n-1}$ . For a matrix  $M$ ,  $|M|$  is the Frobenius norm.
- For two column vectors  $v, w \in \mathbb{R}^n$ ,  $v \otimes w$  is the tensor product of  $v$  and  $w$ , that is, the square matrix  $vw^T$ . In particular, if  $|w| = 1$  we have the identity  $(v \otimes w)w = v$ .
- $P(e) = \mathbb{1} - e \otimes e$  is the projection onto vectors orthogonal to  $e \in \mathbb{S}^{n-1}$ .
- Deformations on  $\mathbb{R}^n$  are denoted by  $\phi$ , and deformations defined on a curve or surface  $\mathcal{M} \subset \mathbb{R}^n$  by  $\varphi$ . The identity deformation is  $\text{id}$ .
- $\Omega \subseteq \mathbb{R}^3$  denotes the computational domain. Every relevant deformation  $\phi$  maps  $\Omega$  into  $\mathbb{R}^n$ .  $\Omega$  has to contain all computationally relevant manifolds  $\mathcal{M}$ .  $\Omega$  has Lipschitz boundary, is open and bounded.
- We use the notation  $\partial_i$  for partial derivatives,  $\nabla$  for the gradient of a scalar function,  $\mathcal{D}$  for the Jacobian matrix of a vector function and  $\mathcal{D}^2$  for the Hessian matrix of a scalar function.
- $\mathcal{M}_1, \mathcal{M}_2$  are closed surfaces with  $C^{2,1}$  boundary. The inside and outside components being well defined by the Jordan-Brouwer separation theorem ([GP74], Chapter 2, Section 5). The signed distance function to  $\mathcal{M}_1, \mathcal{M}_2$  is denoted by  $\mathbf{d}_1, \mathbf{d}_2$ . The sign convention is that  $\mathbf{d}_i$  is negative on the inside of  $\mathcal{M}_i$ , so that  $\mathbf{d}_i(x) = -\text{dist}(x, \mathcal{M}_i)$  if  $x$  is in the inside component of  $\Omega \setminus \mathcal{M}_i$  and  $\mathbf{d}_i(x) = \text{dist}(x, \mathcal{M}_i)$  otherwise, where the distance functions  $\text{dist}(\cdot, \mathcal{M}_i)$ ,  $i = 1, 2$  are the unique viscosity solutions of  $1 - |\nabla \text{dist}(\cdot, \mathcal{M}_i)| = 0$  and  $\text{dist}(\cdot, \mathcal{M}_i) = 0$  on  $\mathcal{M}_i$ . The normal fields to the offsets of  $\mathcal{M}_i$  at a point  $x$  are denoted by  $\mathbf{n}_i(x) := \nabla \mathbf{d}_i(x)$ . A superscript next to  $\mathcal{M}_i$  ( $i = 1, 2$ ), as in  $\mathcal{M}_i^c$ , denotes that we are talking about a level set of  $\mathbf{d}_i$  with value different from zero, so that  $\mathcal{M}_i^c := \mathbf{d}_i^{-1}(c)$ .

$T_x \mathcal{M}_i^{\mathbf{d}_i(x)}$  denotes the tangent space to  $\mathcal{M}_i^{\mathbf{d}_i(x)}$  at  $x$ . The outwards normal to  $\mathcal{M}_i^{\mathbf{d}_i(x)}$  is given by  $\mathbf{n}_i(x)$ , and the set of points where  $\mathbf{d}_i$  is not differentiable is denoted by  $\text{sing } \mathbf{d}_i$ .

We use  $\mathcal{S}_i = \mathcal{D}^2 \mathbf{d}_i$  for the Hessian of  $\mathbf{d}_i$ , which coincides with an extended shape operator of  $\mathcal{M}_i$ .

- $\lambda, \mu$  are the Lamé coefficients of an isotropic material in linearized elasticity.
- $C^0(\Omega; \mathbb{R}^3)$  is the space of continuous functions from the domain  $\Omega$  to the range  $\mathbb{R}^3$ ,  $C^{k,\alpha}$  the Hölder spaces in which the  $k$ -th derivative is  $\alpha$ -Hölder continuous, including the Lipschitz case  $\alpha = 1$ . The range of the spaces is specified unless it is  $\mathbb{R}$ . Sobolev spaces are denoted by  $W^{1,p}$  and the closure of compactly supported smooth functions in them by  $W_0^{1,p}$ .

- The letter  $C$  is reserved for a generic positive constant that may have different values in each appearance. Sequence indexing is usually denoted by a superscript  $k$ , and limits by an overline, e.g.,  $\phi^k \rightarrow \overline{\phi}$ .

## 3.2 Deformation and matching of level set surfaces

We are given two compact, connected embedded surfaces  $\mathcal{M}_1, \mathcal{M}_2$  of class  $C^{2,1}$ , which are diffeomorphic to each other, and both of which are contained in a bounded Lipschitz domain  $\Omega \subset \mathbb{R}^3$ . In this section we deal with the tangential distortion and the change of the shape operator under a deformation  $\phi : \Omega \rightarrow \mathbb{R}^n$ .

For any  $c \in \mathbb{R}$ , we denote the  $c$ -offsets to the surface  $\mathcal{M}_i$  by  $\mathcal{M}_i^c := \{x \in \Omega \mid \mathbf{d}_i(x) = c\}$ . Furthermore, we define the singularity set  $\text{sing } \mathbf{d}_i$  as the set of points where  $\mathbf{d}_i$  is not twice differentiable. With the regularity of  $\mathcal{M}_i$  that we have assumed, it is well known (e.g., Theorem 1.1, Corollary 1.3 and Remark 1.4 of [LN05]) that  $\text{sing } \mathbf{d}_i$  has Lebesgue measure zero and  $\text{dist}(\mathcal{M}_i, \text{sing } \mathcal{M}_i) > 0$ .

The gradient of the signed distance function  $\nabla \mathbf{d}_i(x)$  is the outward-pointing unit normal  $\mathbf{n}_i(x)$  to  $\mathcal{M}_i^{\mathbf{d}_i(x)}$  at a point  $x$ . The tangent space to  $\mathcal{M}_i^{\mathbf{d}_i(x)}$  at  $x$ , denoted by  $T_x \mathcal{M}_i^{\mathbf{d}_i(x)}$ , consists of all vectors orthogonal to  $\mathbf{n}_i(x)$ . Then, the corresponding projection matrices onto the tangent spaces are defined by

$$\mathbf{P}_i(x) := \mathbf{P}(\mathbf{n}_i(x)) = \mathbb{1} - \mathbf{n}_i(x) \otimes \mathbf{n}_i(x).$$

Note that  $\mathcal{S}_i(x) := \mathcal{D}^2 \mathbf{d}_i(x) = \mathcal{D} \mathbf{n}_i(x) \mathbf{P}_i(x)$  is the shape operator of the immersed surface  $\mathcal{M}_i^{\mathbf{d}_i(x)}$  at a point  $x$ . In fact, from  $|\mathbf{n}_i(x)|^2 = 1$  we deduce by differentiation that  $\mathbf{n}_i^T(x) \mathcal{S}_i(x) = 0$ . This, together with the fact that  $\mathbf{n}_i \otimes \mathbf{n}_i$  is the projection onto the normal of the surface  $\mathcal{S}_i$  shows that

$$\mathbf{P}_i(x) \mathcal{D} \mathbf{n}_i(x) = \mathcal{D} \mathbf{n}_i(x).$$

With our choice of signs for  $\mathbf{d}_i$ , the symmetric matrices  $\mathcal{S}_i$  are positive definite for convex surfaces  $\mathcal{M}_i$ . Further information on tangential calculus for level set functions may be found in Chapter 9 of [DZ11].

### 3.2.1 Tangential derivative and area and length distortion

First, let us assume that  $\phi$  exactly maps  $\mathcal{M}_1^c$  onto  $\mathcal{M}_2^c$ , for all  $c > 0$ . Then,  $T_x \mathcal{M}_1^{\mathbf{d}_1(x)} = \text{im } \mathbf{P}_1(x)$  and  $T_{\phi(x)} \phi(\mathcal{M}_1^{\mathbf{d}_1(x)}) = T_{\phi(x)} \mathcal{M}_2^{\mathbf{d}_2(\phi(x))} = \text{im } \mathbf{P}_2(\phi(x))$  and we define the tangential derivative induced by the deformation  $\phi$  as

$$\mathcal{D}_{\text{tg}} \phi(x) := \mathbf{P}_2(\phi(x)) \mathcal{D} \phi(x) \mathbf{P}_1(x), \quad (3.2.1)$$

capturing the tangential variation of  $\phi(x)$  on  $\mathcal{M}_2$  along tangential directions on  $\mathcal{M}_1$ . In the variational model we consider below an energy term depending on  $\mathcal{D}_{\text{tg}} \phi(x)$  will reflect the tangential distortion of the deformation in the context of a matching of the two surfaces  $\mathcal{M}_1$  and  $\mathcal{M}_2$  even though  $\phi(\mathcal{M}_1)$  does not necessarily equal  $\mathcal{M}_2$ . Indeed, in the case  $\mathcal{M}_2 \neq \phi(\mathcal{M}_1)$  the variation along a tangent direction on  $\mathcal{M}_1$  is still projected via  $\mathcal{D}_{\text{tg}} \phi(x)$  onto the tangent space

$T_{\phi(x)}\mathcal{M}_2^{\mathbf{d}_2(\phi(x))}$  and not onto the tangent space of the deformed surface  $\phi(\mathcal{M}_1)$  (cf. Fig. 3.1). Therefore there may exist tangential directions  $v \in T_x\mathcal{M}_1^{\mathbf{d}_1(x)}$ , such that  $\mathcal{D}_{\text{tg}}\phi(x)v = 0$  even though  $\mathcal{D}\phi v \neq 0$ . Thus  $\mathcal{D}_{\text{tg}}\phi(x)$  can only be considered a measure of tangential distortion if  $\phi(\mathcal{M}_1)$  is sufficiently close to  $\mathcal{M}_2$  in the sense of closeness of tangent bundles.

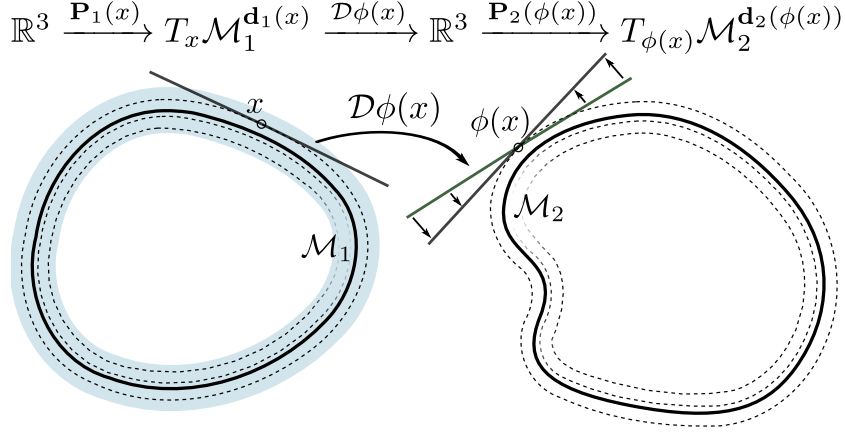


FIGURE 3.1: A sketch of the tangential derivative  $\mathcal{D}_{\text{tg}}\phi$  in the non-exact matching case with  $\phi(\mathcal{M}_1) \neq \mathcal{M}_2$ .

For a general deformation  $\psi : \mathbb{R}^n \rightarrow \mathbb{R}^n$  the Cauchy-Green strain tensor  $\mathcal{D}\psi^T \mathcal{D}\psi$  describes (up to first order) the deformation in a frame invariant (with respect to rigid body motions) way. In the case of deformation of surfaces and for a suitably extended deformation gradient  $\mathcal{D}_{\text{tg}}\phi + \mathbf{n}_2 \circ \phi \otimes \mathbf{n}_1$  we define the **extended Cauchy-Green strain tensor** of the tangential distortions:

$$(\mathcal{D}_{\text{tg}}\phi + (\mathbf{n}_2 \circ \phi) \otimes \mathbf{n}_1)^T (\mathcal{D}_{\text{tg}}\phi + (\mathbf{n}_2 \circ \phi) \otimes \mathbf{n}_1) = \mathcal{D}_{\text{tg}}\phi^T \mathcal{D}_{\text{tg}}\phi + \mathbf{n}_1 \otimes \mathbf{n}_1. \quad (3.2.2)$$

The term  $\mathbf{n}_2(\phi(x)) \otimes \mathbf{n}_1(x)$  is used to complement directions that are removed by the projections in the definition of the tangential distortion  $\mathcal{D}_{\text{tg}}\phi$  and can be seen to realize a nonlinear Kirchhoff-Love assumption [Cia00, Page 336], which postulates that lines normal to the middle surface of a shell remain normal after the deformation without stretching.

Next, we investigate the area and length distortion due to the tangential derivative  $\mathcal{D}_{\text{tg}}\phi$ . For a given vector  $e \in \mathbb{R}^n$  we denote by  $Q(e)$  any proper rotation such that  $Q(e) \cdot e_n = e$ , where  $e_n$  denotes the  $n$ -th element of the canonical basis of  $\mathbb{R}^n$ . Note that this condition does not specify a unique  $Q(e)$ . Then, for every  $B \in \mathbb{R}^{n \times n}$  satisfying  $w \in \ker B$  and  $\text{im } B \subseteq v^\perp$  for some unit vectors  $v, w \in \mathbb{S}^{n-1}$ , we have

$$Q(v)^T (B + v \otimes w) Q(w) = Q(v)^T B Q(w) + e_n \otimes e_n = \left( \begin{array}{c|c} \tilde{B} & 0 \\ \hline 0 & 1 \end{array} \right), \quad (3.2.3)$$

where  $\tilde{B}$  is the upper left  $(n-1) \times (n-1)$  submatrix of  $Q(w)^T B Q(v)$ . Obviously (3.2.3) implies

$$\begin{aligned} \det(B + v \otimes w) &= \det(\tilde{B}), \\ |B + v \otimes w|^2 &= \text{tr}((B + v \otimes w)^T (B + v \otimes w)) = 1 + |\tilde{B}|^2. \end{aligned}$$

Hence, for  $\phi(\mathcal{M}_1) = \mathcal{M}_2$  and  $v = n_2(\phi(x))$ ,  $w = n_1(x)$  the area distortion under the surface matching deformation  $\phi$  at some position  $x$  is described by  $\det(\mathcal{D}_{\text{tg}}\phi(x) + \mathbf{n}_2(\phi(x)) \otimes \mathbf{n}_1(x))$ , which equals the positive square root of the determinant of the above Cauchy-Green strain tensor  $\mathcal{D}_{\text{tg}}\phi^T \mathcal{D}_{\text{tg}}\phi + \mathbf{n}_1 \otimes \mathbf{n}_1$ . The squared tangential length distortion (in the sense of summing all squared distortions with respect to an orthogonal basis) is described by  $|\mathcal{D}_{\text{tg}}\phi(x) + \mathbf{n}_2(\phi(x)) \otimes \mathbf{n}_1(x)|^2$  and equals the trace of the Cauchy-Green strain tensor.

### 3.2.2 Surface bending and curvature mismatch

Now, we quantify the change of curvature directions and magnitudes under the deformation  $\phi$ . Our approach is motivated by models describing bending of elastic shells, because in our application the surfaces are considered as thin shells.

In order to quantify the changes of curvature we first assume that  $\phi(\mathcal{M}_1) = \mathcal{M}_2$ , and compute the difference of the pull back of the shape operator  $\mathcal{S}_2$  on  $\mathcal{M}_2$  onto  $\mathcal{M}_1$  under the deformation  $\phi$  and the shape operator  $\mathcal{S}_1$  on  $\mathcal{M}_1$ , which, for two arbitrary directions  $v, w \in \mathbb{R}^n$ , is given by

$$\mathcal{S}_2(\phi(x))\mathcal{D}\phi(x)v \cdot \mathcal{D}\phi(x)w - \mathcal{S}_1(x)v \cdot w = \left( \mathcal{D}\phi(x)^T \mathcal{S}_2(\phi(x))\mathcal{D}\phi(x) - \mathcal{S}_1(x) \right) v \cdot w.$$

If  $v, w$  are tangent vectors in  $T_x\mathcal{M}_1$ , this difference describes the **relative shape operator**.

We define the extended **relative shape operator**

$$\mathcal{S}_{\text{rel}}(x) := \mathcal{D}\phi(x)^T \mathcal{S}_2(\phi(x))\mathcal{D}\phi(x) - \mathcal{S}_1(x). \quad (3.2.4)$$

For  $n = 3$  when  $\phi$  is an isometric deformation between  $\mathcal{M}_1$  and  $\mathcal{M}_2$  (that is  $\mathcal{D}\phi(x)$  is an orthogonal mapping on  $T_x\mathcal{M}_1$  for all  $x \in \mathcal{M}_1$ )  $\mathcal{S}_{\text{rel}}$  appears in physical models for thin elastic shells in the context of the  $\Gamma$ -limit of 3D hyperelasticity [Fri+03]. Even though we do not necessarily expect our deformations to be tangentially isometric, we use this ansatz to compare curvatures of level sets in deformed and undeformed configuration, respectively. The following calculations shed some light on the properties of  $\mathcal{S}_{\text{rel}}$ :

$$\mathcal{D}^2(\mathbf{d}_2 \circ \phi)(x) = \mathcal{D}(\mathbf{n}_2(\phi(x))) \cdot \mathcal{D}\phi(x) = \mathcal{D}\phi(x)^T \mathcal{S}_2(\phi(x))\mathcal{D}\phi(x) + \sum_{k=1}^n (\mathbf{n}_2)_k^T \mathcal{D}^2\phi^k(x). \quad (3.2.5)$$

The assumption that  $\phi(\mathcal{M}_1) = \mathcal{M}_2$  can be rewritten as  $\mathbf{d}_2 \circ \phi(x) = 0$  for  $x \in \mathcal{M}_1$ . Let us assume that in addition  $\mathbf{d}_2 \circ \phi$  is a distance function (that is  $|\nabla(\mathbf{d}_2 \circ \phi)| = 1$ ), then  $\mathbf{d}_2 \circ \phi$  is again a distance function, and since  $\mathbf{d}_2 \circ \phi = 0$  it follows that the left hand side of (3.2.5) is the shape operator of the surface  $\mathcal{M}_1$ . The first term in the right hand side is the pullback of  $\mathcal{S}_2$ .

The second term measures the additional curvature induced by  $\phi$  that is observed on  $\mathcal{M}_2$ , but was not present in the preimage  $\phi^{-1}(\mathcal{M}_2) = \mathcal{M}_1$ .

Let us remark that the appearance of a second fundamental form is consistent with Koiter's nonlinear thin shell theory [Koi66], [Cia00, Section 11.1]. Regardless of whether  $\mathbf{d}_2 \circ \phi$  is a



distance function or not, (3.2.5) implies that

$$\begin{aligned} \mathcal{D}\phi(x)^T \mathcal{S}_2(\phi(x)) \mathcal{D}\phi(x) - \mathcal{S}_1(x) &= - \sum_{k=1}^n (\mathbf{n}_2)_k^T \mathcal{D}^2 \phi^k(x) + \mathcal{D}^2(\mathbf{d}_2 \circ \phi - \mathbf{d}_1)(x) \\ &= - \sum_{k=1}^n (\mathbf{n}_2)_k^T \mathcal{D}^2 \phi^k(x), \end{aligned} \quad (3.2.6)$$

in case  $\mathbf{d}_2 \circ \phi = \mathbf{d}_1$ .

In what follows, we will use the extended shape operator to derive a variational model for the mismatch of curvatures.

### 3.3 Energy functional

Given two surfaces  $\mathcal{M}_1$  and  $\mathcal{M}_2$  our ultimate goal is to describe best matching deformations  $\phi$ , which map  $\mathcal{M}_1$  onto  $\mathcal{M}_2$  as the minimizer of a suitable energy. Thereby, different energy terms will reflect a set of matching conditions for a volumetric deformation  $\phi : \Omega \rightarrow \mathbb{R}^3$  and without a hard constraint  $\phi(\mathcal{M}_1) = \mathcal{M}_2$ :

- A membrane deformation energy  $E_{\text{mem}}$  penalizes the tangential distortion measured through  $\mathcal{D}_{\text{tg}}\phi$ .
- A bending energy  $E_{\text{bend}}$  penalizes bending as reflected by the relative shape operator.
- A matching penalty  $E_{\text{match}}$  ensures a proper matching of the two surfaces  $\mathcal{M}_1$  onto  $\mathcal{M}_2$  via a narrow band approach.
- A volume energy  $E_{\text{vol}}$  enforces a regular deformation on the whole computational domain  $\Omega$ .

Our approach is based on level sets. Hence, we replace the integration over a single surface (i.e.,  $\mathcal{M}_1$ ) for the first three terms by a weighted integration over a narrow band of width  $\sigma$  with  $0 < \sigma < \text{dist}(\mathcal{M}_1, \text{sing } \mathbf{d}_1)$ . To this end we will make use of a cutoff function  $\eta_\sigma \in C_0^\infty(\mathbb{R})$  with  $\int_{\mathbb{R}} \eta_\sigma(t) dt = 1$  and  $\text{supp } \eta_\sigma = [-\sigma, \sigma]$ . In what follows we will discuss the four energy contributions separately.

#### 3.3.1 Tangential distortion energy

Picking up the insight gained in Section 3.2.1 we formulate the membrane energy in terms of the length and area change associated with the tangential distortion  $\mathcal{D}_{\text{tg}}\phi$ :

$$E_{\text{mem}}[\phi] = \delta \int_{\Omega} \eta_\sigma(\mathbf{d}_1(x)) W(\mathcal{D}_{\text{tg}}\phi(x) + \mathbf{n}_2(\phi(x)) \otimes \mathbf{n}_1(x)) dx, \quad (3.3.1)$$

where  $W$  is a nonnegative polyconvex energy density vanishing at  $\text{SO}(3)$ . The weight  $\delta$  reflects the proper scaling of the tangential distortion energy in case of a thin shell model with shell thickness  $\delta$ .



The energy (3.3.1) vanishes only on deformations  $\phi$  whose Jacobian matrix  $\mathcal{D}\phi(x)$  maps  $T\mathcal{M}_1^{\mathbf{d}_1(x)}$  isometrically onto  $T\mathcal{M}_2^{\mathbf{d}_2(\phi(x))}$  for every point  $x \in \text{supp } \eta_\sigma \circ \mathbf{d}_1$ . In consequence, both tangential expansion and compression are penalized.

Let us remark, that the extension  $\mathcal{D}_{\text{tg}}\phi(x) + \mathbf{n}_2(\phi(x)) \otimes \mathbf{n}_1(x)$  of the tangential derivative  $\mathcal{D}_{\text{tg}}\phi$  defined in (3.2.1) with rank  $n - 1$  can degenerate or be orientation-reversing depending on the local configuration of  $\mathcal{M}_1$  and  $\mathcal{M}_2$  at  $x$  (cf. Figure 3.2 for examples). Therefore, under the assumption  $\det \mathcal{D}\phi(x) > 0$  (which is in fact enforced almost everywhere by our volume regularization term (3.3.7) introduced below), the fact that  $W$  has a minimum only on  $\text{SO}(3)$  means that deformations whose extended tangential derivative may be locally isometric (that is,  $\mathcal{D}_{\text{tg}}\phi(x) + \mathbf{n}_2(\phi(x)) \otimes \mathbf{n}_1(x) \in \text{O}(3)$ ), but for which  $\mathbf{n}_1(x) \cdot \mathbf{n}_2(\phi(x)) \leq 0$ , are also penalized. This does not bring any negative consequences, since we aim for deformations matching the inside and outside of the surfaces correctly.

In fact, any density which is minimal precisely at  $\text{O}(3)$  can not lead to lower a semicontinuous functional. To see this, recall that a necessary condition for lower semicontinuity of the energy is convexity of the density along lines directed by rank-one matrices ([Dac08, Theorems 5.3 and 8.1]). But a density minimized only on  $\text{O}(3)$  can not be convex along such a line, since  $\text{O}(3)$  may be written as

$$\text{O}(3) = \text{SO}(3) \cup \text{DSO}(3),$$

where  $D := \text{diag}(-1, 1, 1)$ , and these components may be joined through such rank-one lines. Indeed, it is enough to choose  $\mathbb{1} \in \text{SO}(3)$  and  $T \in \text{DSO}(3)$  to get  $\mathbb{1} - D = \text{diag}(2, 0, \dots, 0)$ , which has rank one. A similar line of reasoning is exploited in Example 3.4.8 of next section.

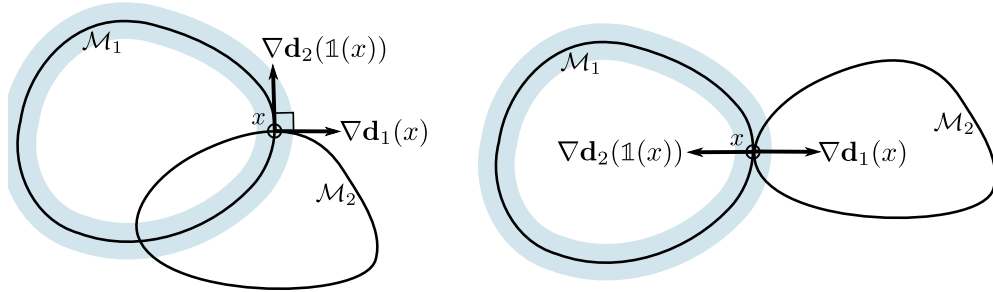


FIGURE 3.2: Configurations in which for the (obviously isometric) identity deformation we have  $\det(\mathcal{D}_{\text{tg}}\mathbb{1}(x) + \mathbf{n}_2(\mathbb{1}x) \otimes \mathbf{n}_1(x)) = 0$  (left) and  $\det(\mathcal{D}_{\text{tg}}\mathbb{1}(x) + \mathbf{n}_2(\mathbb{1}x) \otimes \mathbf{n}_1(x)) < 0$  (right) and thus the extended tangential derivative degenerates or reverses orientation.

Furthermore, the energy density  $W$  should not satisfy  $W(B) \rightarrow \infty$  for  $\det B \rightarrow 0$ . A straightforward modification of the arguments of Ciarlet and Geymonat ([CG82], [Cia88] Theorem 4.10-2) leads to an isotropic, frame-indifferent integrand  $W$  without singularities, and with a Hessian for  $B = \mathbb{1}$  which matches the quadratic energy integrand of the Lamé-Navier model of linearized elasticity. Frame indifference refers to the property  $W(QA) = W(A)$ , and isotropy to  $W(AQ) = W(A)$ , both for any  $A \in \mathbb{R}^{n \times n}$ ,  $Q \in \text{SO}(n)$ . Observe that both of these properties are needed to ensure invariance with respect to the possible tangent planes to  $\mathcal{M}_1$  and  $\mathcal{M}_2$  (cf. (3.2.3)). With given Lamé coefficients  $\lambda, \mu > 0$ , we select the energy

$$W(A) = \frac{\mu}{2}|A|^2 + \frac{\lambda}{4}(\det A)^2 + \left(\mu + \frac{\lambda}{2}\right)e^{-(\det A - 1)} - \frac{(n+2)\mu}{2} - \frac{3\lambda}{4}.$$

This density fits into the notation of (3.1.1), if we choose  $p = q = 2$  and  $\Gamma(t) = ct^2 + de^{-(t-1)}$ .

### 3.3.2 Bending energy

Now, we discuss a variational formulation penalizing deviation from the curvature matching condition  $\mathcal{D}\phi(x)^T \mathcal{S}_2(\phi(x)) \mathcal{D}\phi(x) = \mathcal{S}_1(x)$ , which is equivalent to a vanishing relative shape operator (cf. (3.2.4)), where  $\mathcal{S}_i = \mathcal{D}\mathbf{n}_i \mathbf{P}_i = \mathbf{P}_i \mathcal{D}^2 \mathbf{d}_i \mathbf{P}_i$  for  $i = 1, 2$  are the shape operators on the surfaces  $\mathcal{M}_1$  and  $\mathcal{M}_2$ , respectively. At first sight, it appears natural to formulate a quadratic penalization and to define a bending energy

$$\tilde{E}_{\text{bend}}[\phi] = \int_{\Omega} \eta_{\sigma}(\mathbf{d}_1(x)) |\mathcal{D}\phi(x)^T \mathcal{S}_2(\phi(x)) \mathcal{D}\phi(x) - \mathcal{S}_1(x)|^2 dx.$$

The weight  $\delta^3$  reflects the scaling of the bending energy for thin shells of thickness  $\delta$ . However, this energy is in general not weakly lower semicontinuous. Indeed, already in the simple case  $\mathcal{S}_1 \equiv \mathcal{S}_2 \equiv \mathbb{1}$ , the integrand reduces to  $|\mathcal{D}\phi^T \mathcal{D}\phi - \mathbb{1}|^2$  for which a lack of quasiconvexity is well known [LDR95b].

Thus, we are asking for an alternative lower semicontinuous energy functional which gives preference to deformations  $\phi$  for which  $\mathcal{D}\phi^T (\mathcal{S}_2 \circ \phi) \mathcal{D}\phi$  is close to  $\mathcal{S}_1$ . We show that this can be achieved with the extended shape operators  $\mathcal{S}_i^{\text{ext}} = \mathbf{P}_i \mathcal{D}^2 \mathbf{d}_i \mathbf{P}_i + \mathbf{n}_i \otimes \mathbf{n}_i$  for  $i = 1, 2$  and factorization. For proving this we make use of the following lemma.

**Lemma 3.3.1** (modified curvature matching condition). Assume that  $M, N$  are two symmetric, positive definite matrices satisfying

$$M = \mathbf{P}_1 M \mathbf{P}_1 + \mathbf{n}_1 \otimes \mathbf{n}_1 \text{ and } N = \mathbf{P}_2 N \mathbf{P}_2 + \mathbf{n}_2 \otimes \mathbf{n}_2.$$

Moreover, assume that  $A \in \mathbb{R}^{n \times n}$  satisfies

$$A \mathbf{P}_1 = \mathbf{P}_2 A,$$

then the following statements are equivalent:

$$A^T \mathbf{P}_2 N \mathbf{P}_2 A = \mathbf{P}_1 M \mathbf{P}_1 \tag{3.3.2}$$

and

$$\Lambda[M, N, A] = \mathbf{P}_2 N^{\frac{1}{2}} \mathbf{P}_2 A \mathbf{P}_1 M^{-\frac{1}{2}} \mathbf{P}_1 + \mathbf{n}_2 \otimes \mathbf{n}_1 \in \mathcal{O}(n). \tag{3.3.3}$$

*Proof.* By definition, the matrix  $\Lambda[M, N, A]$  is orthogonal if  $\Lambda[M, N, A]^T \Lambda[M, N, A] = \mathbb{1}$ . Therefore, if (3.3.3) holds, then

$$\begin{aligned} \mathbb{1} &= (\mathbf{P}_2 N^{\frac{1}{2}} \mathbf{P}_2 A \mathbf{P}_1 M^{-\frac{1}{2}} \mathbf{P}_1 + \mathbf{n}_2 \mathbf{n}_1^T)^T (\mathbf{P}_2 N^{\frac{1}{2}} \mathbf{P}_2 A \mathbf{P}_1 M^{-\frac{1}{2}} \mathbf{P}_1 + \mathbf{n}_2 \mathbf{n}_1^T) \\ &= \mathbf{P}_1 M^{-\frac{1}{2}} \mathbf{P}_1 A^T \mathbf{P}_2 N^{\frac{1}{2}} \mathbf{P}_2 \mathbf{P}_2 N^{\frac{1}{2}} \mathbf{P}_2 A \mathbf{P}_1 M^{-\frac{1}{2}} \mathbf{P}_1 + \mathbf{n}_1 \mathbf{n}_2^T \mathbf{n}_2 \mathbf{n}_1^T \\ &= \mathbf{P}_1 M^{-\frac{1}{2}} A^T \mathbf{P}_2 (\mathbf{P}_2 N^{\frac{1}{2}} \mathbf{P}_2)^2 \mathbf{P}_2 A M^{-\frac{1}{2}} \mathbf{P}_1 + \mathbf{n}_1 \mathbf{n}_1^T. \end{aligned}$$

If we multiply this equation from left and right by  $P_1 M^{\frac{1}{2}} P_1$  and take into account that  $(P_2 N^{\frac{1}{2}} P_2)^2 = P_2 N P_2$  and  $(P_1 M^{\frac{1}{2}} P_1)^2 = P_1 M P_1$  we see that this is equivalent to

$$P_1 A^T P_2 N P_2 A P_1 = P_1 M P_1.$$

Applying that  $A P_1 = P_2 A$  we finally achieve at the equivalent condition

$$A^T P_2 N P_2 A = P_1 M P_1.$$

The proof of the converse follows the same steps in opposite direction.  $\square$

If the assumptions of this lemma apply to  $M = \mathcal{S}_1^{ext}(x)$ ,  $N = \mathcal{S}_2^{ext}(y)$ , and  $A = \mathcal{D}\phi(x)$  with  $y = \phi(x)$ , then the curvature matching condition

$$(\mathcal{D}\phi(x))^T P_2(y) \mathcal{S}_2^{ext}(y) P_2(y) \mathcal{D}\phi(x) = P_1(x) \mathcal{S}_1^{ext}(x) P_1(x) \quad (3.3.4)$$

is equivalent to  $\Lambda(\mathcal{S}_1^{ext}(x), \mathcal{S}_2^{ext}(\phi(x)), \mathcal{D}\phi(x)) \in \mathcal{O}(n)$  and a lower semicontinuous energy functional penalizing deviations of  $\Lambda(\mathcal{S}_1^{ext}(x), \mathcal{S}_2^{ext}(\phi(x)), \mathcal{D}\phi(x))$  from  $\mathcal{O}(n)$  would be a proper choice for realizing curvature matching. Unfortunately, the positive definiteness assumption of Lemma 3.3.1 is not fulfilled if principal curvatures of  $\mathcal{M}_1$  or  $\mathcal{M}_2$  are negative. Hence, we are replacing the extended shape operator matrices  $\mathcal{S}_i^{ext}$  by symmetric and positive definite curvature classification matrices  $C_i = \mathcal{C}(\mathcal{S}_i^{ext})$ ,  $i = 1, 2$ , respectively.

We have experimented with two different choices for  $\mathcal{C}$ :

- A simple choice is  $\mathcal{C}(\mathcal{S}_i^{ext}) = \mathcal{S}_i^{ext} + \mu \mathbb{1}$ , where  $-\mu$  is a strict lower bound of the principal curvatures. But, in applications surfaces are frequently characterized by strong creases or rather sharp edges leading to very large  $\mu$ . As a consequence the relative difference of the eigenvalues is significantly reduces when dealing with the resulting curvature classification matrices. Thus, the variational approach is less sensitive to different principal curvatures of the input surfaces.
- Another option is to use a truncation of the absolute value function for the eigenvalues of symmetric matrices. For a symmetric matrix  $B \in \mathbb{R}^{n,n}$  with eigenvalues  $\lambda_1, \dots, \lambda_n$  and a diagonalization  $B = Q^T \text{diag}(\lambda_1, \dots, \lambda_n) Q$  we use the classification operator

$$\mathcal{C}(B) = Q^T \text{diag}(|\lambda_1|_\tau, \dots, |\lambda_n|_\tau) Q,$$

where  $|\lambda|_\tau = \max\{|\lambda|, \tau\}$  for some  $\tau > 0$ . This approach properly represents the exact shape operator matching objective in case of principal curvatures of equal sign and absolute value larger than  $\tau$ . A disadvantage of this construction is that it is not able to force the deformation to correctly match curvature directions on the surface with the same absolute value of the principal curvatures but with different signs. In the applications the ansatz performs well in particular in regions of edges and creases (see Section 3.6).

Like for the membrane energy (3.3.1), if  $\mathcal{D}\phi(x)$  is ensured to be orientation-preserving ( $\det \mathcal{D}\phi > 0$ ) and  $\mathbf{n}_1 \cdot (\mathbf{n}_2 \circ \phi) > 0$  (cf. Figure 3.2), the curvature matching condition is equivalent to

$$\Lambda(\mathcal{C}(\mathcal{S}_1^{ext}(x)), \mathcal{C}(\mathcal{S}_2^{ext}(\phi(x))), \mathcal{D}\phi(x)) \in \text{SO}(n).$$

Based on these considerations, a suitable choice for the bending energy is

$$E_{\text{bend}}[\phi] = \delta^3 \int_{\Omega} \eta_{\sigma}(\mathbf{d}_1(x)) W(\Lambda(\mathcal{C}(\mathcal{S}_1^{\text{ext}}(x)), \mathcal{C}(\mathcal{S}_2^{\text{ext}}(\phi(x))), \mathcal{D}\phi(x))) \, dx, \quad (3.3.5)$$

where  $W$  can be chosen as the same polyconvex density already used for  $E_{\text{mem}}$ .

### 3.3.3 Mismatch penalty and volumetric regularization energies

So far, we have defined tangential membrane and bending energies which quantify the appropriateness of deformations  $\phi : \Omega \rightarrow \mathbb{R}^n$  in a narrow band around the surface  $\mathcal{M}_1$ . In the derivation of these energies we assumed the constraint  $\phi(\mathcal{M}_1) = \mathcal{M}_2$ .

However, such a constraint would be very hard to enforce numerically. Thus we use a weaker mismatch penalty instead:

$$E_{\text{match}}[\phi] = \frac{1}{\nu} \int_{\Omega} (\eta_{\sigma} \circ \mathbf{d}_1) |\mathbf{d}_2 \circ \phi - \mathbf{d}_1|^2 \, dx, \quad (3.3.6)$$

where  $1/\nu$  is a penalization parameter.

Moreover, we aim for a regular deformation on the whole computational domain  $\Omega$  which is globally injective. This, in particular, prevents from self-intersections of the deformed surface  $\phi(\mathcal{M}_1)$ . To achieve this we introduce the following volume regularization term based on a polyconvex density  $\hat{W}$  that enforces orientation preservation

$$E_{\text{vol}}[\phi] = \int_{\Omega} \hat{W}(\mathcal{D}\phi, \text{Cof } \mathcal{D}\phi, \det \mathcal{D}\phi) \, dx \text{ with} \quad (3.3.7)$$

$$\hat{W}(\mathcal{D}\phi, \text{Cof } \mathcal{D}\phi, \det \mathcal{D}\phi) = \alpha_p |\mathcal{D}\phi|^p + \beta_q |\text{Cof } \mathcal{D}\phi|^q + \gamma_s (\det \mathcal{D}\phi)^{-s},$$

with  $p > 3$ ,  $q > 3$ ,  $s > 2q/(q-3)$ , and with  $\alpha_p, \beta_q, \gamma_s > 0$  ensuring that the density  $\hat{W}$  has a unique minimum when  $\mathcal{D}\phi^T \mathcal{D}\phi = \mathbf{1}$ . As mentioned in the introduction, such an energy is weakly lower semicontinuous in  $W^{1,p}(\Omega; \mathbb{R}^3)$  when restricted to deformations whose Jacobian determinant is positive almost everywhere, and this condition is closed under weak convergence.

### 3.3.4 Total energy

Summing the above terms, our energy for shape-aware level set matching reads

$$E_{\nu}[\phi] = E_{\text{match}}[\phi] + E_{\text{mem}}[\phi] + E_{\text{bend}}[\phi] + E_{\text{vol}}[\phi], \quad (3.3.8)$$

where the different terms depend on the fixed input geometries  $\mathcal{M}_1$  and  $\mathcal{M}_2$  through  $\mathbf{d}_1$  and  $\mathbf{d}_2$ . We keep the dependence on  $\nu$  explicit in our notation  $E_{\nu}$ , since it plays an important role in our analysis.

### 3.4 Existence of optimal matching deformations

First we prove the following weak continuity lemma, which is a generalization of the classical result given in [Mur87, Theorem 4.1]. Here the coefficients may depend on the deformed configuration.

**Lemma 3.4.1.** Let  $\phi^k \rightharpoonup \phi \in W^{1,p}(\Omega; \mathbb{R}^n)$  and  $p > n$ . Moreover, let  $V_i \in C^0(\overline{\Omega} \times \mathbb{R}^n; \mathbb{S}^{n-1})$ ,  $i = 1, 2$  and we denote

$$\mathbf{n}_i^k(\cdot) := V_i(\cdot, \phi^k(\cdot)) \text{ and } \mathbf{n}_i := V_i(\cdot, \phi(\cdot)), \quad i = 1, 2.$$

Then

$$\det(\mathbf{P}(\mathbf{n}_2^k) \mathcal{D}\phi^k \mathbf{P}(\mathbf{n}_1^k) + \mathbf{n}_2^k \otimes \mathbf{n}_1^k) \xrightarrow{L^{\frac{p}{n}}} \det(\mathbf{P}(\mathbf{n}_2) \mathcal{D}\phi \mathbf{P}(\mathbf{n}_1) + \mathbf{n}_2 \otimes \mathbf{n}_1). \quad (3.4.1)$$

Moreover, for every  $M_i, i = 1, 2$  with  $M_1^{-\frac{1}{2}} \in C^0(\overline{\Omega} \times \mathbb{R}^n; \mathbb{R}^{n \times n})$  and  $M_2^{\frac{1}{2}} \in C^0(\overline{\Omega} \times \mathbb{R}^n; \mathbb{R}^{n \times n})$  and the corresponding compositions

$$M_i^k(\cdot) := M_i(\cdot, \phi^k(\cdot)) \text{ and } \overline{M}_i := M_i(\cdot, \phi(\cdot))$$

we have

$$\begin{aligned} \det \Lambda(M_1^k, M_2^k, \mathcal{D}\phi_k) &= \det(\mathbf{P}(\mathbf{n}_2^k)(M_2^k)^{\frac{1}{2}} \mathbf{P}(\mathbf{n}_2^k) \mathcal{D}\phi^k \mathbf{P}(\mathbf{n}_1^k)(M_1^k)^{-\frac{1}{2}} \mathbf{P}(\mathbf{n}_1^k) + \mathbf{n}_2^k \otimes \mathbf{n}_1^k) \\ &\xrightarrow{L^{\frac{p}{n}}} \det(\mathbf{P}(\mathbf{n}_2)(\overline{M}_2)^{\frac{1}{2}} \mathbf{P}(\mathbf{n}_2) \mathcal{D}\phi \mathbf{P}(\mathbf{n}_1)(\overline{M}_1)^{-\frac{1}{2}} \mathbf{P}(\mathbf{n}_1) + \mathbf{n}_2 \otimes \mathbf{n}_1) = \det \Lambda(\overline{M}_1, \overline{M}_2, \mathcal{D}\phi). \end{aligned} \quad (3.4.2)$$

*Proof.* To prove (3.4.1) let  $\zeta \in L^{\frac{p}{p-n}}(\Omega)$ . We show that

$$I^k := \int_{\Omega} \zeta \det(\mathbf{P}(\mathbf{n}_2^k) \mathcal{D}\phi^k \mathbf{P}(\mathbf{n}_1^k) + \mathbf{n}_2^k \otimes \mathbf{n}_1^k) dx \rightarrow I := \int_{\Omega} \zeta \det(\mathbf{P}(\mathbf{n}_2) \mathcal{D}\phi \mathbf{P}(\mathbf{n}_1) + \mathbf{n}_2 \otimes \mathbf{n}_1) dx.$$

Moreover, we denote

$$\overline{I}^k := \int_{\Omega} \zeta \det(\mathbf{P}(\mathbf{n}_2) \mathcal{D}\phi^k \mathbf{P}(\mathbf{n}_1) + \mathbf{n}_2 \otimes \mathbf{n}_1) dx.$$

Using the inequality (cf. [Fri82, Theorem 4.7])

$$|\det A - \det B| \leq C|A - B| \max(|A|, |B|)^{n-1}$$

and Hölder's inequality it follows that

$$\begin{aligned} |I^k - \overline{I}^k| &\leq C \int_{\Omega} |\zeta| \left| \mathbf{P}(\mathbf{n}_2^k) \mathcal{D}\phi^k \mathbf{P}(\mathbf{n}_1^k) - \mathbf{P}(\mathbf{n}_2) \mathcal{D}\phi^k \mathbf{P}(\mathbf{n}_1) + \mathbf{n}_2^k \otimes \mathbf{n}_1^k - \mathbf{n}_2 \otimes \mathbf{n}_1 \right| \\ &\quad \cdot \max \left( |\mathbf{P}(\mathbf{n}_2^k) \mathcal{D}\phi^k \mathbf{P}(\mathbf{n}_1^k) + \mathbf{n}_2^k \otimes \mathbf{n}_1^k|, |\mathbf{P}(\mathbf{n}_2) \mathcal{D}\phi^k \mathbf{P}(\mathbf{n}_1) + \mathbf{n}_2 \otimes \mathbf{n}_1| \right)^{n-1} dx \\ &\leq C \|\zeta\|_{L^{\frac{p}{p-n}}} \left\| |\mathcal{D}\phi^k|^{n-1} + 1 \right\|_{L^{\frac{p}{n-1}}} \\ &\quad \cdot \left\| \mathbf{P}(\mathbf{n}_2^k) \mathcal{D}\phi^k \mathbf{P}(\mathbf{n}_1^k) - \mathbf{P}(\mathbf{n}_2) \mathcal{D}\phi^k \mathbf{P}(\mathbf{n}_1) + \mathbf{n}_2^k \otimes \mathbf{n}_1^k - \mathbf{n}_2 \otimes \mathbf{n}_1 \right\|_{L^p} \end{aligned}$$

$$\begin{aligned}
&\leq C \|\zeta\|_{L^{\frac{p}{p-n}}} \left( \|\mathcal{D}\phi^k\|_{L^p}^{n-1} + 1 \right) \\
&\quad \cdot \left[ \|\mathcal{D}\phi^k\|_{L^p} \left( \|\mathbf{P}(\mathbf{n}_2^k)\|_{L^\infty} \|\mathbf{P}(\mathbf{n}_1^k) - \mathbf{P}(\mathbf{n}_1)\|_{L^\infty} + \|\mathbf{P}(\mathbf{n}_1)\|_{L^\infty} \|\mathbf{P}(\mathbf{n}_2^k) - \mathbf{P}(\mathbf{n}_2)\|_{L^\infty} \right) \right. \\
&\quad \left. + \left( \|\mathbf{n}_1^k - \mathbf{n}_1\|_{L^\infty} + \|\mathbf{n}_2^k - \mathbf{n}_2\|_{L^\infty} \right) \right],
\end{aligned}$$

Here, we have used that

$$|\mathbf{P}(\mathbf{n}_2)\mathcal{D}\phi^k\mathbf{P}(\mathbf{n}_1) + \mathbf{n}_2 \otimes \mathbf{n}_1|^{n-1} \leq (|\mathcal{D}\phi^k| + 1)^{n-1} \leq C(|\mathcal{D}\phi^k|^{n-1} + 1).$$

By the Rellich-Kondrakov embedding theorem ([AF03], Theorem 6.3 III) there exist subsequences of  $\mathbf{n}_i^k$ ,  $i = 1, 2$ , which for simplicity of notation are again denoted by  $\mathbf{n}_i^k$ ,  $i = 1, 2$ , that converge uniformly to  $\mathbf{n}_i$ ,  $i = 1, 2$ , respectively. Taking into account the Lipschitz continuity estimate

$$|\mathbf{P}(e) - \mathbf{P}(f)| = |(e - f) \otimes e + f \otimes (e - f)| \leq 2\sqrt{n}|e - f|$$

and that  $\mathbf{n}_i^k \rightarrow \mathbf{n}_i$ ,  $i = 1, 2$  in  $L^\infty$  we obtain  $|I^k - \bar{I}^k| \rightarrow 0$  for  $k \rightarrow \infty$ .

Next, we replace  $\mathbf{n}_i$ ,  $i = 1, 2$  in  $\bar{I}^k$  by a piecewise constant approximation on a grid superimposed to the computational domain  $\Omega$ . Explicitly, we consider the finitely many non empty intersection  $\omega_\delta^z = \delta(z + [0, 1]^n) \cap \Omega$  of cubical cells with  $\Omega$  for  $z \in \mathbb{Z}^n$  and define

$$\bar{I}_\delta^k := \sum_{z \in \mathbb{Z}^n} \int_{\omega_\delta^z} \zeta \det(\mathbf{P}(\mathbf{n}_2(z_\delta))\mathcal{D}\phi^k\mathbf{P}(\mathbf{n}_1(z_\delta)) + \mathbf{n}_2(z_\delta) \otimes \mathbf{n}_1(z_\delta)) dx,$$

where  $z_\delta$  is any point in  $\bar{\Omega} \cap \omega_\delta^z$  if this set is nonempty. Using analogous estimates as above we obtain

$$\begin{aligned}
|\bar{I}_\delta^k - \bar{I}^k| &\leq C \|\zeta\|_{L^{\frac{p}{p-n}}} \left( \|\mathcal{D}\phi^k\|_{L^p}^{n-1} + 1 \right) \\
&\quad \cdot \left[ \|\mathcal{D}\phi^k\|_{L^p} \left( \|\mathbf{P}(\mathbf{n}_{1,\delta})\|_{L^\infty} \|\mathbf{P}(\mathbf{n}_{2,\delta}) - \mathbf{P}(\mathbf{n}_2)\|_{L^\infty} + \|\mathbf{P}(\mathbf{n}_1)\|_{L^\infty} \|\mathbf{P}(\mathbf{n}_{1,\delta}) - \mathbf{P}(\mathbf{n}_1)\|_{L^\infty} \right) \right. \\
&\quad \left. + \left( \|\mathbf{n}_{2,\delta} - \mathbf{n}_2\|_{L^\infty} + \|\mathbf{n}_{1,\delta} - \mathbf{n}_1\|_{L^\infty} \right) \right],
\end{aligned}$$

where  $\mathbf{n}_{1,\delta}$  and  $\mathbf{n}_{2,\delta}$  are piecewise constant functions in  $L^\infty$  with  $\mathbf{n}_{1,\delta}|_{\omega_\delta^z} = \mathbf{n}_1(z_\delta)$  and  $\mathbf{n}_{2,\delta}|_{\omega_\delta^z} = \mathbf{n}_2(z_\delta)$ , respectively.

Using the uniform continuity of  $\mathbf{n}_2$  and  $\mathbf{n}_1$  on  $\bar{\Omega}$  we obtain that  $|\bar{I}_\delta^k - \bar{I}^k| \leq \beta(\delta)$  for a monotonically increasing continuous function  $\beta : \mathbb{R}_0^+ \rightarrow \mathbb{R}$  with  $\beta(0) = 0$ . In particular the convergence is uniform with respect to  $k$ . The same argument applies for the difference of  $I$  and

$$\bar{I}_\delta := \sum_{z \in \mathbb{Z}^n} \int_{\omega_\delta^z} \zeta \det(\mathbf{P}(\mathbf{n}_2(z_\delta))\mathcal{D}\phi\mathbf{P}(\mathbf{n}_1(z_\delta)) + \mathbf{n}_2(z_\delta) \otimes \mathbf{n}_1(z_\delta)) dx$$

and we get  $|\bar{I}_\delta - I| < C\beta(\delta)$ . Using (3.2.3) it follows that

$$Q(\mathbf{n}_1(z_\delta))^T (\mathbf{P}(\mathbf{n}_2(z_\delta))A\mathbf{P}(\mathbf{n}_1(z_\delta)) + \mathbf{n}_1(z_\delta) \otimes \mathbf{n}_2(z_\delta)) Q(\mathbf{n}_2(z_\delta)) = \left( \begin{array}{c|c} \tilde{A} & 0 \\ \hline 0 & 1 \end{array} \right).$$

Thus  $\det(\mathbf{P}(\mathbf{n}_2(z_\delta))A\mathbf{P}(\mathbf{n}_1(z_\delta)) + \mathbf{n}_2(z_\delta) \otimes \mathbf{n}_1(z_\delta)) = \det(\tilde{A})$  represents an  $(n-1) \times (n-1)$  minor of the linear mapping corresponding to the matrix  $A$  with respect to different orthogonal basis in preimage space (associated with  $\mathbf{P}(\mathbf{n}_1(z_\delta))$  and  $\mathbf{n}_1(z_\delta)$ ) and the image space (associated with  $\mathbf{P}(\mathbf{n}_2(z_\delta))$  and  $\mathbf{n}_2(z_\delta)$ ). Indeed, for each of the terms in  $\bar{I}_\delta^k$ , denoting  $Q_i := Q(\mathbf{n}_i(z_\delta))$  we have

$$\begin{aligned}
& \int_{\omega_\delta^z} \zeta(x) \det(\mathbf{P}(\mathbf{n}_2(z_\delta))\mathcal{D}\phi^k(x)\mathbf{P}(\mathbf{n}_1(z_\delta)) + \mathbf{n}_2(z_\delta) \otimes \mathbf{n}_1(z_\delta)) dx \\
&= \int_{\omega_\delta^z} \zeta(x) \det(Q_2^T(\mathbf{P}(\mathbf{n}_2(z_\delta))\mathcal{D}\phi^k(x)\mathbf{P}(\mathbf{n}_1(z_\delta)) + \mathbf{n}_2(z_\delta) \otimes \mathbf{n}_1(z_\delta))Q_1) dx \\
&= \int_{\omega_\delta^z} \zeta(x) \det(Q_2^T\mathbf{P}(\mathbf{n}_2(z_\delta))Q_2Q_2^T\mathcal{D}\phi^k(x)Q_1Q_1^T\mathbf{P}(\mathbf{n}_1(z_\delta))Q_1 + e_n \otimes e_n) dx \\
&= \int_{\omega_\delta^z} \zeta(x) \det(\mathbf{P}(e_n)Q_2^T\mathcal{D}\phi^k(x)Q_1\mathbf{P}(e_n) + e_n \otimes e_n) dx \\
&= \int_{Q_1^T\omega_\delta^z} \zeta(Q_1y) \det(\mathbf{P}(e_n)\mathcal{D}(Q_2^T \circ \phi^k \circ Q_1)(y)\mathbf{P}(e_n) + e_n \otimes e_n) dy \\
&= \int_{Q_1^T\omega_\delta^z} \zeta(Q_1y) \text{Cof}_{nn}(\mathcal{D}(Q_2^T \circ \phi^k \circ Q_1)(y)) dy,
\end{aligned}$$

where we have used the orthogonal change of variables  $y = Q_1^T x$  and  $\text{Cof}_{nn}$  denotes the minor obtained by erasing the last column and the last row. This change of orthogonal coordinates is fixed on each cell  $\omega_\delta^z$ . Since for each  $\delta$  the domain  $\Omega$  is covered by finitely many cells  $\omega_\delta^z$ , using the above computation and standard weak continuity results [Dac08, Theorem 8.20] for determinants of minors of the Jacobian we obtain that  $\bar{I}_\delta^k \rightarrow \bar{I}_\delta$  for  $k \rightarrow \infty$ . Finally, for given  $\epsilon$  we first choose  $\delta$  small enough to ensure that  $|\bar{I}_\delta - I| + |\bar{I}_\delta^k - \bar{I}_\delta| \leq \frac{\epsilon}{2}$ . Then we choose  $k$  large enough to ensure that  $|I^k - \bar{I}_\delta^k| + |\bar{I}_\delta^k - \bar{I}_\delta| \leq \frac{\epsilon}{2}$ . This proves that a subsequence of  $I^k$  converges to  $I$  for  $k \rightarrow \infty$ . Since the limit does not depend on the subsequence, we finally obtain weak convergence for the whole sequence.

To prove (3.4.2), consider the three sequences of matrix functions

$$\mathbf{P}(\mathbf{n}_2^k)(M_2^k)^{\frac{1}{2}}\mathbf{P}(\mathbf{n}_2^k) + \mathbf{n}_2^k \otimes \mathbf{n}_2^k, \quad \mathbf{P}(\mathbf{n}_2^k)\mathcal{D}\phi^k\mathbf{P}(\mathbf{n}_1^k) + \mathbf{n}_2^k \otimes \mathbf{n}_1^k \quad \text{and} \quad \mathbf{P}(\mathbf{n}_1^k)(M_1^k)^{-\frac{1}{2}}\mathbf{P}(\mathbf{n}_1^k) + \mathbf{n}_1^k \otimes \mathbf{n}_1^k. \quad (3.4.3)$$

The determinant of the second expression above converges weakly as  $k \rightarrow \infty$  by the first part of the lemma, while the determinants of the first and third can be assumed to converge uniformly. Moreover, the matrices in (3.4.3) have the block structure shown in (3.2.3), so multiplying the three together and taking into account that  $\mathbf{P}$  is a projection (depending on the argument) recovers the matrix

$$\mathbf{P}(\mathbf{n}_2^k)(M_2^k)^{\frac{1}{2}}\mathbf{P}(\mathbf{n}_2^k)\mathcal{D}\phi^k\mathbf{P}(\mathbf{n}_1^k)(M_1^k)^{-\frac{1}{2}}\mathbf{P}(\mathbf{n}_1^k) + \mathbf{n}_2^k \otimes \mathbf{n}_1^k$$

appearing in the statement. Multiplicativity of the determinant and the fact that a product of strongly converging and one weakly converging sequence converges weakly then finishes the proof.  $\square$

An analogous result for minors of dimension smaller than  $n-1$  can be proved in an entirely analogous manner, but we only need the statement above. Notice also that the regularity is not optimal, since the determinants of  $(n-1)$ -dimensional minors (in fixed directions) converge

weakly in  $L^{\frac{p}{n-1}}$ , but our proof gives only weak convergence in  $L^{\frac{p}{n}}$ . This can be improved through a different choice of exponents in the application of Hölder's inequality, like for example  $(p+1-n)/p, (n-1-\varepsilon)/p, \varepsilon/p$ , for any  $\varepsilon \in (0, 1)$ .

We are now in a position to prove existence of a minimizing deformation for the surface matching energy  $E$  in a suitable set of admissible deformations. Of particular difficulty is that derivatives of  $\mathbf{d}_2$  are not defined in the whole of  $\Omega$  and in the functional these derivatives are evaluated at deformed positions. We handle this by ensuring that the involved deformations are such that terms involving these derivatives are not evaluated near the singularities. We obtain the following theorem:

**Theorem 3.4.2** (Existence of minimizing deformations). Let  $\mathcal{M}_1, \mathcal{M}_2$  be  $C^{2,1}$  compact embedded surfaces in  $\mathbb{R}^3$  ( $n = 3$ ), be such that a  $C^1$  diffeomorphism  $\varphi : \mathcal{M}_1 \rightarrow \mathcal{M}_2$  exists between them.

Assume further that

$$0 < \sigma < \min(\text{dist}(\mathcal{M}_1, \text{sing } \mathbf{d}_1), \text{dist}(\mathcal{M}_2, \text{sing } \mathbf{d}_2)), \quad (3.4.4)$$

where  $\text{sing } \mathbf{d}_i$  is the set of points where  $\mathbf{d}_i$  is not twice differentiable, and that  $r : \mathbb{R}^{3 \times 3} \rightarrow \text{SPD}(3)$  is continuous. Then there exists a constant  $0 < \nu_0 := \nu_0(\Omega, \mathcal{M}_1, \mathcal{M}_2, \sigma)$  such that for  $0 < \nu \leq \nu_0$ , the functional  $E_\nu$  has at least one minimizer  $\phi$  among deformations in the space  $W_0^{1,p}(\Omega; \mathbb{R}^3) + \text{id}$ . Moreover,  $\phi$  is a homeomorphism of  $\Omega$  into  $\Omega$ , and  $\phi^{-1} \in W^{1,\theta}(\Omega; \mathbb{R}^3)$ , where  $\theta$  is given by  $\theta = q(1+s)/(q+s)$ .

*Proof.* We proceed in several steps.

*Step 1: Coercivity.* First we point out the coercivity enjoyed by our functional. Using the Poincaré and Morrey inequalities ([Leo09], Theorem 12.30 and 11.34), and the Dirichlet boundary conditions we have

$$\|\phi\|_{C^{0,\alpha}(\Omega)} \leq C\|\phi\|_{W^{1,p}(\Omega)} \leq C(1 + \|\mathcal{D}\phi\|_{L^p(\Omega)}) \leq C(1 + E_\nu[\phi]^{\frac{1}{p}}), \quad (3.4.5)$$

for any  $\phi \in W_0^{1,p}(\Omega) + \text{id}$  and  $\alpha = 1 - 3/p$ .

*Step 2: Lower semicontinuity along sequences of constrained deformations.* For the remainder of the proof, a deformation  $\phi \in W_0^{1,p}(\Omega; \mathbb{R}^3) + \text{id}$ ,  $p > 3$  is termed  $\rho$ -admissible for  $\rho > 0$ , if

- $E_{\text{vol}}[\phi] < +\infty$ ,
- $\det \mathcal{D}\phi(x) > 0$  for a.e.  $x \in \Omega$ , and
- for all  $x \in \text{supp } (\eta_\sigma \circ \mathbf{d}_1)$  and every  $y \in \text{sing}(\mathbf{d}_2)$ , we have  $|\phi(x) - y| \geq \rho$ .

Notice that since  $p > 3$ ,  $\phi$  has a unique continuous representative, so the third property is well defined.

First, notice that with the assumption (3.4.4) we have

$$\text{supp } (\eta_\sigma \circ \mathbf{d}_i) = \{|\mathbf{d}_i| \leq \sigma\} \subset \Omega \setminus \overline{\text{sing}(\mathbf{d}_i)}, \quad i = 1, 2. \quad (3.4.6)$$



Let  $\phi^k$  be a sequence of  $\rho$ -admissible deformations with  $E_{\text{vol}}[\phi^k] \leq C$ . By (3.4.5) and using the Banach-Alaoglu and Rellich-Kondrakov theorems, a subsequence (again denoted by  $(\phi^k)$ ) converges to a deformation  $\phi$ , both in the  $W^{1,p}$ -weak and uniform topologies.

Now, we have ([Dac08, Theorem 8.20])

$$(\det \mathcal{D}\phi^k, \text{Cof } \mathcal{D}\phi^k) \rightharpoonup (\det \mathcal{D}\phi, \text{Cof } \mathcal{D}\phi) \text{ in } L^{\frac{p}{3}}(\Omega) \times \left(L^{\frac{p}{2}}(\Omega)\right)^9. \quad (3.4.7)$$

Additionally, since (3.4.7) holds and because  $E_{\nu}[\phi_k]$  is uniformly bounded,  $\int_{\Omega} (\det \mathcal{D}\phi_k)^{-s} dx$  is uniformly bounded by the definition of  $\hat{W}$  and  $\det \mathcal{D}\phi_k \geq 0$  a.e. Together with (3.4.7), we have

$$\det \mathcal{D}\phi(x) > 0 \text{ a. e.} \quad (3.4.8)$$

so that  $\phi$  is again  $\rho$ -admissible.

Notice also that by a.e. positivity of the determinants, (3.4.7) and a standard lower semicontinuity result for convex integrands (see e.g. [Dac08, Theorem 3.23]) implies

$$E_{\text{vol}}[\phi] \leq \liminf_{k \rightarrow \infty} E_{\text{vol}}[\phi^k],$$

and uniform convergence of  $\phi^k$  immediately leads to

$$E_{\text{match}}[\phi] = \lim_{k \rightarrow \infty} E_{\text{match}}[\phi^k].$$

We claim that under the assumptions of this theorem, we also have that

$$E_{\text{mem}}[\phi] \leq \liminf_{k \rightarrow \infty} E_{\text{mem}}[\phi^k] \quad (3.4.9)$$

and

$$E_{\text{bend}}[\phi] \leq \liminf_{k \rightarrow \infty} E_{\text{bend}}[\phi^k]. \quad (3.4.10)$$

To see this, notice that  $\phi^k, \phi$  being  $\rho$ -admissible ensures that the normal vectors satisfy

$$\mathbf{n}_1, \mathbf{n}_2 \circ \phi^k, \mathbf{n}_2 \circ \phi \in C^0(\{|\mathbf{d}_1| \leq \sigma\}; \mathbb{R}^n).$$

Consequently, the first part of Lemma 3.4.1 implies

$$\chi_{\{|\mathbf{d}_1| \leq \sigma\}} \left( \mathcal{D}_{\text{tg}} \phi^k, \det(\mathcal{D}_{\text{tg}} \phi^k) \right) \rightharpoonup \chi_{\{|\mathbf{d}_1| \leq \sigma\}} \left( \mathcal{D}_{\text{tg}} \phi, \det(\mathcal{D}_{\text{tg}} \phi) \right) \text{ in } (L^p(\Omega))^9 \times L^{\frac{p}{3}}(\Omega), \quad (3.4.11)$$

with  $\chi_{\{|\mathbf{d}_1| \leq \sigma\}}$  denoting the indicator function. Combining (3.4.11) with the polyconvexity of  $W$ , defining the function  $E_{\text{mem}}$ , both introduced in (3.3.1) we find the assertion (3.4.9).

Furthermore, by our assumptions on  $\mathcal{M}_i$  (see section 3.2), we have that

$$\chi_{\{|\mathbf{d}_i| \leq \sigma\}} \mathcal{S}_i = \chi_{\{|\mathbf{d}_i| \leq \sigma\}} \mathcal{D}^2 \mathbf{d}_i \in C^{0,1}(\bar{\Omega}; \mathbb{R}^{3 \times 3}).$$

Since  $\mathcal{C}$  produces uniformly positive matrices, we have  $\chi_{\{|\mathbf{d}_1| \leq \sigma\}} (\mathcal{C}(\mathcal{S}_1^{\text{ext}}))^{-1} \in C^0(\bar{\Omega}; \mathbb{R}^{3 \times 3})$ . We can then use a continuity result for square roots of nonnegative definite matrix-valued

functions defined on  $\Omega$  [CH97, Theorem 1.1] to see that

$$\chi_{\{|\mathbf{d}_1| \leq \sigma\}}(\mathcal{C}(\mathcal{S}_1^{ext}))^{-\frac{1}{2}}, \chi_{\{|\mathbf{d}_1| \leq \sigma\}}(\mathcal{C}(\mathcal{S}_2^{ext}) \circ \phi^k)^{\frac{1}{2}}, \chi_{\{|\mathbf{d}_1| \leq \sigma\}}(\mathcal{C}(\mathcal{S}_2^{ext}) \circ \phi)^{\frac{1}{2}} \in C^0(\overline{\Omega}; \mathbb{R}^{3 \times 3}).$$

The second part of Lemma 3.4.1 implies the weak convergence

$$\begin{aligned} & \chi_{\{|\mathbf{d}_1| \leq \sigma\}} \left( \Lambda(\mathcal{C}(\mathcal{S}_1^{ext}(\phi^k)), \mathcal{C}(\mathcal{S}_2^{ext}(\phi^k)), \mathcal{D}\phi^k), \det \Lambda(\mathcal{C}(\mathcal{S}_1^{ext}), \mathcal{C}(\mathcal{S}_2^{ext}(\phi^k)), \mathcal{D}\phi^k) \right) \\ & \xrightarrow{L^{\frac{p}{n}}} \chi_{\{|\mathbf{d}_1| \leq \sigma\}} \left( \Lambda(\mathcal{C}(\mathcal{S}_1^{ext}), \mathcal{C}(\mathcal{S}_2^{ext}(\phi)), \mathcal{D}\phi), \det \Lambda(\mathcal{C}(\mathcal{S}_1^{ext}), \mathcal{C}(\mathcal{S}_2^{ext}(\phi)), \mathcal{D}\phi) \right), \end{aligned}$$

from which (3.4.10) follows by using the polyconvexity of  $W$ .

*Step 3: Existence of minimizers restricted to admissible deformations.* Since we have already seen that the set of  $\rho$ -admissible deformations is weakly closed and weakly compact, and that every term of  $E$  is weakly lower semicontinuous on this set, we just need to check that for all fixed  $\nu > 0$ , the set of  $\rho$ -admissible deformations, with adequate  $\rho$ , is not empty.

For some given  $\sigma$  satisfying  $\text{dist}(\mathcal{M}_2, \text{sing } \mathbf{d}_2) - \sigma > 0$  let  $\rho$  satisfy

$$0 < \rho < \text{dist}(\mathcal{M}_2, \text{sing } \mathbf{d}_2) - \sigma. \quad (3.4.12)$$

We construct a deformation  $\hat{\varphi}$ , which is  $\rho$ -admissible and satisfies  $E_\nu[\hat{\varphi}] < \infty$ . By assumption, there exists a diffeomorphism  $\varphi : \mathcal{M}_1 \rightarrow \mathcal{M}_2$ . Thus, we construct an extension of this diffeomorphism to  $\{|\mathbf{d}_1| \leq \sigma\}$  along the normal directions using

$$\hat{\varphi}(x + s\mathbf{n}_1(x)) := \varphi(x) + s\mathbf{n}_2(\varphi(x)), \text{ for } x \in \mathcal{M}_1, -\sigma \leq s \leq \sigma. \quad (3.4.13)$$

We can then extend  $\hat{\varphi}$  to the inside and outside components  $\Omega_i, \Omega_o$  of  $\Omega \setminus \{|\mathbf{d}_1| \leq \sigma\}$  by solving the minimization problems for  $E_{\text{vol}}$  with Dirichlet boundary conditions given by (3.4.13) on  $\partial\Omega_i$  and  $\partial\Omega_o \setminus \partial\Omega$ , and by  $\hat{\varphi}(x) = x$  on  $\partial\Omega$ . For the resulting  $\hat{\varphi}$  we have

$$E_{\text{match}}[\hat{\varphi}] = 0, E_{\text{vol}}[\hat{\varphi}] < \infty, E_{\text{mem}}[\hat{\varphi}] < \infty, E_{\text{bend}}[\hat{\varphi}] < \infty,$$

where the first two statements follow by construction, and the last two by virtue of  $\varphi$  being a diffeomorphism and the choice of  $\sigma$ . Moreover, we note that since  $\hat{\varphi}$  has finite energy and the growth conditions assumed for  $\hat{W}$  (see (3.3.7)), the condition  $\det \mathcal{D}\hat{\varphi}(x) > 0$  for a.e.  $x$  is also satisfied [Bal81].

*Step 4: A priori estimate to remove the constraint.* Next, we show that for any  $\rho$  satisfying (3.4.12) there exists a parameter  $\nu_0 > 0$  such that for all  $0 < \nu < \nu_0$  the constrained minimizers of  $E_\nu$  subject to (3.4.4) solves the unconstrained optimization problem, consisting in minimizing  $E_\nu$  on  $W_0^{1,p} + \text{id}$ .

To this end, we verify that every  $\phi$  that satisfies

$$E_\nu[\phi] \leq E_\nu[\hat{\varphi}] \quad (3.4.14)$$

is  $\rho$ -admissible. It is immediate from (3.4.14) that  $E_{\text{vol}}(\phi) < +\infty$ , and from the definition of  $\hat{W}$  in (3.3.7) it follows with the same arguments as in (3.4.8) that  $\det \phi > 0$  a.e.

We prove now that for all deformations  $\phi$  satisfying (3.4.14) also satisfy

$$\|\mathbf{d}_2 \circ \phi\|_{L^\infty(\{|\mathbf{d}_1| \leq \sigma\})} \leq \text{dist}(\mathcal{M}_2, \text{sing } \mathbf{d}_2) - \rho. \quad (3.4.15)$$

This is sufficient because from (3.4.15) it follows for all  $x$  satisfying  $|\mathbf{d}_1(x)| \leq \sigma$  by the triangle inequality that

$$\begin{aligned} \rho &\leq \text{dist}(\mathcal{M}_2, \text{sing } \mathbf{d}_2) - \|\mathbf{d}_2 \circ \phi\|_{L^\infty(\{|\mathbf{d}_1| \leq \sigma\})} \\ &= \text{dist}(\mathcal{M}_2, \text{sing } \mathbf{d}_2) - \text{dist}(\phi(x), \mathcal{M}_2) \\ &\leq \text{dist}(\phi(x), \text{sing } \mathbf{d}_2), \end{aligned}$$

which is the third property of a  $\rho$ -admissible deformation  $\phi$ .

To prove (3.4.15) we use the triangle inequality and estimate

$$\|\mathbf{d}_2 \circ \phi\|_{L^\infty(\{|\mathbf{d}_1| \leq \sigma\})} \leq \sigma + \|\mathbf{d}_2 \circ \phi - \mathbf{d}_1\|_{L^\infty(\{|\mathbf{d}_1| \leq \sigma\})}. \quad (3.4.16)$$

By the monotonicity of  $\eta_\sigma$  and the fact that the signed distance functions  $\mathbf{d}_i$  are Lipschitz continuous with constant 1 we have, for each  $\hat{\sigma} \in (0, \sigma)$  that

$$\begin{aligned} &\|\mathbf{d}_2 \circ \phi - \mathbf{d}_1\|_{L^\infty(\{|\mathbf{d}_1| \leq \sigma\})} \\ &\leq \left(1 + \|\phi\|_{C^{0,\alpha}(\{\sigma - \hat{\sigma} \leq |\mathbf{d}_1| \leq \sigma\})}\right) \hat{\sigma}^\alpha + \frac{\|\eta_\sigma \circ \mathbf{d}_1(\mathbf{d}_2 \circ \phi - \mathbf{d}_1)\|_{L^\infty(\{|\mathbf{d}_1| < \sigma - \hat{\sigma}\})}}{\eta_\sigma(\sigma - \hat{\sigma})}. \end{aligned} \quad (3.4.17)$$

Estimates (3.4.5) and (3.4.14) imply in turn

$$\|\phi\|_{C^{0,\alpha}(\{\sigma - \hat{\sigma} \leq |\mathbf{d}_1| \leq \sigma\})} \leq C\|\phi\|_{W^{1,p}(\Omega)} \leq C(1 + E_\nu[\hat{\varphi}]^{\frac{1}{p}}). \quad (3.4.18)$$

Finally, combining (3.4.16), (3.4.17), and (3.4.18) we obtain

$$\begin{aligned} &\|\mathbf{d}_2 \circ \phi\|_{L^\infty(\{|\mathbf{d}_1| \leq \sigma\})} \\ &\leq \sigma + \left(1 + C(1 + E_\nu[\hat{\varphi}]^{\frac{1}{p}})\right) \hat{\sigma}^\alpha + \frac{1}{\eta_\sigma(\sigma - \hat{\sigma})} \|\eta_\sigma \circ \mathbf{d}_1(\mathbf{d}_2 \circ \phi - \mathbf{d}_1)\|_{L^\infty(\{|\mathbf{d}_1| < \sigma - \hat{\sigma}\})}. \end{aligned} \quad (3.4.19)$$

Now we can apply Ehring's lemma [RR04, Theorem 7.30] for the embeddings  $W^{1,p}(\Omega) \subset L^\infty(\Omega) \subset L^2(\Omega)$  to control the last term in (3.4.19). Taking into account the Poincaré inequality and Dirichlet boundary conditions, we obtain for any  $\epsilon > 0$  a constant  $C(\epsilon) > 0$  such that

$$\begin{aligned} &\|\eta_\sigma \circ \mathbf{d}_1(\mathbf{d}_2 \circ \phi - \mathbf{d}_1)\|_{L^\infty(\{|\mathbf{d}_1| < \sigma - \hat{\sigma}\})} \leq \|\eta_\sigma \circ \mathbf{d}_1(\mathbf{d}_2 \circ \phi - \mathbf{d}_1)\|_{L^\infty(\Omega)} \\ &\leq C(\epsilon) \|\eta_\sigma \circ \mathbf{d}_1(\mathbf{d}_2 \circ \phi - \mathbf{d}_1)\|_{L^2(\Omega)} + \epsilon C \left( \|\nabla(\eta_\sigma \circ \mathbf{d}_1(\mathbf{d}_2 \circ \phi - \mathbf{d}_1))\|_{L^p(\Omega)} + 1 \right). \end{aligned} \quad (3.4.20)$$

Now, for the first term in the right hand side of (3.4.20) we can estimate

$$\|\eta_\sigma \circ \mathbf{d}_1(\mathbf{d}_2 \circ \phi - \mathbf{d}_1)\|_{L^2(\Omega)} = \nu^{\frac{1}{2}} E_{\text{match}}[\phi]^{\frac{1}{2}} \leq \nu^{\frac{1}{2}} E_\nu[\hat{\varphi}]^{\frac{1}{2}}. \quad (3.4.21)$$

For the second term, denoting  $\text{diam } \Omega = \sup_{x,y \in \Omega} |x - y|$ ,

$$\begin{aligned} &\|\nabla(\eta_\sigma \circ \mathbf{d}_1(\mathbf{d}_2 \circ \phi - \mathbf{d}_1))\|_{L^p(\Omega)} \\ &\leq \|\nabla(\eta_\sigma \circ \mathbf{d}_1)(\mathbf{d}_2 \circ \phi - \mathbf{d}_1)\|_{L^p(\Omega)} + \|(\eta_\sigma \circ \mathbf{d}_1) \nabla(\mathbf{d}_2 \circ \phi - \mathbf{d}_1)\|_{L^p(\Omega)} + 1 \end{aligned}$$

$$\begin{aligned}
&\leq C\nu^{\frac{1}{p}} \left( \|\mathbf{d}_2 \circ \phi - \mathbf{d}_1\|_{L^\infty(\Omega)}^{\frac{p-2}{p}} E_{\text{match}}[\phi]^{\frac{1}{p}} \right) + C(\|\mathcal{D}\phi\|_{L^p(\Omega)} + \|\nabla \mathbf{d}_1\|_{L^p(\Omega)} + 1) \\
&\leq C\nu^{\frac{1}{p}} \left( (\|\phi\|_{C^{0,\alpha}(\Omega)} + 2 \operatorname{diam} \Omega)^{\frac{p-2}{p}} E_\nu[\hat{\phi}]^{\frac{1}{p}} \right) + C(E_\nu[\hat{\phi}]^{\frac{1}{p}} + 1) \\
&\leq C\nu^{\frac{1}{p}} \left( (1 + E_\nu[\hat{\phi}]^{\frac{1}{p}})^{\frac{p-2}{p}} E_\nu[\hat{\phi}]^{\frac{1}{p}} \right) + C(E_\nu[\hat{\phi}]^{\frac{1}{p}} + 1), \tag{3.4.22}
\end{aligned}$$

where we have applied the product rule, the definition of  $E_{\text{match}}$ ,  $\eta_\sigma \in C_0^\infty$ ,  $\eta_\sigma \leq C$ , that  $|\nabla \mathbf{d}_i| = 1$  a.e.,  $i = 1, 2$ , the chain rule, and (3.4.14). The use of the chain rule is justified by [MM72, Theorem 2.2], since  $\mathbf{d}_2$  has Lipschitz constant 1.

Together, (3.4.20), (3.4.21), and (3.4.22) imply

$$\begin{aligned}
&\|\eta_\sigma \circ \mathbf{d}_1(\mathbf{d}_2 \circ \phi - \mathbf{d}_1)\|_{L^\infty(\{|\mathbf{d}_1| < \sigma - \hat{\sigma}\})} \\
&\leq \nu^{\frac{1}{p}} \left( C(\epsilon)\nu^{\frac{1}{2}-\frac{1}{p}} E_\nu[\hat{\phi}]^{\frac{1}{2}} + \epsilon C(1 + E_\nu[\hat{\phi}]^{\frac{1}{p}})^{\frac{p-2}{p}} E_\nu[\hat{\phi}]^{\frac{1}{p}} \right) + \epsilon C(E_\nu[\hat{\phi}]^{\frac{1}{p}} + 1). \tag{3.4.23}
\end{aligned}$$

In light of (3.4.19) and (3.4.23), and since  $E_\nu[\hat{\phi}]$  is independent of  $\nu$ , we can now choose first  $\hat{\sigma}$ , then  $\epsilon$  and finally  $\nu$  small enough to obtain

$$\|\mathbf{d}_2 \circ \phi\|_{L^\infty(\{|\mathbf{d}_1| \leq \sigma\})} \leq \sigma + (\operatorname{dist}(\mathcal{M}_2, \operatorname{sing} \mathbf{d}_2) - \sigma - \rho) \leq \operatorname{dist}(\mathcal{M}_2, \operatorname{sing} \mathbf{d}_2) - \rho.$$

*Step 5: Injectivity.* The injectivity and regularity of the inverse follow by the growth conditions satisfied by  $E_{\text{vol}}$  and classical results of Ball [Bal81, Theorems 2 and 3]. Note that although Theorem 3 in [Bal81] is stated in terms of minimizers, the boundary conditions and finiteness of the energy are all that is needed.  $\square$

We have particularized the statement of Theorem 3.4.2 to the case of surfaces ( $n = 3$ ) and Dirichlet boundary conditions to use standard growth assumptions on  $\hat{W}$  that ensure global invertibility of deformations of finite energy in  $\mathbb{R}^3$ . However, the existence results generalizes easily to different dimensions  $n$ . Furthermore, as stated in Corollary 3.4.3 we also have existence of minimizing deformations also for the case of Neumann boundary conditions.

**Corollary 3.4.3** (Natural boundary conditions). Under the assumptions of Theorem 3.4.2 above, there exists a constant

$$0 < \nu_N = \nu_N(\Omega, \mathcal{M}_1, \mathcal{M}_2, \sigma)$$

such that for  $0 < \nu \leq \nu_N$ , the functional  $E_\nu$  possesses at least one minimizer among deformations in the space  $W^{1,p}(\Omega; \mathbb{R}^3)$ .

*Proof.* The proof follows the same arguments used for Theorem 3.4.2, so we only point out the necessary modifications. We need a replacement for the coercivity estimate (3.4.5) and claim

$$\|\phi\|_{W^{1,p}(\Omega)} \leq C(1 + \nu^{\frac{1}{2}} E_{\text{match}}[\phi]^{\frac{1}{2}} + \|\mathcal{D}\phi\|_{L^p(\Omega)}) \leq C(1 + \nu^{\frac{1}{2}} E_\nu[\phi]^{\frac{1}{2}} + E_\nu[\phi]^{\frac{1}{p}}). \tag{3.4.24}$$

To verify this let us consider  $\omega := \{|\mathbf{d}_1| \leq \sigma/2\}$ . An adequate Poincaré inequality (see e.g. [Leo09, Theorem 12.23]) implies that

$$\|\phi\|_{W^{1,p}(\Omega)} \leq C \left( \|\mathcal{D}\phi\|_{L^p(\Omega)} + \left| \int_\omega \phi \, dx \right| \right),$$

and we estimate the second term in the right hand side by

$$\begin{aligned}
\left| \int_{\omega} \phi \, dx \right| &\leq \int_{\omega} |\phi| \, dx \leq \int_{\omega} |\mathbf{d}_2 \circ \phi| \, dx + |\omega| \sup_{x \in \mathcal{M}_2} |x| \\
&\leq \int_{\omega} |\mathbf{d}_2 \circ \phi - \mathbf{d}_1| \, dx + \int_{\omega} |\mathbf{d}_1| \, dx + |\omega| \sup_{x \in \mathcal{M}_2} |x| \\
&\leq \eta_{\sigma} \left( \frac{\sigma}{2} \right)^{-1} |\omega|^{-\frac{1}{2}} (\nu E_{\text{match}}[\phi])^{\frac{1}{2}} + \int_{\omega} |\mathbf{d}_1| \, dx + |\omega| \sup_{x \in \mathcal{M}_2} |x|,
\end{aligned}$$

where Hölder's inequality has been used to compare  $L^1$  and  $L^2$  norms. Therefore, (3.4.24) follows.

The proof of the estimate for  $\|\mathbf{d}_2 \circ \phi\|_{L^{\infty}(\{\mathbf{d}_1 \leq \sigma\})}$  (to ensure that deformations stay away from the singularities of  $\mathbf{d}_2$ ) is still valid with minor modifications, since  $\nu$  appears in (3.4.24) multiplicatively.  $\square$

We conclude this section with the following proposition, which explores the penalization limit in which the parameter  $\nu$  tends to zero. It is partially based on a computation contained in the introduction to [EG87a] that is developed in more generality in [EG87b].

**Proposition 3.4.4.** Let  $\{\nu_k\}_{k \in \mathbb{N}}$  be a sequence of penalty matching parameters such that  $\nu_k \rightarrow 0$  as  $k \rightarrow \infty$ , and  $\phi^k$  be solutions of the Dirichlet minimization problem for  $E_{\nu_k}$ . Then, up to a choice of subsequence, the  $\phi^k$  converge strongly in  $W^{1,p}$  to a solution of the constrained problem in which the condition  $\phi(\mathcal{M}_1^{\ell}) = \mathcal{M}_2^{\ell}$  for all  $\ell \in (-\sigma, \sigma)$  is imposed.

*Proof.* First, notice that the energy  $E$  may be written as

$$\begin{aligned}
E_{\nu}[\phi] &= \frac{1}{\nu} \int_{\Omega} \eta_{\sigma} \circ \mathbf{d}_1 |\mathbf{d}_2 \circ \phi - \mathbf{d}_1|^2 + \alpha_p |\mathcal{D}\phi|^p \\
&\quad + H\left(\det \mathcal{D}\phi, \text{Cof} \mathcal{D}\phi, \mathcal{D}_{\text{tg}} \phi, \det(\mathcal{D}_{\text{tg}} \phi + \mathbf{n}_2 \circ \phi \otimes \mathbf{n}_1), \right. \\
&\quad \left. \Lambda(\mathcal{C}(\mathcal{S}_1^{\text{ext}}, \mathcal{C}(\mathcal{S}_2^{\text{ext}} \circ \phi)), \mathcal{D}\phi), \det(\Lambda(\mathcal{C}(\mathcal{S}_1^{\text{ext}}, \mathcal{C}(\mathcal{S}_2^{\text{ext}} \circ \phi)), \mathcal{D}\phi))\right) dx,
\end{aligned} \tag{3.4.25}$$

where  $H : \mathbb{R}^+ \times \mathbb{R}^{3 \times 3} \times \mathbb{R}^{3 \times 3} \times \mathbb{R} \times \mathbb{R}^{3 \times 3} \times \mathbb{R} \rightarrow \mathbb{R}^+$  is smooth and convex.

Denote by  $\hat{\phi}$  the extension of a diffeomorphism between  $\mathcal{M}_1$  and  $\mathcal{M}_2$  used in the proof of Theorem 3.4.2. Since  $E_{\text{match}}[\hat{\phi}] = 0$ , we have that  $E_{\nu_k}[\phi^k] \leq E_1[\hat{\phi}]$ . By the coercivity estimate (3.4.5) the  $\phi^k$  are then bounded in  $W^{1,p}$  and we may extract a (not relabeled) subsequence converging uniformly and weakly in  $W^{1,p}$  to some limit  $\phi$ . Since  $\{E_{\nu_k}[\phi^k]\}$  is bounded and  $\nu_k \rightarrow 0$ , the uniform convergence of  $\phi^k$  implies that

$$\int_{\Omega} \eta_{\sigma}(\mathbf{d}_1) |\mathbf{d}_2 \circ \phi^k - \mathbf{d}_1|^2 \, dx \xrightarrow{k \rightarrow \infty} \int_{\Omega} \eta_{\sigma}(\mathbf{d}_1) |\mathbf{d}_2 \circ \phi - \mathbf{d}_1|^2 \, dx = 0. \tag{3.4.26}$$

In consequence,  $\phi(\mathcal{M}_1^{\ell}) = \mathcal{M}_2^{\ell}$  for all  $\ell \in (-\sigma, \sigma)$ . Therefore,  $\phi$  is admissible for all  $\nu_k$  and  $E_{\nu_k}[\phi^k] \leq E_1[\hat{\phi}]$ . Combined with lower semicontinuity and (3.4.25), the above implies

$$\int_{\Omega} \alpha_p |\mathcal{D}\phi^k|^p + H(\det(\mathcal{D}\phi^k), \dots) \, dx \xrightarrow{k \rightarrow \infty} \int_{\Omega} \alpha_p |\mathcal{D}\phi|^p + H(\det(\mathcal{D}\phi), \dots) \, dx. \tag{3.4.27}$$

From this convergence, the fact that  $H$  is convex and differentiable, and  $\mathcal{D}\phi^k \rightharpoonup \mathcal{D}\phi$  in  $L^p$  it follows that

$$\begin{aligned} 0 &= \limsup_{k \rightarrow \infty} \left( \int_{\Omega} \alpha_p \left( |\mathcal{D}\phi^k|^p - |\mathcal{D}\phi|^p \right) + H(\det(\mathcal{D}\phi^k), \dots) - H(\det(\mathcal{D}\phi), \dots) dx \right) \\ &\geq \limsup_{k \rightarrow \infty} \left( \int_{\Omega} \alpha_p \left( |\mathcal{D}\phi^k|^p - |\mathcal{D}\phi|^p \right) + \mathcal{D}H(\det(\mathcal{D}\phi), \dots) \cdot (\det(\mathcal{D}\phi^k) - \det(\mathcal{D}\phi), \dots) dx \right) \\ &= \limsup_{k \rightarrow \infty} \int_{\Omega} \alpha_p |\mathcal{D}\phi^k|^p dx - \int_{\Omega} \alpha_p |\mathcal{D}\phi|^p dx . \end{aligned}$$

This together with the weak lower semicontinuity of the  $L^p$ -norm, the above shows that

$$\int_{\Omega} \alpha_p |\mathcal{D}\phi|^p dx = \lim_{k \rightarrow \infty} \int_{\Omega} \alpha_p |\mathcal{D}\phi^k|^p dx .$$

Because  $L^p(\Omega)$  has the Radon-Riesz property ([Meg98, p. 2.5.26]), weak convergence and convergence of the norm guarantees strong convergence in  $L^p$ . Since  $\phi_k$  was assumed to converge uniformly, we have also  $\phi_k \rightarrow \phi$  in  $L^p$ , and this shows that  $\phi_k \rightarrow \phi$  in  $W^{1,p}(\Omega; \mathbb{R}^3)$ .

That  $\phi$  is a minimizer of the constrained problem follows directly ([Bra02], Theorem 1.21) from the fact that the  $E_{\nu_k}$  are an equicoercive family of functionals,  $\Gamma$ -converging in the weak topology of  $W^{1,p}$ . Equicoercivity follows easily from the above, while  $\Gamma$ -convergence is implied by the fact that  $E_{\nu_k}$  is an increasing sequence of weakly lower semicontinuous functionals ([Bra02], Remark 1.40), since  $\nu_k \rightarrow 0$  appears as a denominator in  $E_{\text{match}}$ .  $\square$

**Remark 3.4.5.** By the coercivity estimate (3.4.24) of Corollary 1, an entirely analogous result holds for minimizers with Neumann boundary conditions.

**Remark 3.4.6.** Contrary to what might be expected, the limit problem we have obtained is not a surface problem, since all the level sets are still coupled through the volume energy  $E_{\text{vol}}$ . The line of reasoning above depends heavily on the fact that the coefficients of the volume term are held fixed, since the equicoercivity and uniform strict quasiconvexity (in the language of [EG87b]) both require the presence of  $\|\mathcal{D}\phi\|_{L^p(\Omega)}^p$  in the functional.

### 3.4.1 Oscillations and lack of rank-one convexity for the naive approach

To model the tangential distortion energy we have considered a frame indifferent energy density with the argument  $\mathcal{D}_{\text{tg}}\phi + (\mathbf{n}_2 \circ \phi) \otimes \mathbf{n}_1$ . Let us now consider a simpler version of the membrane energy (3.3.6), where we use as an argument of the energy density directly the tangential Cauchy-Green strain tensor (cf (3.2.2))  $(\tilde{\mathcal{D}}_{\text{tg}}\phi(x))^T (\tilde{\mathcal{D}}_{\text{tg}}\phi(x)) + \mathbf{n}_1(x) \otimes \mathbf{n}_1(x)$ , and define the membrane energy

$$\tilde{E}_{\text{mem}}[\phi] := \int_{\Omega} \eta_{\sigma}(\mathbf{d}_1(x)) W\left((\tilde{\mathcal{D}}_{\text{tg}}\phi(x))^T \tilde{\mathcal{D}}_{\text{tg}}\phi(x) + \mathbf{n}_1(x) \otimes \mathbf{n}_1(x)\right) dx, \quad (3.4.28)$$

with  $\tilde{\mathcal{D}}_{\text{tg}}\phi := \mathcal{D}\phi P_1$  defined as the tangential part of the derivative along  $T_x \mathcal{M}_1^{\mathbf{d}_1(x)}$ , and  $W : \mathbb{R}^{2 \times 2} \rightarrow \mathbb{R}$  a frame indifferent energy density that has a strict minimum at  $\text{SO}(2)$ .

The expression  $\det(\tilde{\mathcal{D}}_{\text{tg}}\phi^T \tilde{\mathcal{D}}_{\text{tg}}\phi + \mathbf{n}_1 \otimes \mathbf{n}_1)$  appearing above can not be reduced to a squared determinant of a minor of  $\mathcal{D}\phi$ , in contrast to the corresponding construction (3.2.2) for our

tangential derivative  $\mathcal{D}_{\text{tg}}\phi$ . In fact, a density which is polyconvex in  $\tilde{\mathcal{D}}_{\text{tg}}\phi$  would give rise to a lower semicontinuous energy, but no such energy can be useful for our purpose as a measure of tangential area distortion. An application of the Binet-Cauchy formula ([EG92, Section 3.2, Theorem 4]) yields

$$(\det(\tilde{\mathcal{D}}_{\text{tg}}\phi^T \tilde{\mathcal{D}}_{\text{tg}}\phi + \mathbf{n}_1 \otimes \mathbf{n}_1))^2 = \sum_{j=1}^3 \left( \det(\text{Cof}(\tilde{\mathcal{D}}_{\text{tg}}\phi Q(\mathbf{n}_1))_{j3}) \right)^2,$$

where the last column of the matrix  $\tilde{\mathcal{D}}_{\text{tg}}\phi Q(\mathbf{n}_1) \in \mathbb{R}^{3 \times 3}$  vanishes. Therefore, the condition for lack of area distortion  $\det(\tilde{\mathcal{D}}_{\text{tg}}\phi^T \tilde{\mathcal{D}}_{\text{tg}}\phi + \mathbf{n}_1 \otimes \mathbf{n}_1) = 1$  expresses that a triplet of determinants of minors of  $\tilde{\mathcal{D}}_{\text{tg}}\phi$  belongs to  $\mathbb{S}^2$ , which is not a convex set.

In fact, this energy is no longer lower semicontinuous. To this end, we present explicit counterexamples (in dimension  $n = 2$ ).

**Example 3.4.7** (Oscillation patterns). We construct an explicit sequence for which lower semicontinuity of the membrane energy  $\tilde{E}_{\text{mem}}$  fails. Fix  $0 < R < 1$  and  $\mathcal{M}_1 = \mathbb{S}^1$  with the parametrization  $\xi \rightarrow e^{i\xi}$ . Consider a sequence of deformations  $\varphi_k : \mathbb{S}^1 \rightarrow \mathbb{R}^2$  defined in polar coordinates of  $(r, \theta)$  by the condition

$$\partial_\xi \varphi_k(\xi) = (R \sin k\xi) e_r(r(\varphi_k(\xi)), \theta(\varphi_k(\xi))) + \left(1 - R^2 \sin^2 k\xi\right)^{\frac{1}{2}} e_\theta(r(\varphi_k(\xi)), \theta(\varphi_k(\xi))), \quad (3.4.29)$$

where  $e_r = (\cos \theta, \sin \theta)^T$ ,  $e_\theta = (-\sin \theta, \cos \theta)^T$  for given  $\phi_k(0)$ . Note that for any  $k$  and  $\theta$  that  $|\partial_\theta \varphi_k(\theta)| = 1$ , so that the transformations are tangentially isometric. We define  $\varphi_k(0)$  via two integration constants  $r_0$  and  $\theta_0$  for the initialization of  $r$  and  $\theta$  at  $\xi = 0$ . We set  $\theta_0 = 0$  and choose  $r_0$  such that the curve  $\varphi_k$  is closed and simple, which imposes  $r_0 = r(\varphi_k(0)) = r(\varphi_k(2\pi))$  since the first term in (3.4.29) has zero average. From the second term, taking into account that  $e_\theta(r, \theta)$  is independent of  $r$ , we get the condition

$$2\pi r_0 = \int_0^{2\pi} \left(1 - R^2 \sin^2 k\xi\right)^{\frac{1}{2}} d\xi = \frac{1}{k} \int_0^{2\pi k} \left(1 - R^2 \sin^2 \zeta\right)^{\frac{1}{2}} d\zeta,$$

where we have applied the change of variables  $\zeta = k\xi$ . By periodicity the right hand side (an incomplete elliptic integral of the second kind with modulus  $R$ ) is independent of  $k$  and thus determines  $r_0$ . The resulting  $\varphi_k$  for several values of  $k$  are depicted in Figure 3.3.

We observe that  $\partial_\theta \varphi_k(\theta) \rightharpoonup r_0 e_\theta$  in  $L^p$ , for any  $1 \leq p < \infty$  (and also weak-\* in  $L^\infty$ ). Therefore, the weak  $W^{1,p}$ -limit  $\phi$  of the  $\varphi_k$  is the function defined by  $\phi(\theta) = r_0 e_r$  and obviously not an isometry. Assuming  $0 < \sigma < 1$  and extending  $\varphi_k, \phi$  along the radial direction  $e_r$  to the annulus  $\{1 - \sigma \leq r \leq 1 + \sigma\}$ , we obtain corresponding deformations given by

$$\phi^k(r, \theta) = \varphi_k(\theta) + (r - 1)Q_{\frac{\pi}{2}}\partial_\theta \varphi_k(\theta), \text{ and } \phi(r, \theta) = \phi(\theta) + (r - 1)r_0 e_r = r r_0 e_r,$$

where  $Q_{\frac{\pi}{2}}$  stands for clockwise rotation by  $\pi/2$ , so that  $Q_{\frac{\pi}{2}}\partial_\theta \varphi_k(\theta)$  is the unit outward normal to  $\varphi_k(\mathbb{S}^1)$ . Clearly also  $\phi^k \rightharpoonup \phi$  in  $W^{1,p}$ . From (3.4.29) and since  $e_r, e_\theta$  are unit vectors, we have that  $\tilde{E}_{\text{mem}}[\phi^k] = 0$ , but  $\tilde{E}_{\text{mem}}[\phi] > 0$ , so  $\tilde{E}_{\text{mem}}$  is not weakly lower semicontinuous for  $\mathcal{M}_1 = \mathbb{S}^1$ .

An intuitive explanation for this failure of lower semicontinuity is that we are trying to control

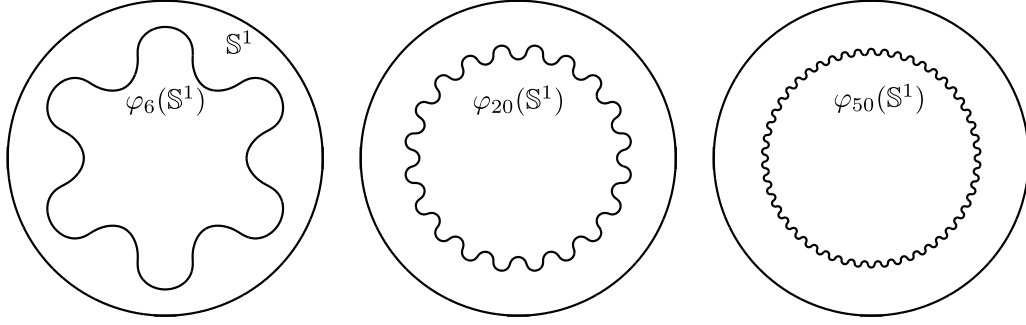


FIGURE 3.3: Explicit oscillations for a simplified model.  $\varphi_k$  for  $R = 0.95$ ,  $k = 6, 20, 50$

through determinants the  $n$  components of  $T\phi(\mathcal{M}_1^c)$  (which is  $n - 1$  dimensional, but we don't know a priori in which directions) with just the  $n - 1$  directions in  $T\mathcal{M}_1^c$ . Therefore, we cannot get enough cancellation (in the sense of compensated compactness [Tar79]) to obtain weak continuity of the area distortion, nor weak lower semicontinuity of the functionals, and thus oscillations are encouraged when trying to impose an isometry constraint. In fact, it is well known that the partial differential relations arising from low-regularity isometric immersion of a  $n - 1$  dimensional surface in  $\mathbb{R}^n$  have a large amount of solutions.

The celebrated Nash-Kuiper theorem [Nas54; Kui55] states that it is possible to uniformly approximate any short  $C^\infty$  immersion by  $C^1$  isometric ones. Our explicit oscillations around  $r_0\mathbb{S}^1$  is just one example of this phenomenon. Notice that a bending term of the type  $E_{\text{bend}}$  introduced in our model only compares the curvatures of  $\mathcal{M}_1^{\mathbf{d}_1(x)}$  and  $\mathcal{M}_2^{\mathbf{d}_2(\phi(x))}$ . It therefore does not penalize oscillations, since it does not detect the curvature of  $\phi(\mathcal{M}_1)$  at all.

It is, however, plausible that the volume term (3.3.7) penalizes such oscillations strongly enough to recover lower semicontinuity (notice that the  $\phi^k$  in our example are eventually not injective), but we do not pursue this direction here. Let us mention that the limit theories for thin plates and shells with energy scaling linearly on their width [LDR95a; LDR96] also do not properly account for compression resistance, since in the (strong  $L^p$ )  $\Gamma$ -limit a quasiconvex envelope appears, forcing the resulting oscillations to be 'averaged away'.

**Example 3.4.8.** [Lack of rank-one convexity] We present an additional example of a configuration for which the integrand of an energy of the type  $\tilde{E}_{\text{mem}}$  is not rank-one convex. Rank-one convexity of the complete energy density, i.e., , convexity in  $t \in \mathbb{R}$  when composed with the function  $A + tB$  for any matrix  $A$  and any rank one matrix  $B$ , is known to be a necessary condition for quasiconvexity ([Dac08], Theorem 5.3). Quasiconvexity, in turn, is necessary for weak lower semicontinuity of integral functionals in Sobolev spaces ([Dac08], Theorem 8.1 and Remark 8.2).

Let  $\Omega = [-1, 1]^2$ , and  $\mathcal{M}_1 = [-1, 1] \times \{0\}$ . In this situation, the tangential derivatives are just partial derivatives along the first coordinate, yielding

$$\tilde{\mathcal{D}}_{tg}\phi = \mathcal{D}\phi\mathbf{P}(e_2) = \begin{pmatrix} \partial_1\phi_1 & 0 \\ \partial_1\phi_2 & 0 \end{pmatrix}, \text{ and } \tilde{\mathcal{D}}_{tg}\phi^T \tilde{\mathcal{D}}_{tg}\phi = \begin{pmatrix} (\partial_1\phi_1)^2 + (\partial_1\phi_2)^2 & 0 \\ 0 & 0 \end{pmatrix}.$$



Hence the tangential area distortion measure reduces to

$$\mathrm{tr}(\tilde{\mathcal{D}}_{tg}\phi^T \tilde{\mathcal{D}}_{tg}\phi) = \det(\tilde{\mathcal{D}}_{tg}\phi^T \tilde{\mathcal{D}}_{tg}\phi + e_2 \otimes e_2) = (\partial_1 \phi_1)^2 + (\partial_1 \phi_2)^2, \quad (3.4.30)$$

where  $e_2 = (0, 1)^T$ . Defining now the convex function

$$F(a, d) = \frac{1}{2}a + \frac{1}{2}d + d^{-1} - 2,$$

which has a unique minimum with value 0 for  $a = d = 1$ , we have that the energy density

$$W_F(B) = F\left(\mathrm{tr}(B^T B), \det(B^T B + e_2 \otimes e_2)\right)$$

has a pointwise minimum, with value zero, whenever  $\mathcal{D}\phi$  is such that  $(\partial_1 \phi_1)^2 + (\partial_1 \phi_2)^2 = 1$ . Note that although the length and area distortion measures are the same in the case of curves, the corresponding energy fits in (3.4.28) in any dimension, and so do the calculations below (with the obvious modifications).

Consider now, for  $0 \leq \lambda \leq 1$ , the family of matrices

$$B(\lambda) = \begin{pmatrix} \lambda & 0 \\ (1-\lambda) & 0 \end{pmatrix} = \lambda \begin{pmatrix} 1 & 0 \\ 0 & 0 \end{pmatrix} + (1-\lambda) \begin{pmatrix} 0 & 0 \\ 1 & 0 \end{pmatrix}. \quad (3.4.31)$$

Clearly  $B(\lambda)$  is rank one. But we have  $W_F(B(\lambda)) = \lambda^2 + (1-\lambda)^2 + \frac{1}{\lambda^2 + (1-\lambda)^2} - 2$  and therefore

$$W_F(B(0)) = F(B(1)) = 0, \text{ but } W_F(B(1/2)) = \frac{1}{2},$$

which demonstrates that  $W_F$  is not rank-one convex.

Observe that the situation is not improved by adding a simple regularization term, like for example considering a density of the type  $W_\varepsilon(\mathcal{D}\phi) := W(\mathcal{D}\phi) + \varepsilon|\mathcal{D}\phi|^2$ , since in this case we have

$$W_F^\varepsilon(B(0)) = W_F^\varepsilon(B(1)) = \varepsilon, \text{ and } W_F^\varepsilon(B(1/2)) = \frac{1}{2} + \frac{\varepsilon}{4},$$

and therefore if  $\varepsilon < \frac{2}{3}$ , the function  $W_F^\varepsilon$  is also not convex on this particular rank-one segment.

### 3.5 Finite element discretization based on adaptive octrees

We adopt a ‘discretize, then optimize’ approach and consider a finite element approximation and optimize for the coefficients of the solution. Since the energy  $E_\nu$  is highly nonlinear and nonconvex, we use a cascadic multilevel minimization scheme in which the solution for one grid level is used as the initial data for the minimization on the next finer grid. We use an adaptive refinement of the underlying meshes around the surfaces  $\mathcal{M}_1, \mathcal{M}_2$  (Algorithm 2).

One of the main characteristics of our functional is the pervasive presence of coefficients depending on the deformed position  $\phi(x)$ . Indeed, this is how the functional takes into account the geometry of target surface, through the projection  $P_2$  and shape operator  $\mathcal{S}_2$ . From an implementation perspective, however, this means that frequently discrete functions have to

evaluated at deformed positions. Therefore, the ability to efficiently search the index of an element containing a given position is of paramount importance, so a hierarchical data structure that allows for efficient searching is needed. The model only contains first derivatives of the unknown deformation. Hence, multilinear finite elements already allow a conforming discretization. For these reasons we use multilinear FEM on octree grids. The grids used are such that all of the elements are either squares or cubes of side length  $h = 2^{-\ell}$ , for an integer  $\ell$  to which we refer as grid level of the element. In what follows let us detail the different ingredients of the algorithm.

---

**Algorithm 2** Cascadic minimization scheme.

---

```

Starting grid: Uniform of level  $\ell_{\min}$ ,  $h = 2^{-\ell_{\min}}$ 
 $\phi \leftarrow \mathbb{1}$ 
for  $l \leftarrow \ell_{\min}$  to  $\ell_{\max}$  do
    Regenerate  $\mathbf{d}_1, \mathbf{d}_2$  on grid by aFMM.
    Compute  $\mathbf{n}_1, \mathbf{n}_2, \mathcal{S}_1, \mathcal{S}_2$  from  $\mathbf{d}_1, \mathbf{d}_2$ .
     $\beta \leftarrow \beta_{\max}$ 
    while  $\beta > \beta_{\min}$  do
         $\phi \leftarrow H^1\text{-CG-descent}(\beta, \phi)$ 
         $\beta \leftarrow \beta/2$ 
    end while
    Mark all elements intersecting  $\mathcal{M}_1$  or  $\mathcal{M}_2$ .
    Refine the grid ( $h \leftarrow 2^{-\ell+1}$ ).
end for
return  $\phi$ 

```

---

**Multilinear Finite Elements on Octrees.** We assume  $n = 3$  for the presentation here. Using an adaptive octree grid based on cubic cells leads to hanging nodes (see Figure 3.4), nodes which are on the facet of a cell without being one of its vertices. Enforcing continuity of the finite element functions leads to constraints for function values on hanging nodes and these hanging nodes are not degrees of freedom. Additionally, to minimize the complexity of the required interpolation rules, the subdivision is propagated in such a way that the grid level of neighboring elements sharing a cell facet differs at most by one.

**Octrees and the access to degrees of freedom via hashtables.** Even though the tree structure gives a natural hierarchical structure to the elements of the mesh, maintaining consistent linear indices for degrees of freedom, hanging nodes, and elements can be delicate. Consistent rules could be devised to maintain consistency with the element octree for a given mesh, but these would not be easy to update when the grid is refined. In order to keep track of vertex indices in a simple manner without sacrificing efficiency, hash maps ([Cor+09], Chapter 11) are maintained to keep track of the indices of degrees of freedom, hanging nodes, and cells. The keys used in the hashmap are a combination of a level value  $\ell$  and point coordinates as integer multiples of  $h = 2^{-\ell}$ . These keys uniquely identify nodes or elements, with the convention that an element is identified with its lower-left-back corner. Whenever a query for a node or cell is made, there are two possible outcomes. If it is already contained in the corresponding hash table, a linear

index for it can be retrieved. Otherwise, a new entry of the hash table is created and the node or cell is given the next unused index. Since we do not require coarsening of the mesh, this scheme guarantees a consistent linear set of indices with a computational cost for insertions and queries that is, on average, independent of the mesh size.

**Computing distance functions on octrees.** In our model we have assumed that the distance functions to our surfaces are given. In practice, especially when using adaptive grids, we need to compute signed distance functions on such grids. This has been accomplished by a straightforward adaptation of the Fast Marching Method on Cartesian grids [Set99] exploiting the fact that our grids still are subgrids of a regular Cartesian grid. In the implemented variant hanging nodes are not taken into account for the propagation, their values being linearly interpolated to accommodate the constraints needed for conformality. The initialization for the distance computation has been performed starting from triangular meshes of the surfaces (for  $n = 3$ ; for  $n = 2$  two-bit segmentation of interior and exterior of the curves has been used). The signs of the distance functions have to be computed separately, by detecting which points of the grid are inside (resp. outside) the initial surface data. In our case, they have been computed with the provably correct algorithm given in [BA05].

**Computation of the coefficients.** The discretization for the unknown deformation  $\phi$ , as already mentioned, is done by multilinear finite elements. However, the coefficients of our model include first and second derivatives of the signed distance functions  $\mathbf{d}_i$ , for the normal vectors  $\mathbf{n}_i$  and shape operators  $\mathcal{S}_i$  ( $i = 1, 2$ ), respectively. The approximations are required to be robust, since they appear in the highest order terms of the model. For the normal vectors  $\mathbf{n}_i$ , we compute the  $L^2$  projection of the finite element derivative of  $\mathbf{d}_i$  to recover the nodal values of a piecewise multilinear function, followed by a orthogonal projection to the unit sphere to restore the constraint  $|\mathbf{n}_i| = 1$ .

In the case of the shape operators, our approach is to approximate the distance functions  $\mathbf{d}_i$  by a quadratic polynomial supported on a neighborhood of each point. Given a fixed integer neighborhood size  $r$ , for each non hanging node  $x_k$  (i.e., the neighborhood  $B_r(x_k)$  contains the  $r$  closest other degrees of freedom of the adaptive grid) the local quadratic polynomial  $p_k$  is defined as the one minimizing the least-squares error

$$\sum_{x_j \in B_r(x_k)} (p_k(x_j) - \mathbf{d}_i(x_j))^2 .$$

which can be easily computed by inverting a small matrix. The Hessian of  $\mathbf{d}_i$  at the node  $x_k$  is then approximated by the Hessian of  $p_k$ .

For the computation of matrix square roots and their inverses, we have used the method described in [Fra89], taking appropriate care to truncate almost-singular matrices, since the resulting square roots also appear inverted.

**Minimization strategy.** For the minimization at each level, we have opted for a Fletcher-Reeves nonlinear conjugate gradient method ([NW06], Section 5.2), with gradients computed

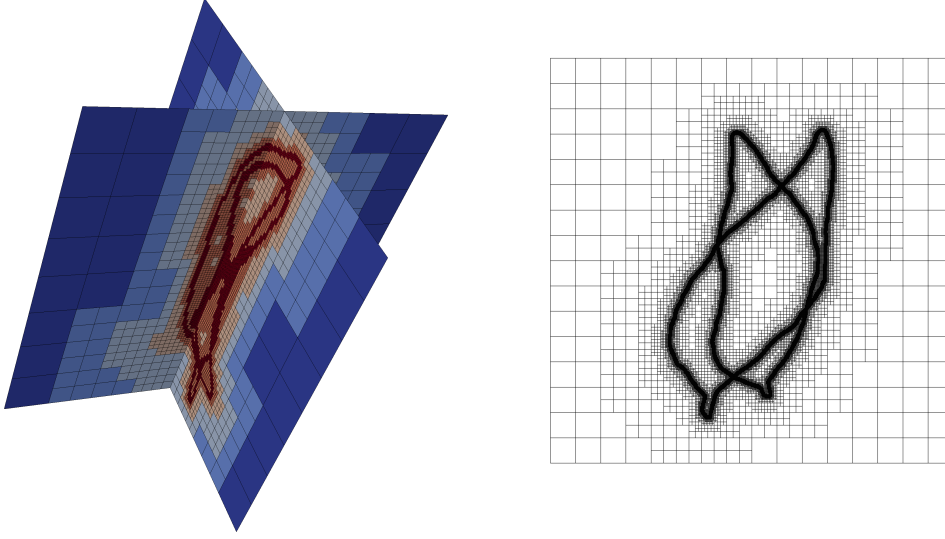


FIGURE 3.4: Hierarchical grids corresponding to the dolphin surfaces (different 2D slices in 3D, grid level 8, 178584 DOFs, 1.1% of the amount of DOFs in the full grid case) and leaf contours (2D, level 10).

with respect to a  $H_\beta^1$  metric, thereby introducing additional smoothing to mitigate the nonconvexity of the problem, i.e.,

$$\nabla_{H_\beta^1} E_\nu[\phi] = (1 + \frac{\beta^2}{2} \Delta)^{-1} \nabla_{L^2} E_\nu[\phi],$$

where  $\Delta$  is the Laplacian corresponding to the chosen boundary conditions, and  $\nabla_{L^2} E_\nu$  is the usual  $L^2$  gradient appearing in the Euler-Lagrange equation for  $E_\nu$ . The  $L^2$  gradient of  $E_\nu$ , whose computation is involved but elementary, was implemented directly. The parameter  $\alpha$  is progressively reduced when a further feasible descent step is not found, according to an Armijo line search ([NW06], Section 3.1).

### 3.6 Numerical results

All of our results have been computed on the unit cube  $\Omega = [0, 1]^3$  for the matching of surfaces in 3D, and the unit square  $[0, 1]^2$  for the matching of contour curves in 2D. In practice, we have used homogeneous Neumann boundary conditions, since this allows to have relatively large shapes  $\mathcal{M}_i$  in comparison to the size of the domain  $\Omega$  without creating excessive volume energies near the boundary (for the justification we refer to Corollary 3.4.3). However, if the boundary is not fixed, the deformed domain  $\phi(\Omega)$  is not necessarily contained in  $\Omega$ , so evaluation of coefficients on deformed positions has to be appropriately handled numerically. We use a projection of outside position onto the boundary of  $\Omega$  for sufficient large  $\text{dist}(\mathcal{M}_2, \partial\Omega)$ .

For the membrane and the bending energy we use the material parameters  $\lambda = \mu = 1$ , corresponding to the density

$$W(A) = \frac{1}{2}|A|^2 + \frac{1}{4}(\det A)^2 + \frac{3}{2}e^{-(\det A-1)} - \frac{13}{4}.$$

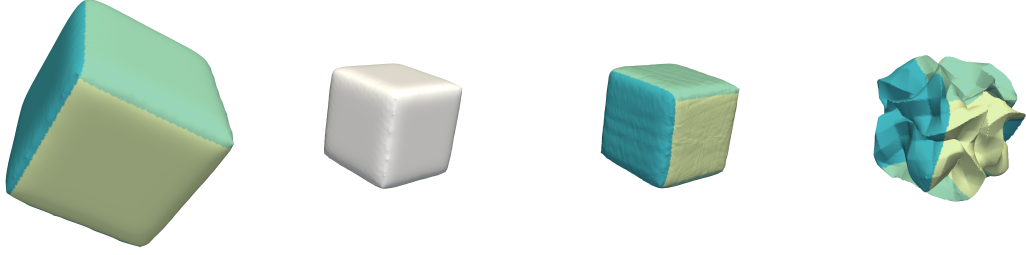


FIGURE 3.5: Behavior of the optimal (numerical) deformation in the presence of strong compression. From left to right: Textured  $\mathcal{M}_1$ ,  $\mathcal{M}_2$ , resulting deformed shape  $\phi(\mathcal{M}_1)$  after level 7 with our model, and corresponding result for the final grid level 4 when  $P_2$  is not present in  $E_{\text{mem}}$ .

In the bending term, the shape operators have been regularized through the truncated absolute value function with  $\tau = 1$ . Since we work on the unit cube, this corresponds to a comparatively large curvature radius.

We have run the stated minimization scheme beginning from a uniform grid of level  $\ell_{\min} = 2$  or  $\ell_{\min} = 3$  with  $9^3 = 729$  nodes, and refined up to  $\ell_{\max} = 7$  or 8 for 3D examples. For 2D cases a reasonable range turned out to be  $\ell_{\min} = 4$ ,  $\ell_{\max} = 10$ . The finest grids used for two of the examples below are depicted in Figure 3.4. The width of the narrow band was chosen proportional the finest resolution of the mesh ( $\sigma = 2h$ ) since a small value of  $\sigma$  clearly produces inaccurate results when  $\eta_\sigma$  is evaluated on coarse grids. However, the constraint  $\int_\Omega \eta_\sigma = 1$  ensures that the overall strength of the surface terms  $E_{\text{match}}$ ,  $E_{\text{mem}}$  and  $E_{\text{bend}}$  is not affected. The value of the penalty constraint  $\nu$  was divided by 8 for each grid refinement, which is justified by Proposition 3.4.4. Furthermore, the coefficients  $\alpha_p, \beta_q, \gamma_s$  are also halved per level to allow for simultaneously higher initial regularization and close final matches. Note that this reduction is much slower than that of the matching parameter.

All figures have been produced by deforming the input data (polygonal curve or triangulated surface) via the resulting deformation  $\phi$ . This is in contrast to deforming the grid and plotting the resulting extracted level sets (which effectively visualizes the *inverse* deformation), as commonly done in the registration literature, and also in [Igl+13].

**Test case.** First we present a simple test case to underline the qualitative properties of our model. Figure 3.5 shows a configuration in which a high amount of compression, combined with rotation, is required. Our model finds the intuitively correct deformation, but oscillations typical for the lack of lower semicontinuity of the underlying energy are induced when  $P_2$  is not used in the membrane and bending terms. The bending term assists in matching the curvatures even if the deformation is not rigid. Note, however, that for the optimal match the curvature energy  $E_{\text{bend}}$  is not expected to vanish, as can easily be seen from (3.3.4), (3.2.6) and the related discussion in 3.3.

**Shape matching applications.** We now turn our attention to high resolution examples with real data. Figure 3.6 demonstrates the effect of the multilevel descent scheme, in which details

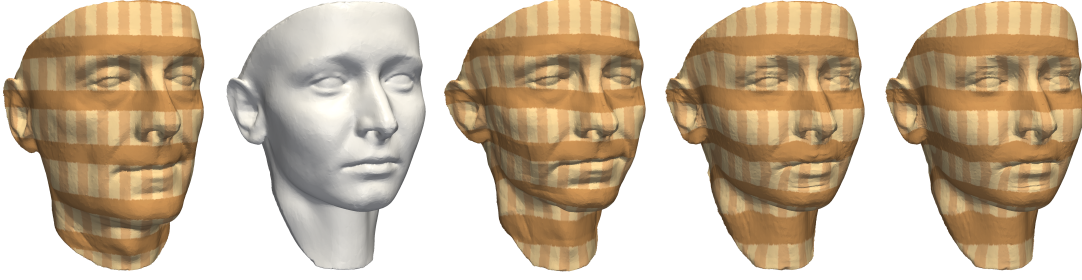


FIGURE 3.6: Detail is added progressively in the cascadic coarse-to-fine scheme. From left to right: Textured  $\mathcal{M}_1$ ,  $\mathcal{M}_2$ , resulting deformed shape  $\phi(\mathcal{M}_1)$  after the computation on grid level 4, 6 and 8, respectively.

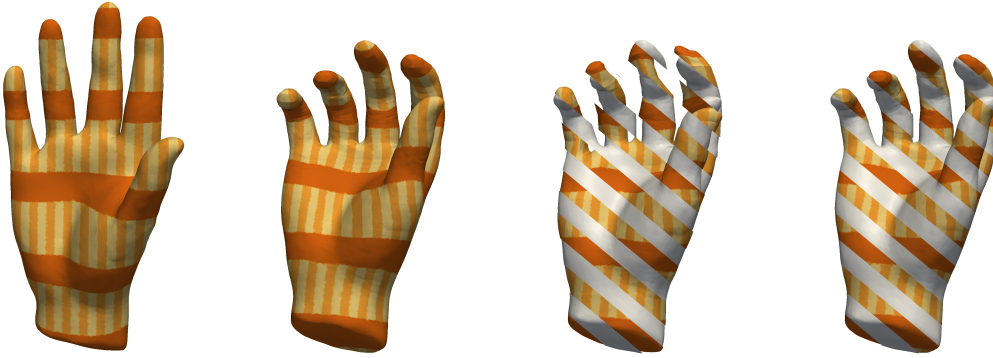


FIGURE 3.7: From left to right: Textured hand shape  $\mathcal{M}_1$ , resulting deformed shape  $\phi(\mathcal{M}_1)$  after level 7 in the minimization scheme, comparison of target and obtained shapes after the computation on grid level 4 and 7, respectively.

are added progressively to avoid spurious local minima. In Figure 3.10 a high-resolution 2D example is presented. Figures 3.7, 3.8 and 3.9 show 3D examples in which the influence of the curvature matching is indispensable to obtain shape sensitive matching deformations.

For these examples, the width parameter  $\delta$  was chosen relatively high with a typical value of  $\delta = 0.35$ , since the curvature matching term  $E_{\text{bend}}$  is a major driving force to obtain correct matching of geometric features. The initial values of  $\nu$  and the coefficients of the volume term  $\alpha_p, \beta_q, \gamma_s$  were set significantly smaller than  $\delta$ . For example, for Figure 3.7 the computation was run from levels  $\ell_{\min} = 2$  to  $\ell_{\max} = 7$ , with  $\delta = 0.39$ ,  $p = s = 2$ ,  $\beta_q = 0$ , initial  $\alpha_p = \gamma_s = 0.01$ , and initial  $\nu = 9.8 \cdot 10^{-2}$ .

## Acknowledgements

This research was supported by the Austrian Science Fund (FWF) through the National Research Network ‘Geometry+Simulation’ (NFN S117) and Doctoral Program ‘Dissipation and Dispersion in Nonlinear PDEs’ (W1245). Furthermore, the authors acknowledge support of the Hausdorff Center for Mathematics at the University of Bonn. The shapes for Figure 3.8 are originally from the McGill 3D Shape Benchmark [Sid+08]. The scanned faces of Figure 3.6 are part of the 3D





FIGURE 3.8: From left to right: Textured dolphin  $\mathcal{M}_1$ ,  $\mathcal{M}_2$ , resulting deformed shape  $\phi(\mathcal{M}_1)$  after level 8 in the minimization scheme, comparison of target and obtained shapes after the computation on grid level 4 and 8, respectively. The corresponding final grid is depicted in Figure 3.4.

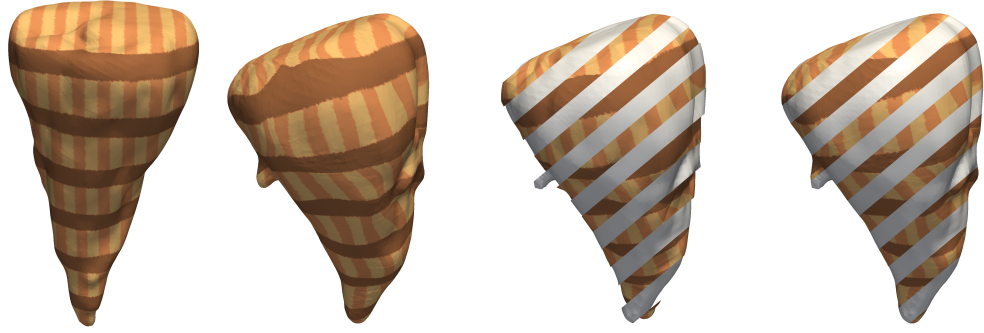


FIGURE 3.9: From left to right: Textured sugar beet shape  $\mathcal{M}_1$ , resulting deformed shape  $\phi(\mathcal{M}_1)$  after level 8 in the minimization scheme, comparison of target sugar beet shape and obtained shapes after the computation on grid level 4 and 8, respectively.

Basel Face Model dataset [Pay+09]. The laser-scanned sugar beets of Figure 3.9 and the original shapes for Figure 3.7 were kindly provided by Behrend Heeren.

## References

- [AF03] R. A. Adams and J. J. F. Fournier. *Sobolev spaces*. Second. Vol. 140. Pure and Applied Mathematics (Amsterdam). Elsevier/Academic Press, Amsterdam, 2003, pp. xiv+305.
- [BA05] J. A. Baerentzen and H. Aanaes. “Signed distance computation using the angle weighted pseudonormal”. *IEEE Trans. Vis. Comput. Graphics* 11.3 (May 2005), pp. 243–253.
- [Bal77] J. M. Ball. “Convexity conditions and existence theorems in nonlinear elasticity”. *Arch. Ration. Mech. Anal.* 63 (1977), pp. 337–403.

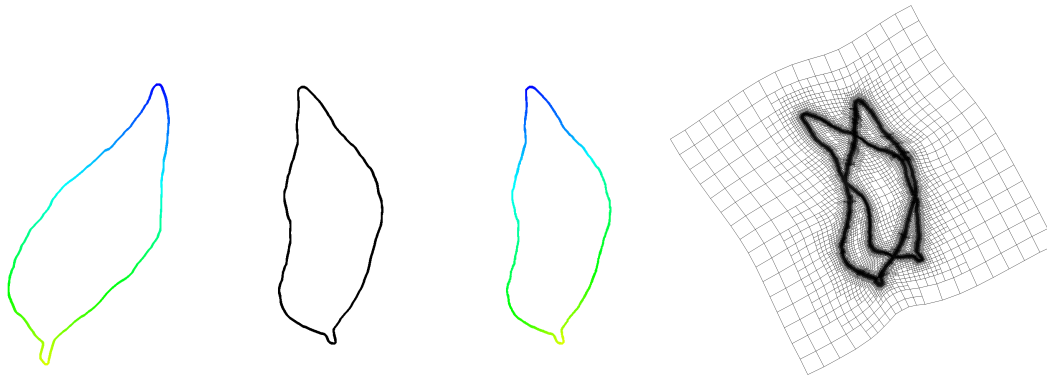


FIGURE 3.10: 2D example. From left to right: Colored leaf contours  $\mathcal{M}_1, \mathcal{M}_2$ , resulting deformed leaf shape  $\phi(\mathcal{M}_1)$  after the computation on grid level 10 and corresponding deformed grid. The corresponding undeformed grid is depicted in Figure 3.4.

- [Bal81] J. M. Ball. “Global invertibility of Sobolev functions and the interpenetration of matter”. *Proc. Roy. Soc. Edinburgh Sect. A* 88 (1981), pp. 315–328.
- [BMR13] M. Burger, J. Modersitzki, and L. Ruthotto. “A Hyperelastic Regularization Energy for Image Registration”. *SIAM J. Sci. Comput.* 35.1 (2013), B132–B148.
- [BNP10] A. Bonito, R. H. Nochetto, and M. S. Pauletti. “Parametric FEM for geometric biomembranes”. *J. Comput. Phys.* 229 (2010), pp. 3171–3188.
- [Bot+06] M. Botsch, M. Pauly, M. Gross, and L. Kobbelt. “PriMo: Coupled Prisms for Intuitive Surface Modeling”. In: *Proceedings of the Fourth Eurographics Symposium on Geometry Processing*. Eurographics Association, 2006, pp. 11–20.
- [BPW13] K. Bredies, T. Pock, and B. Wirth. “Convex Relaxation of a Class of Vertex Penalizing Functionals”. *J. Math. Imaging Vis.* 47.3 (2013), pp. 278–302.
- [BPW15] K. Bredies, T. Pock, and B. Wirth. “A convex, lower semicontinuous approximation of Euler’s elastica energy”. *SIAM J. Math. Anal.* 47.1 (2015), pp. 566–613.
- [Bra02] A. Braides.  *$\Gamma$ -convergence for beginners*. Vol. 22. Oxford Lecture Series in Mathematics and its Applications. Oxford: Oxford University Press, 2002. xii+218.
- [BS08] M. Botsch and O. Sorkine. “On Linear Variational Surface Deformation Methods”. *IEEE Trans. Vis. Comput. Graph.* 14.1 (Jan. 2008), pp. 213–230.
- [CFK04] G. Charpiat, O. Faugeras, and R. Keriven. “Approximations of Shape Metrics and Application to Shape Warping and Empirical Shape Statistics”. *Found. Comp. Math.* 5 (2004), pp. 1–58.
- [CG82] P.G. Ciarlet and G. Geymonat. “Sur les lois de comportement en élasticité non linéaire compressible”. *CR Acad. Sci. Paris Sér. II* 295 (1982), pp. 423–426.
- [CH97] Z. Chen and Z. Huan. “On the Continuity of the m-th Root of a Continuous Nonnegative Definite Matrix-valued Function”. *J. Math. Anal. Appl.* 209.1 (1997), pp. 60–66.



- [Cha+10] I. Chao, U. Pinkall, P. Sanan, and P. Schröder. “A simple geometric model for elastic deformations”. *ACM Trans. Graph.* 29 (4 July 2010), 38:1–38:6.
- [Cia00] P. G. Ciarlet. *Mathematical elasticity, volume III: Theory of shells*. Amsterdam: North-Holland, 2000.
- [Cia88] P. G. Ciarlet. *Mathematical elasticity, volume I: Three-dimensional elasticity*. Vol. 20. Mathematics and its Applications. Amsterdam: North-Holland, 1988.
- [Cor+09] T. H. Cormen, C. E. Leiserson, R. L. Rivest, and C. Stein. *Introduction to Algorithms, 3rd Edition*. 3rd. The MIT Press, 2009.
- [Dac08] B. Dacorogna. *Direct methods in the calculus of variations*. 2nd ed. Vol. 78. Applied Mathematical Sciences. New York: Springer, 2008. xii+619.
- [DZ11] M. C. Delfour and J.-P. Zolésio. *Shapes and geometries*. Second. Vol. 22. Advances in Design and Control. Metrics, analysis, differential calculus, and optimization. Society for Industrial and Applied Mathematics (SIAM), Philadelphia, PA, 2011, pp. xxiv+622.
- [DZ94] M.C. Delfour and J.-P. Zolésio. “Shape analysis via oriented distance functions”. *J. Funct. Anal.* 123 (1994), pp. 129–201.
- [DZ95] M.C. Delfour and J.-P. Zolésio. “A boundary differential equation for thin shells”. *J. Differential Equations* 119.2 (1995), pp. 426–449.
- [EG87a] L. C. Evans and R. F. Gariepy. “Blowup, compactness and partial regularity in the calculus of variations”. *Indiana Univ. Math. J.* 36.2 (1987), pp. 361–371.
- [EG87b] L. C. Evans and R. F. Gariepy. “Some remarks concerning quasiconvexity and strong convergence”. *Proc. Roy. Soc. Edinburgh Sect. A* 106 (1-2 Jan. 1987), pp. 53–61.
- [EG92] L. C. Evans and R. F. Gariepy. *Measure theory and fine properties of functions*. Studies in Advanced Mathematics. Boca Raton, FL: CRC Press, 1992. viii+268.
- [Fra89] L. P. Franca. “An algorithm to compute the square root of a  $3 \times 3$  positive definite matrix”. *Comput. Math. Appl.* 18.5 (1989), pp. 459–466.
- [Fri+03] G. Friesecke, R.D. James, M.G. Mora, and S. Müller. “Derivation of nonlinear bending theory for shells from three-dimensional nonlinear elasticity by Gamma-convergence”. *C. R. Acad. Sci. Paris Sér I Math.* 336.8 (2003), pp. 697–702.
- [Fri82] S. Friedland. “Variation of tensor powers and spectra”. *Linear and Multilinear Algebra* 12.2 (1982/83), pp. 81–98.
- [Fuc+09] M. Fuchs, B. Jüttler, O. Scherzer, and H. Yang. “Shape metrics based on elastic deformations”. *J. Math. Imaging Vis.* 35.1 (2009), pp. 86–102.
- [GP74] V. Guillemin and A. Pollack. *Differential topology*. Prentice-Hall, Inc., 1974, pp. xvi+222.

- [Gri+03] E. Grinspun, A. N. Hirani, M. Desbrun, and P. Schröder. “Discrete shells”. In: *Proceedings of the 2003 ACM SIGGRAPH/Eurographics symposium on Computer animation*. SCA '03. Eurographics Association, 2003, pp. 62–67.
- [Igl+13] J.A. Iglesias, B. Berkels, M. Rumpf, and O. Scherzer. “A Thin Shell Approach to the Registration of Implicit Surfaces”. In: *Proceedings of the Vision, Modeling, and Visualization Workshop 2013*. Eurographics Association, 2013, pp. 89–96.
- [KFF06] S. Kabus, A. Franz, and B. Fischer. “Variational Image Registration with Local Properties”. In: *Biomedical Image Registration*. Ed. by J. P. W. Pluim, B. Likar, and F. A. Gerritsen. Vol. 4057. Lecture Notes in Computer Science. Springer Berlin Heidelberg, 2006, pp. 92–100.
- [KL10] S. Kabus and C. Lorenz. “Fast elastic image registration”. In: *Proceedings of the Medical Image Analysis For The Clinic: A Grand Challenge, MICCAI, Beijing, China*. 2010, pp. 81–89.
- [Koi66] W. T. Koiter. “On the nonlinear theory of elastic shells”. *Proc. Kon. Ned. Akad. Wetesch.* B69 (1966), pp. 1–54.
- [KR05] S. L. Keeling and W. Ring. “Medical image registration and interpolation by optical flow with maximal rigidity”. *J. Math. Imaging Vision* 23.1 (2005), pp. 47–65.
- [KU03] J. Kybic and M. Unser. “Fast parametric elastic image registration”. *IEEE Trans. Image Process.* 12.11 (Nov. 2003), pp. 1427–1442.
- [Kui55] N.H. Kuiper. “On  $C^1$ -isometric imbeddings I”. *Nederl. Akad. Wetensch. Proc. Ser. A*. 58 (1955), pp. 545–556.
- [LDR95a] H. Le Dret and A. Raoult. “The nonlinear membrane model as variational limit of nonlinear three-dimensional elasticity”. *J. Math. Pures Appl.* 74 (1995), pp. 549–578.
- [LDR95b] H. Le Dret and A. Raoult. “The quasiconvex envelope of the Saint Venant-Kirchhoff stored energy function”. *Proc. Roy. Soc. Edinburgh Sect. A* 125 (06 Jan. 1995), pp. 1179–1192.
- [LDR96] H. Le Dret and A. Raoult. “The membrane shell model in nonlinear elasticity: A variational asymptotic derivation”. *J. Nonlinear Sci.* 6 (1 1996), pp. 59–84.
- [Leo09] G. Leoni. *A first course in Sobolev spaces*. Vol. 105. Graduate Studies in Mathematics. American Mathematical Society, Providence, RI, 2009, pp. xvi+607.
- [Lit+05] N. Litke, M. Droske, M. Rumpf, and P. Schröder. “An Image Processing Approach to Surface Matching”. In: *Symposium on Geometry Processing*. Ed. by M. Desbrun and H. Pottmann. 2005, pp. 207–216.
- [LL08] T.-Y. Lee and S.-H. Lai. “3D non-rigid registration for MPU implicit surfaces”. In: *CVPR Workshop on Non-Rigid Shape Analysis and Deformable Image Alignment*. 2008.

- [LN05] Y.Y. Li and L. Nirenberg. “The distance function to the boundary, Finsler geometry, and the singular set of viscosity solutions of some Hamilton-Jacobi equations”. *Comm. Pure Appl. Math.* 58.1 (2005), pp. 85–146.
- [Meg98] R. E. Megginson. *An Introduction to Banach Space Theory*. Vol. 183. Graduate Texts in Mathematics. New York: Springer Verlag, 1998.
- [MM72] M. Marcus and V. J. Mizel. “Absolute continuity on tracks and mappings of Sobolev spaces”. *Arch. Ration. Mech. Anal.* 45.4 (1972), pp. 294–320.
- [Mod04] J. Modersitzki. *Numerical Methods for Image Registration*. OUP Oxford, 2004.
- [MR12] D. P. Mukherjee and N. Ray. “Contour interpolation using level-set analysis”. *Int. J. Img. Graph.* 12.1 (2012), p. 1250004.
- [Mur87] F. Murat. “A survey on compensated compactness”. In: *Contributions to modern calculus of variations (Bologna, 1985)*. Vol. 148. Pitman Res. Notes Math. Ser. Harlow: Longman Sci. Tech., 1987, pp. 145–183.
- [Nas54] J. Nash. “ $C^1$ -isometric imbeddings”. *Ann. Math.* 60.3 (1954), pp. 383–396.
- [NW06] J. Nocedal and S. Wright. *Numerical Optimization*. Second. Springer, 2006.
- [Pay+09] P. Paysan, R. Knothe, B. Amberg, S. Romdhani, and T. Vetter. “A 3D Face Model for Pose and Illumination Invariant Face Recognition”. In: *Proc. Advanced Video and Signal based Surveillance*. 2009.
- [RR04] M. Renardy and R.C. Rogers. *An Introduction to Partial Differential Equations*. Second. Vol. 13. Texts in Applied Mathematics. Springer, 2004.
- [RSW10] P. Risholm, E. Samset, and III Wells W. “Bayesian Estimation of Deformation and Elastic Parameters in Non-rigid Registration”. In: *Biomedical Image Registration*. Ed. by B. Fischer, B. M. Dawant, and C. Lorenz. Vol. 6204. Lecture Notes in Computer Science. Springer, 2010, pp. 104–115.
- [RW09] M. Rumpf and B. Wirth. “A nonlinear elastic shape averaging approach”. *SIAM J. Imaging Sci.* 2.3 (2009), pp. 800–833.
- [Set99] J. A. Sethian. *Level set methods and fast marching methods*. 2nd ed. Vol. 3. Cambridge Monographs on Applied and Computational Mathematics. Evolving interfaces in computational geometry, fluid mechanics, computer vision, and materials science. Cambridge: Cambridge University Press, 1999. xx+378.
- [Sid+08] K. Siddiqi, J. Zhang, D. Macrini, A. Shokoufandeh, S. Bouix, and S. Dickinson. “Retrieving articulated 3-D models using medial surfaces”. *Machine Vision and Applications* 19.4 (2008), pp. 261–275.
- [Sri+09] A. Srivastava, C. Samir, S. H. Joshi, and M. Daoudi. “Elastic Shape Models for Face Analysis Using Curvilinear Coordinates”. *J. Math. Imaging. Vis.* 33 (2009), pp. 253–265.

- [Tar79] L. Tartar. “Compensated compactness and applications to partial differential equations”. In: *Nonlinear analysis and mechanics: Heriot-Watt Symposium, Vol. IV*. Vol. 39. Res. Notes in Math. Boston, Mass.: Pitman, 1979, pp. 136–212.
- [Win+11] T. Windheuser, U. Schlickewei, F. R. Schmidt, and D. Cremers. “Geometrically consistent elastic matching of 3D shapes: A linear programming solution”. In: *International Conference on Computer Vision*. 2011, pp. 2134–2141.

# 4

---

## Convective Regularization for Optical Flow

### Abstract

We argue that the time derivative in a fixed coordinate frame may not be the most appropriate measure of time regularity of an optical flow field. Instead, for a given velocity field  $v$  we consider the convective acceleration  $v_t + \nabla vv$  which describes the acceleration of objects moving according to  $v$ . Consequently we investigate the suitability of the nonconvex functional  $\|v_t + \nabla vv\|_{L^2}^2$  as a regularization term for optical flow. We demonstrate that this term acts as both a spatial and a temporal regularizer and has an intrinsic edge-preserving property. We incorporate it into a contrast invariant and time-regularized variant of the Horn-Schunck functional, prove existence of minimizers and verify experimentally that it addresses some of the problems of basic quadratic models. For the minimization we use an iterative scheme that approximates the original nonlinear problem with a sequence of linear ones. We believe that the convective acceleration may be gainfully introduced in a variety of optical flow models.

### 4.1 Introduction

**Motivation.** Optical flow is the apparent motion in a sequence of images and can be described by a velocity field. Using variational techniques to estimate this velocity field requires the design of an appropriate energy functional. Typically such a functional is a sum of two parts. The first part, sometimes called data term, measures the accuracy with which the velocity field describes the observable image motion. By ensuring consistency of the flow field, the second part, also called regularization term, gives information the data term cannot provide and thereby addresses the inherent ill-posedness of the optical flow problem. Naturally, related research has to a large degree been concerned with tuning the second term to optimally capture the characteristics of velocities of real-world image sequences.

Generally speaking regularization terms for optical flow fall into two categories: those which only penalize spatial derivatives of the velocity field, and those where derivatives in both space and time are penalized. The first category is by far the more popular one. Its developments have closely followed those of variational image restoration, because the regularity of images dictates to a significant degree the spatial regularity of velocity fields describing their motion. In other words, image discontinuities tend to coincide with motion discontinuities. These, it was found, can be appropriately dealt with using subquadratic or anisotropic regularization.

Research on the second category, i.e. that of spatiotemporal regularization, is relatively scarce. Again this is in analogy with the field of image processing, where the joint restoration of image sequences is quite under-represented as compared to the restoration of single frames. The inclusion of time derivatives has the obvious disadvantage of turning a series of decoupled 2D

problems into one 3D problem. In the early days of computer vision limited computer memory and processing power was prohibitive to such approaches. Clearly this is no longer the case. On the contrary, recent publications have articulated and addressed the need for time-coupled models even for data with three instead of two space dimensions. See for example [AMK13; Sch+13].

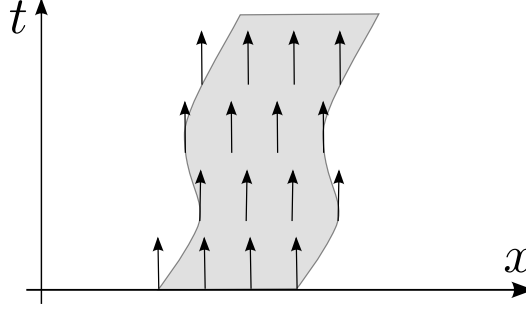


FIGURE 4.1: Using partial time derivatives in flow regularization can blur across object boundaries. Here, the shaded area represents the space-time signature of a moving object and the time direction points both inside and outside of it at different points.

It is well-known that indiscriminate smoothing in space can lead to blurring at the boundaries of objects. This statement is equally true in the space-time domain, if we identify objects with their space-time signature (Figure 4.1). In particular, blind penalization of the partial time derivative of a velocity field can lead to a loss of accuracy, especially at the boundaries of *moving* objects. Therefore we suggest to take the time derivative only along the movement of the object.

This derivative has a very natural physical interpretation. Let  $v(t, x)$  be a time dependent velocity field on  $\mathbb{R}^d$ , and let  $t \mapsto \gamma(t; x_0)$  be the trajectory of a certain object initially located at  $x_0 \in \mathbb{R}^d$  that moves according to  $v$ . The translation into mathematical terms of this connection between  $\gamma$  and  $v$  is the following initial value problem

$$\begin{aligned}\gamma'(t; x_0) &= v(t, \gamma(t; x_0)) \\ \gamma(0; x_0) &= x_0.\end{aligned}\tag{4.1.1}$$

Taking time derivatives on both sides of the differential equation above gives a formula in terms of  $v$  for the acceleration of the object moving along  $\gamma$

$$\begin{aligned}\gamma''(t; x_0) &= \frac{d}{dt}v(t, \gamma(t; x_0)) \\ &= \frac{\partial}{\partial t}v(t, \gamma(t; x_0)) + \nabla v(t, \gamma(t; x_0)) v(t, \gamma(t; x_0))\end{aligned}$$

This expression, which is sometimes called *convective acceleration*, is to be contrasted with the partial time derivative of  $v$  evaluated at  $(t, \gamma(t; x_0))$

$$\frac{\partial}{\partial t}v(t, \gamma(t; x_0)),$$

which has a notably different physical meaning. In this article we argue that in some situations the former can be more appropriate for the regularization of optical flow.

This work is devoted to investigating the suitability of the functional

$$v \mapsto \|v_t + \nabla v v\|_{L^2}^2 \quad (4.1.2)$$

as a smoothness term for optical flow. We believe a sensible way to do so is to include this term into a simple optical flow model and to compare the results with those of the same model without the new term. The reference model we choose for this task is a contrast invariant and time-regularized version of the Horn-Schunck functional [HS81]. Incorporating (4.1.2) into our model comes, however, at the cost of leading to a nonconvex functional and to nonlinear optimality conditions. Numerically, we approximate the problem by a sequence of convex quadratic ones.

We stress that it is not the aim of the proposed model to compete in the highest ranks of motion estimation benchmarks. Instead we want to point out a certain aspect of optical flow regularization, which we feel has not received its due amount of attention. Even though it leads to a more challenging variational problem, we demonstrate that a reasonable approximation is numerically tractable and pays off in terms of accuracy.

**Related work.** Horn and Schunck [HS81] are generally credited with having laid the groundwork for variational optical flow models. Penalizing the squared  $L^2$ -norms of the spatial derivatives, their model regularizes the optical flow isotropically as well as homogeneously over the image domain. In [Nag83] Nagel proposed to suppress smoothing across image discontinuities by only penalizing the derivatives of the vector field along the level lines of the image. This idea was subsequently extended to the space-time domain in [Nag90].

A different route to spatiotemporal regularization was taken by Weickert and Schnörr. In [WS01b] they used an isotropic but essentially subquadratic regularizer. While still convex this approach leads to nonlinear optimality conditions. In the survey [WS01a] the same authors classify convex spatial as well as spatiotemporal regularizers for optical flow. According to their nomenclature our approach would classify as anisotropic and flow-driven. It is, however, fundamentally different from the regularizers considered there, not only because of nonconvexity. In [WS01a] the anisotropy of flow-driven regularizers is determined by the Jacobian of the velocity field, whereas in our approach it is determined by the velocity itself.

Chaudhury and Mehrotra pursue an interesting trajectory-based regularization strategy [CM95]. Motivated by the principle of least action and the inertia of motion they postulate that both length and curvature of trajectories of moving objects should be minimal. There is a close connection between a trajectory's curvature and the convective acceleration of an object moving along that trajectory. We discuss this connection in the next section. More recently, Salgado and Sánchez [SS07] as well as Volz and coauthors [Vol+11] have proposed time-discrete models using explicit trajectorial regularization. The present article tries to capture the essence of trajectorial regularization for optical flow in an entirely continuous setting.

Finally, we note that for the problem of image sequence reconstruction it is not uncommon to regularize the sequence along the optical flow, which can be either precomputed or estimated simultaneously. This derivative along the optical flow is just the convective derivative of the image sequence. See [CCBT03; Pre+08] for example.

**Outline.** In Section 4.2 we introduce our model. In Sec. 4.2.1 we discuss the convective acceleration of vector fields. Section 4.2.2 contains properties of the functional  $\|v_t + \nabla v v\|_{L^2}^2$  as a regularization term. The last part of Sec. 4.2 treats our choice of data term. Section 4.3 is dedicated to discussing our numerical minimization approach. Finally, we present experimental results in Section 4.4.

## 4.2 Model

### 4.2.1 Convective acceleration

**Notation.** Let  $\Omega \subset \mathbb{R}^2$  be a bounded Lipschitz domain,  $T > 0$ , and set  $E = (0, T) \times \Omega$ . We denote points in  $\Omega$  by  $x = (x^1, x^2)^\top$ . Let  $\phi : E \rightarrow \Omega$  be a flow on  $\Omega$ : That is, for fixed  $t \in (0, T)$  the map  $\phi(t, \cdot)$  is a diffeomorphism of  $\Omega$ , while for fixed  $x_0 \in \Omega$  the trajectory described by  $\phi(\cdot, x_0)$  is smooth. The vector field on  $E$  that gathers the velocities of all trajectories associated to  $\phi$  is defined by

$$u(t, x) = \phi_t(t, x_0) \Big|_{x_0=\phi^{-1}(t, x)} \quad (4.2.1)$$

where  $\phi_t$  is the partial derivative of  $\phi$  with respect to its first argument and  $\phi^{-1}(t, x)$  denotes the inverse of  $\phi(t, \cdot)$  evaluated at  $x$ . Notice that  $u(t, x)$  describes the velocity of the trajectory passing through  $x$  at the time  $t$ , so  $u(s, x)$  in general corresponds to a different trajectory, if  $s \neq t$ .

Let  $f : E \rightarrow \mathbb{R}^N$  be a possibly vector-valued quantity on  $E$ . We define the convective derivative of  $f$  along  $\phi$  as

$$\begin{aligned} D_u f(t, x) &= \frac{d}{dt} f(t, \phi(t, x_0)) \Big|_{x_0=\phi^{-1}(t, x)} \\ &= f_t(t, x) + \nabla f(t, x) u(t, x). \end{aligned} \quad (4.2.2)$$

Here  $\nabla f = (f_{x^1}, f_{x^2}) \in \mathbb{R}^{N \times 2}$  is the spatial gradient of  $f$ . Notice that the convective derivative only depends on  $u(t, x)$ , thereby justifying the notation  $D_u f$ . Using the notation  $\bar{\nabla} f = (f_t, \nabla f)$  and  $\bar{u} = (1, u^\top)^\top$  we can write  $D_u f = \bar{\nabla} f \bar{u}$ . If we set  $f = u$ , the resulting vector field

$$D_u u = u_t + \nabla u u = \bar{\nabla} u \bar{u} \quad (4.2.3)$$

is called the *convective acceleration* of the flow  $\phi$ .

**Flows with vanishing convective acceleration.** When proposing a new regularization term, it is always helpful to know when it is minimal. Therefore, we briefly discuss what conditions must be met so that a vector field  $u$  satisfies

$$D_u u = 0, \quad \text{for all } (t, x) \in E, \quad (4.2.4)$$

and give a few examples afterwards.

From the definition of the convective derivative (4.2.2) and (4.2.1) it follows that

$$D_u u(t, \phi(t, x_0)) = \phi_{tt}(t, x_0),$$



for all  $x_0 \in \Omega$  and  $t \in (0, T)$ . Now fix an  $x_0 \in \Omega$  and, for simplicity, denote the trajectory  $\phi(\cdot, x_0)$  by  $\gamma(\cdot)$ , so that we have  $D_u u = \gamma''$ . Assuming that  $\gamma'$  does not vanish on  $(0, T)$ , we can write

$$\begin{aligned}\gamma'' &= \frac{d}{dt} \left( |\gamma'| \frac{\gamma'}{|\gamma'|} \right) \\ &= \frac{d|\gamma'|}{dt} \frac{\gamma'}{|\gamma'|} + |\gamma'| \frac{d}{dt} \frac{\gamma'}{|\gamma'|}.\end{aligned}$$

Since the unit tangent vector  $\gamma'/|\gamma'|$  is always perpendicular to its derivative, the convective acceleration  $\gamma''$  is a sum of two mutually orthogonal vectors. Such a sum can only vanish, if both vectors vanish. Due to the assumption that  $\gamma' \neq 0$ , we conclude that

$$\begin{aligned}\frac{d|\gamma'|}{dt} &= 0, \quad \text{and} \\ \frac{d}{dt} \frac{\gamma'}{|\gamma'|} &= 0.\end{aligned}$$

This proves the quite intuitive fact that, if a flow has vanishing convective acceleration, then all its trajectories must be straight lines and have constant speed. Below we give a few examples of such vector fields.

*Example 1.* Let  $g : \mathbb{R} \rightarrow \mathbb{R}$  be a differentiable function. The two vector fields  $v_1, v_2 : E \rightarrow \mathbb{R}^2$  defined by

$$v_1(t, x^1, x^2) = \begin{pmatrix} 0 \\ g(x^1) \end{pmatrix}, \quad v_2(t, x^1, x^2) = \begin{pmatrix} g(x^2) \\ 0 \end{pmatrix}$$

do not depend on time and satisfy  $\nabla v_i v_i = 0$ . Thus, by formula (4.2.3) they have vanishing convective acceleration. Their integral curves are parallel to the  $x_2$ - and  $x_1$ -axes, respectively.

*Example 2.* Let  $0 \notin \Omega$ . Denote by  $e_r$  the unit vector in radial direction and let  $g : \mathbb{R} \rightarrow \mathbb{R}$  be a differentiable function with period  $2\pi$ . The vector field  $v : E \rightarrow \mathbb{R}^2$  which in polar coordinates is given by

$$v(t, r, \varphi) = g(\varphi) e_r$$

has zero convective acceleration. In contrast to the previous example the integral lines of  $v$  are not all mutually parallel.

*Example 3.* The vector fields in the previous examples were all constant in time. Time-dependent examples can be constructed from time-dependent solutions  $u$  of the inviscid Burgers' equation in one space dimension ([Eva10], Section 3.4). That is, let  $u : E \rightarrow \mathbb{R}$  solve (4.2.4) with  $E = (0, T) \times \mathbb{R}$ . Then

$$v_1(t, x^1, x^2) = \begin{pmatrix} u(t, x^1) \\ 0 \end{pmatrix}, \quad v_2(t, x^1, x^2) = \begin{pmatrix} 0 \\ u(t, x^2) \end{pmatrix}$$

satisfy  $D_{v_i} v_i = 0$  while having partial time derivatives that do not vanish identically. As in the first example the integral curves are mutually parallel straight lines. The main difference, however, is that two trajectories passing through the same point in space but at different times, might do so at different speeds.

**Relation to curvature.** Given a curve  $\gamma : (0, T) \rightarrow \Omega$ , we can define its curvature as the normal part of the arclength derivative of the unit tangent vector

$$\kappa_\gamma = \left( \frac{\gamma'}{|\gamma'|} \right)^\perp \cdot \frac{1}{|\gamma'|} \frac{d}{dt} \frac{\gamma'}{|\gamma'|} = \frac{\gamma'^\perp \cdot \gamma''}{|\gamma'|^3},$$

where  $(a, b)^\top{}^\perp = (-b, a)^\top$ . If  $\gamma$  is arc length parametrized, that is  $|\gamma'| \equiv 1$ , then the expression simplifies to  $\kappa_\gamma = |\gamma''|$ , because in that case  $\gamma'^\perp = \gamma''/|\gamma''|$ .

For a given  $x_0 \in \Omega$  we can apply the formula above to the trajectory  $t \mapsto \phi(t, x_0)$  of a flow  $\phi$ . Recall that in this case  $\gamma'$  becomes  $u$  and  $\gamma''$  becomes  $D_u u$ . Thus we get

$$\kappa_{\phi(\cdot, x_0)} = \frac{u^\perp \cdot D_u u}{|u|^3}.$$

In particular, whenever  $|u(t, \phi(t, x_0))| \equiv 1$  on some subinterval of  $(0, T)$ , then the norm of the convective acceleration  $|D_u u|$  coincides with the absolute value of the curvature of  $\phi(\cdot, x_0)$  on this subinterval

$$\kappa_{\phi(\cdot, x_0)} = \pm |D_u u|.$$

## 4.2.2 Convective regularization

In this section we study some properties of the functional

$$u \mapsto \frac{1}{2} \|D_u u\|_{L^2}^2 \tag{4.2.5}$$

as a regularization term for optical flow. By  $\|\cdot\|_{L^2}$  we mean the norm of  $L^2(E, \mathbb{R}^2)$ . Below we continue to use this shorthand whenever convenient.

**Interpretation of the convective term.** Functional (4.2.5) has two interpretations, one as a smoothing term and another one as a projection term. Recalling the bar-notation we introduced in Section 4.2.1, the integrand of (4.2.5) can be written as a quadratic form in the partial derivatives of  $u$

$$|D_u u|^2 = (\bar{\nabla} u^1)^\top \bar{u} \bar{u}^\top \bar{\nabla} u^1 + (\bar{\nabla} u^2)^\top \bar{u} \bar{u}^\top \bar{\nabla} u^2, \tag{4.2.6}$$

Observe that the diffusion tensor

$$\bar{u} \bar{u}^\top = \begin{pmatrix} 1 & u^\top \\ u & uu^\top \end{pmatrix},$$

is a projection matrix onto the span of  $\bar{u}$  composed with a scaling by  $|\bar{u}|^2$ . Therefore, minimization of (4.2.5) leads to smoothing of the vector field  $u$  only in direction  $\bar{u}$ , where precedence is given to regions where the magnitude of  $u$  is relatively large. Clearly, since  $\bar{u} \neq (1, 0, 0)^\top$  in general, the proposed convective regularization term is not a purely temporal regularizer, but it also enforces spatial smoothness of the vector field in a way that is consistent with the motion. Figure 4.2 illustrates this behaviour.

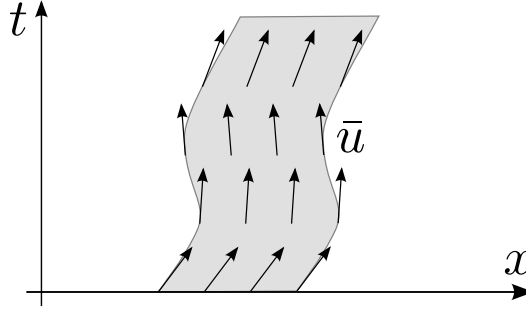


FIGURE 4.2: The shaded area represents the space-time signature of a moving object. The arrows not only indicate the space-time velocity  $\bar{u}$  of the object but also the direction of diffusion enforced by the tensor  $\bar{u}\bar{u}^\top$ . As opposed to the situation with the time derivative (Figure 4.1), object boundaries are respected.

On the other hand, the roles of  $\bar{u}$  and  $\bar{\nabla}u^i$  can be exchanged so that (4.2.6) rewrites as a sum of two quadratic forms in  $\bar{u}$

$$|D_u u|^2 = \bar{u}^\top \bar{\nabla}u^1 (\bar{\nabla}u^1)^\top \bar{u} + \bar{u}^\top \bar{\nabla}u^2 (\bar{\nabla}u^2)^\top \bar{u}. \quad (4.2.7)$$

The matrix  $\bar{\nabla}u^i (\bar{\nabla}u^i)^\top$  projects onto the span of  $\bar{\nabla}u^i$  and scales by the squared magnitude of  $\bar{\nabla}u^i$ . From this point of view minimizing (4.2.5) amounts to forcing  $\bar{u}$  to be orthogonal to the directions of greatest change of both  $u^1$  and  $u^2$ , where precedence is again given whenever this change is relatively drastic. Note that the outer product of a vector with itself is always a positive semidefinite matrix, so that there can be no cancellations in (4.2.6), (4.2.7).

The concurrence of the two different interpretations above is made explicit by looking at the Euler-Lagrange equation of (4.2.5), given by

$$\left( \nabla u^1 (\bar{\nabla}u^1)^\top + \nabla u^2 (\bar{\nabla}u^2)^\top \right) \bar{u} - \bar{\nabla} \cdot \left( \bar{\nabla}u \bar{u} \bar{u}^\top \right) = 0. \quad (4.2.8)$$

Here, the space-time divergence operator  $\bar{\nabla} \cdot$  acts along rows.

**Variational properties.** In the following we adopt the notation  $A \lesssim B$  whenever  $A \leq B$  holds up to multiplication by a positive constant. According to the basic estimate

$$\|D_u u\|_{L^2}^2 \lesssim \|u_t\|_{L^2}^2 + \|u\|_{L^\infty}^2 \|\nabla u\|_{L^2}^2$$

a seemingly natural space over which to minimize, for a given image sequence  $f$ , the optical flow functional

$$\mathcal{F}(u) = \|D_u f\|_{L^2}^2 + \alpha \|D_u u\|_{L^2}^2$$

would be  $X = H^1(E, \mathbb{R}^2) \cap L^\infty(E, \mathbb{R}^2)$ . Now, in order to show existence of minimizers using the direct method [Dac08], we need to ensure existence of a minimizing sequence which converges. This is typically done by establishing a coercivity condition of the type

$$\mathcal{F}(u) \gtrsim \|u\|_X^p - b$$

for some  $b \geq 0$  and  $p \geq 1$ . In the examples above we have seen, however, that there are vector fields  $u$  with vanishing convective acceleration but nonzero partial derivatives. This implies that not even the inequality

$$\|D_u u\|_{L^2}^2 \gtrsim \|\bar{\nabla} u\|_{L^2}^p - b$$

holds true. Therefore, in order to guarantee existence of minimizers we consider the functional

$$\begin{aligned} \mathcal{E} : H^1(E, \mathbb{R}^2) &\rightarrow [0, +\infty] \\ \mathcal{E}(u) &= \|\lambda D_u f\|_{L^2}^2 + \alpha \|D_u u\|_{L^2}^2 + \beta \|\bar{\nabla} u\|_{L^2}^2, \end{aligned} \quad (4.2.9)$$

where  $\alpha, \beta > 0$  and  $\lambda : E \rightarrow \mathbb{R}_+$  is a weighting function which is specified in Sec. 4.2.3. In addition we have to make the assumption introduced in [Sch91] that the partial derivatives of  $f$  are linearly independent in  $L^2(E)$ , that is

$$\langle f_{x^1}, f_{x^2} \rangle_{L^2} < \|f_{x^1}\|_{L^2} \|f_{x^2}\|_{L^2}. \quad (4.2.10)$$

**Proposition 1.** *Let  $f \in W^{1,\infty}(E)$  satisfy (4.2.10) and assume that  $\lambda \in L^\infty(E)$  is such that  $\text{ess inf } \lambda > 0$ . Then the minimization of  $\mathcal{E}$  over  $H^1(E, \mathbb{R}^2)$  has at least one solution.*

*Proof.* We show that  $\mathcal{E}$  is proper, coercive and lower semicontinuous with respect to the weak topology of  $H^1(E, \mathbb{R}^2)$ . That  $\mathcal{E}$  is proper follows from nonnegativity and the assumptions on  $f$  and  $\lambda$ .

Next we prove the coercivity estimate

$$\mathcal{E}(u) \gtrsim \|u\|_{H^1}^2 - b$$

for  $b \geq 0$ . We obviously have  $\mathcal{E}(u) \geq \beta \|\bar{\nabla} u\|_{L^2}^2$ . So it remains to show that  $\mathcal{E}(u) \gtrsim \|u\|_{L^2}^2 - b$ . Denoting the average of  $u$  by  $u_E = 1/|E| \int_E u$  we have

$$\begin{aligned} \|u\|_{L^2}^2 &\lesssim \|u_E\|_{L^2}^2 + \|u - u_E\|_{L^2}^2 \\ &\lesssim \|u_E \cdot \nabla f\|_{L^2}^2 + \|\bar{\nabla} u\|_{L^2}^2 \\ &\lesssim \|u \cdot \nabla f\|_{L^2}^2 + \|(u - u_E) \cdot \nabla f\|_{L^2}^2 + \|\bar{\nabla} u\|_{L^2}^2 \\ &\lesssim \|D_u f\|_{L^2}^2 + \|f_t\|_{L^2}^2 + \|\bar{\nabla} u\|_{L^2}^2 \\ &\lesssim \mathcal{E}(u) + \|f_t\|_{L^2}^2, \end{aligned} \quad (4.2.11)$$

which proves coercivity. There are three main ingredients in the above estimate. The first one is a quadratic variant of the triangle inequality

$$\|v + w\|^2 \leq 2\|v\|^2 + 2\|w\|^2.$$

The second one

$$\|u_E\|_{L^2}^2 \lesssim \|u_E \cdot \nabla f\|_{L^2}^2$$

uses the assumption of linear independence of  $f_{x^1}$  and  $f_{x^2}$  and is proved in [Sch91, p. 29]. The third ingredient is the Poincaré inequality  $\|u - u_E\|_{L^2} \lesssim \|\bar{\nabla} u\|_{L^2}$  ([LL01], Theorem 8.11). Also note that the fourth inequality in (4.2.11) requires the assumption  $f \in W^{1,\infty}(E)$ , while the last one uses  $\text{ess inf } \lambda > 0$ .

Let  $\{u_n\} \subset H^1(E, \mathbb{R}^2)$  converge to  $\hat{u}$  in the weak topology of  $H^1(E, \mathbb{R}^2)$ . In particular,  $\bar{\nabla} u_n$  converges weakly in  $L^2(E, \mathbb{R}^6)$  to the corresponding gradient  $\bar{\nabla} \hat{u}$ . By the compact embedding of  $H^1(E, \mathbb{R}^2)$  into  $L^2(E, \mathbb{R}^2)$ , up to choosing a subsequence we may assume that  $u_n$  also converges strongly in  $L^2$  to  $\hat{u}$ . As is made apparent in (4.2.6), the expression  $|D_u u|^2$  is convex in  $\bar{\nabla} u$  for fixed  $u$ , and  $\mathcal{E}$  is always nonnegative. We can therefore apply a standard result ([Dac08], Theorem 3.23) to obtain that  $\mathcal{E}$  is lower semicontinuous.  $\square$

There is no reason to expect minimizers of  $\mathcal{E}$  to be unique. The following example demonstrates that  $\mathcal{E}$  is not convex in general.

*Example 4.* Let  $v_1, v_2$  be the two vector fields from Example 1 with  $g$  being the identity, that is

$$v_1(t, x^1, x^2) = \begin{pmatrix} 0 \\ x^1 \end{pmatrix}, \quad v_2(t, x^1, x^2) = \begin{pmatrix} x^2 \\ 0 \end{pmatrix}$$

They satisfy  $D_{v_1} v_1 = D_{v_2} v_2 \equiv 0$ , while

$$D_w w = \frac{1}{4} \begin{pmatrix} x^1 \\ x^2 \end{pmatrix},$$

where  $w = (v_1 + v_2)/2$ . We conclude

$$0 = \|D_{v_1} v_1\|_{L^2}^2 = \|D_{v_2} v_2\|_{L^2}^2 < \|D_w w\|_{L^2}^2 = \frac{T}{16} \int_{\Omega} |x|^2 dx$$

so that the functional  $u \mapsto \|D_u u\|_{L^2}^2$  cannot be convex. This clearly implies that there are  $\alpha, \beta, f$  such that  $\mathcal{E}$  is not convex.

### 4.2.3 Data term and contrast invariance.

Contrast invariance is a useful property of image processing operators. Let  $h$  be a change of contrast, that is, a differentiable real function with  $h' > 0$ . An operator  $A$  is called contrast invariant, if it commutes with all such contrast changes:

$$A \circ h(f) = h \circ A(f)$$

for all images  $f$  ([Alv+93], Sec. 2.3).

A similar property can be postulated for operators estimating image motion, since an order-preserving rearrangement of the grey values of an image sequence should certainly not change velocities. Therefore, we call an operator  $A$  that maps image sequences  $f$  to velocity fields *contrast invariant*, if it satisfies

$$A(f) = A \circ h(f).$$

However, a typical optical flow model of the form

$$f \mapsto \arg \min_u \{ \|D_u f\|_{L^p}^p + \alpha \mathcal{R}(u) \} \quad (4.2.12)$$

does not have this property. A simple counterexample is multiplication by a positive number  $h(f) = cf$ . For a model like (4.2.12) this change of contrast effectively amounts to dividing the regularization parameter  $\alpha$  by  $c^p$  and therefore definitely influences the result. There is, however, also a local effect of this contrast dependence, which is easy to confirm experimentally. Consider a scene with a dark background and two moving objects which are similar in shape and size and which move at similar velocities, but which have significantly different average brightnesses. This is precisely the case in the example of Figure 4.3. Then, the velocities of the darker object, i.e. the one with lower values of  $f$ , will be regularized more strongly than those of the brighter one, if a data term like the above is used.

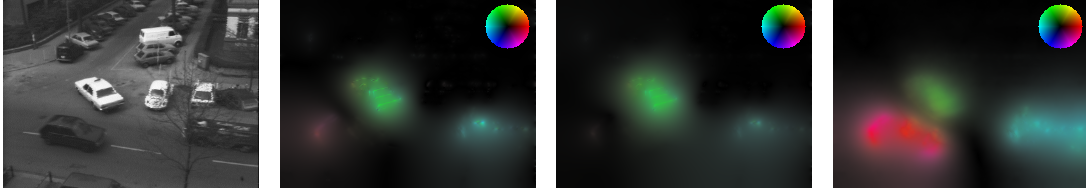


FIGURE 4.3: Effect of the data term weighting for  $\mathcal{E}$  with  $\alpha = 0$ . When it is omitted, the data term inappropriately favours high-contrast objects. Shown are, from left to right, one frame of  $f$ , the corresponding results without weighting and  $\beta = 0.2$ , without weighting and  $\beta = 0.5$ , and weighted with  $\omega = \sqrt{|\bar{\nabla} f|^2 + \epsilon^2}$  and  $\beta = 0.005$ .

However, contrast dependence is not an inherent property of optical flow. Observe that, if  $u$  solves  $D_u f = 0$ , then it also solves  $D_u(h \circ f) = 0$ , because  $D_u(h \circ f) = h' D_u f$  and  $h' > 0$  by assumption. Therefore, it should rather be regarded a side-effect of the variational regularization approach. Contrast invariance can be restored by weighting the data term with  $\lambda = 1/\omega$ , where  $\omega$  is a positively 1-homogeneous function that depends only on the first order derivatives of  $f$ . It then follows that

$$\frac{D_u(h \circ f)}{\omega(\bar{\nabla}(h \circ f))} = \frac{h' D_u f}{h' \omega(\bar{\nabla} f)} = \frac{D_u f}{\omega(\bar{\nabla} f)}. \quad (4.2.13)$$

Such weighted data terms have already been used, although it seems with a different reasoning. In [LV98; ZBW11], for example, the weight was chosen to be  $\omega = \sqrt{|\nabla f|^2 + \epsilon^2}$ . In this paper we experiment with the weight  $\omega = \sqrt{|\bar{\nabla} f|^2 + \epsilon^2}$ . With this choice the data term essentially measures the orthogonal projection of  $\bar{u}$  onto the span of  $\bar{\nabla} f$ , since

$$\frac{D_u f}{\omega} \approx \frac{\bar{\nabla} f}{|\bar{\nabla} f|} \cdot \bar{u}.$$

The effectiveness of this choice is illustrated in Figure 4.3, in which the relative velocities of the vehicles are recovered correctly even though they have widely different contrast levels.

Finally, observe that weights which do not depend on first derivatives of  $f$  (only), like  $\omega = |f| + \epsilon$  for instance, do not yield full contrast invariance. While they work fine for the special case of rescaling  $h(f) = cf$ , they fail in general since the factor  $h'$  in (4.2.13) does not cancel.

### 4.3 Numerical solution

We now seek to formulate a numerical approach for the minimization of the functional  $\mathcal{E}$ . As shown above, the convective regularization term is nonconvex and leads to nonlinear optimality conditions. Therefore, we propose an iterative scheme to arrive at an adequate flow field.

**Iterative scheme.** Consider the functional

$$\mathcal{G}(u, w) = \|\lambda D_u f\|_{L^2}^2 + \alpha \|D_w u\|_{L^2}^2 + \beta \|\bar{\nabla} u\|_{L^2}^2,$$

which satisfies  $\mathcal{E}(u) = \mathcal{G}(u, u)$ . For fixed  $w \in L^\infty(E, \mathbb{R}^2)$ , the mapping  $u \mapsto \mathcal{G}(u, w)$  is a convex and quadratic functional, and  $\mathcal{G}(u, w) < +\infty$  for any  $u \in H^1(E)$ . Our iterative method then reads as follows.

- Given an image sequence  $f$  and parameters  $\beta_0, \alpha_1, \beta_1$ :
- Find an initial guess  $u_0$  by minimizing  $\mathcal{G}(u, 0)$  over  $u$ , with  $\alpha = 0, \beta = \beta_0$ . This induces isotropic regularization in time and space, corresponding to a time-regularized variant of the Horn-Schunck model.
- Compute  $u_{k+1}$  by minimizing over the variable  $u$  the functional  $\mathcal{G}(u, u_k)$  with parameters  $\alpha = \alpha_1, \beta = \beta_1$ .

Each of these steps corresponds to finding an optical flow field using anisotropic regularization with the diffusion tensor  $\alpha \bar{w} \bar{w}^\top + \beta \text{Id}$ , where  $\text{Id}$  is the  $3 \times 3$  identity matrix. Therefore, this particular scheme is based on the diffusion interpretation of the convective regularization term, as reflected in (4.2.6). Indeed, upon fixing  $w$  the first term in the complete Euler-Lagrange equation (4.2.8) does not appear. In all of our experiments, apparent convergence of  $u_k$  is attained in a few iterations, typically by  $k = 3$  or  $4$ . Even though convergence to a minimizer of  $\mathcal{E}$  is not guaranteed, the obtained vector fields closely satisfy the desired properties used as a guide for our modelling.

By the properties of  $\mathcal{G}$  listed above, each of these minimization problems can be performed by solving the corresponding linear Euler-Lagrange equation

$$\bar{\nabla} \cdot (\bar{\nabla} u (\alpha \bar{w} \bar{w}^\top + \beta \text{Id})) - \lambda^2 (\nabla f \cdot u) \nabla f = \lambda^2 f_t \nabla f, \quad (4.3.1)$$

coupled with natural boundary conditions

$$n \cdot (\bar{\nabla} u (\alpha \bar{w} \bar{w}^\top + \beta \text{Id})) = 0 \quad \text{on } \partial E,$$

where  $n$  is the outward normal to  $E$ . Our approach of discretizing (4.3.1) is specified next.

**Discretization.** The model has been discretized using a multilinear finite element formulation on a regular rectangular grid, so that each vertex in the grid corresponds to one pixel of one video frame. The grid used is such that the spacing between nodes in space is one, while the spacing in time (from frame to frame) may be smaller. We emphasize that the relation of the two grid step sizes implicitly controls the relative amount of regularization done in time and space, since

the derivatives of the functional scale accordingly. Usually, using the same spacing will lead to results that are highly over-regularized in time. In the presented examples, the time step was divided by a factor of 8 with respect to that of space.

Both the input  $f$  and the unknown vector field  $u$  are represented by their nodal values, leading to continuous piecewise multilinear functions. Since the Euler-Lagrange equation (4.3.1) is actually a system for the two components  $u^1, u^2$ , the resulting linear system is represented by a block matrix, with the different blocks describing the interactions between components. The entries of these blocks are assembled from the integrals over different elements arising in the weak formulation, as per finite element practice [QV08]. Such integrals are computed exactly through an adequate Gauss quadrature. Note that boundary conditions do not need to be imposed explicitly.

A consequence of representing  $f$  by a piecewise multilinear function is that the corresponding partial derivatives  $f_{x^i}, f_t$  appearing in the right hand side  $\lambda^2 f_t \nabla f$  of (4.3.1) do not belong to the same finite element space as  $f$ . However, our finite element matrices act on the nodal values of functions in this space, so an interpolation step is needed to obtain functions with the appropriate smoothness. To this end, we have performed an  $L^2$  projection of these partial derivatives into the space of piecewise multilinear functions, whose nodal values are then multiplied together and used as the right hand side for our linear system. Computationally each projection requires the solution of an additional linear system, which needs to be done only once.

## 4.4 Experiments

In Figures 4.4, 4.5 and 4.6 we present some examples of flows computed through the numerical scheme of the previous section, approximating minimizers of

$$\mathcal{E}(u) = \|\lambda D_u f\|_{L^2}^2 + \alpha \|D_u u\|_{L^2}^2 + \beta \|\bar{\nabla} u\|_{L^2}^2,$$

which are compared with corresponding results with basic isotropic regularization, that is, minimizers of

$$\mathcal{H}(u) = \|\lambda D_u f\|_{L^2}^2 + \beta \|\bar{\nabla} u\|_{L^2}^2.$$

In the sequences used, the time derivative of the vector field at a given position is likely not appropriate, since isolated objects travel across the images. In the results with isotropic regularization, some of the disadvantages of basic quadratic regularizers are apparent. With lower regularization parameters (Figures 4.4(b) and 4.5(b)) inner edges of rigidly moving objects are visible. With higher regularization parameter values, the support of the vector field is enlarged and interactions between distinct objects moving ensue, creating cancellations when the objects move in different directions (Figure 4.4(c)) or artificial reinforcement when they move in similar directions (Figure 4.5(c)). However, with convective regularization both of these disadvantages can be avoided (Figures 4.4(d) and 4.5(d)).

Additionally, one needs to choose the regularization constant  $\epsilon$  for the weight  $\sqrt{|\bar{\nabla} f|^2 + \epsilon^2}$  in the data term. Clearly, choosing a too large  $\epsilon$  will diminish the effect of the weighting scheme, while choosing it too small may overemphasize very low contrast regions and potentially amplify noise. Since the 8-bit input images were normalized so that their values are of the form  $k/255$



with  $k = 0 \dots 255$ , we chose  $\epsilon = 0.01$ . That is,  $\epsilon$  is roughly of the size of the smallest nonzero derivative that may appear in the data.

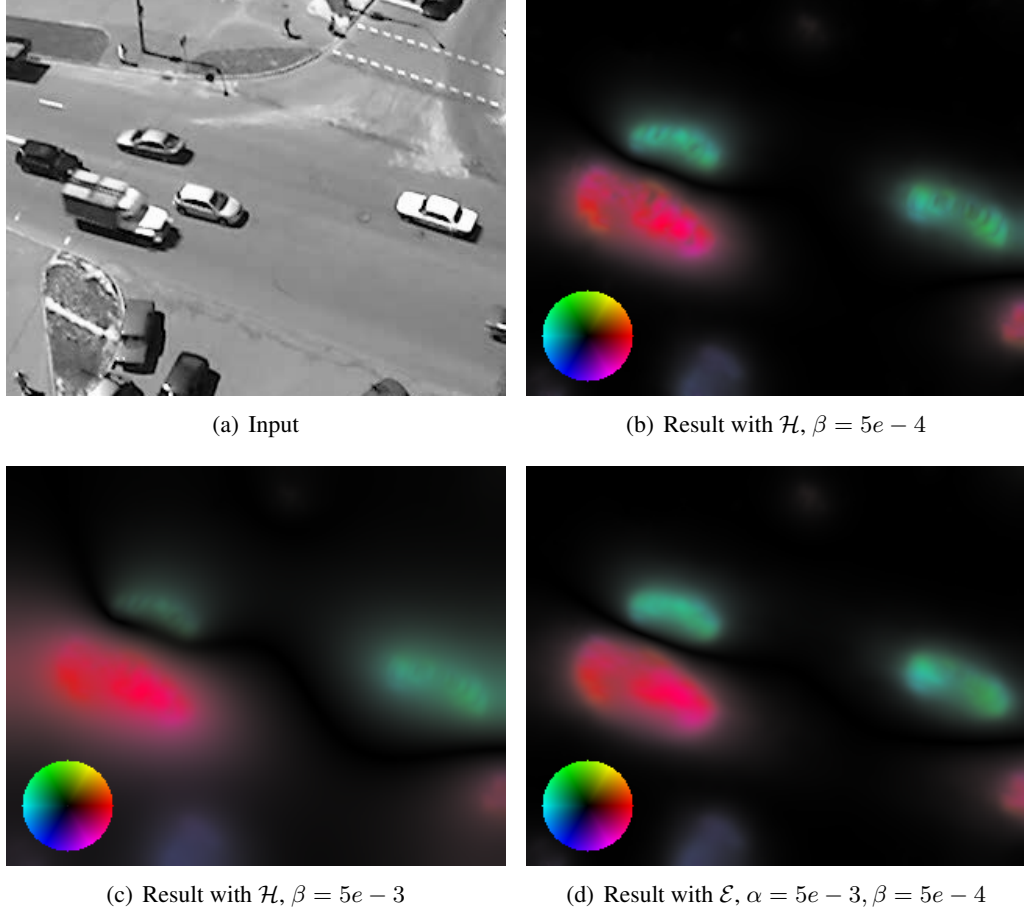


FIGURE 4.4: Comparison of isotropic and convective regularization.

In our experiments the parameter  $\beta_1$  may be chosen quite small to preserve the boundaries of objects, while using a relatively large  $\alpha_1$  for the convective regularization term. By using the convective derivative, the information from other frames is used in a consistent way to correctly fill the flow field inside objects even in the absence of texture. The initial isotropic parameter  $\beta_0$  for starting the iterative scheme was chosen to be  $\beta_0 = \alpha_1$  in all cases.

## 4.5 Conclusion

In this article we presented an entirely continuous optical flow model that is based on the assumption that velocities should vary smoothly not at fixed points in space but along motion trajectories. The resulting regularization term has a variety of different interpretations. First, this term penalizes the proper acceleration of objects moving according to the velocity field. Second, it has a direct relation to the curvature of motion trajectories. Finally, when minimized it

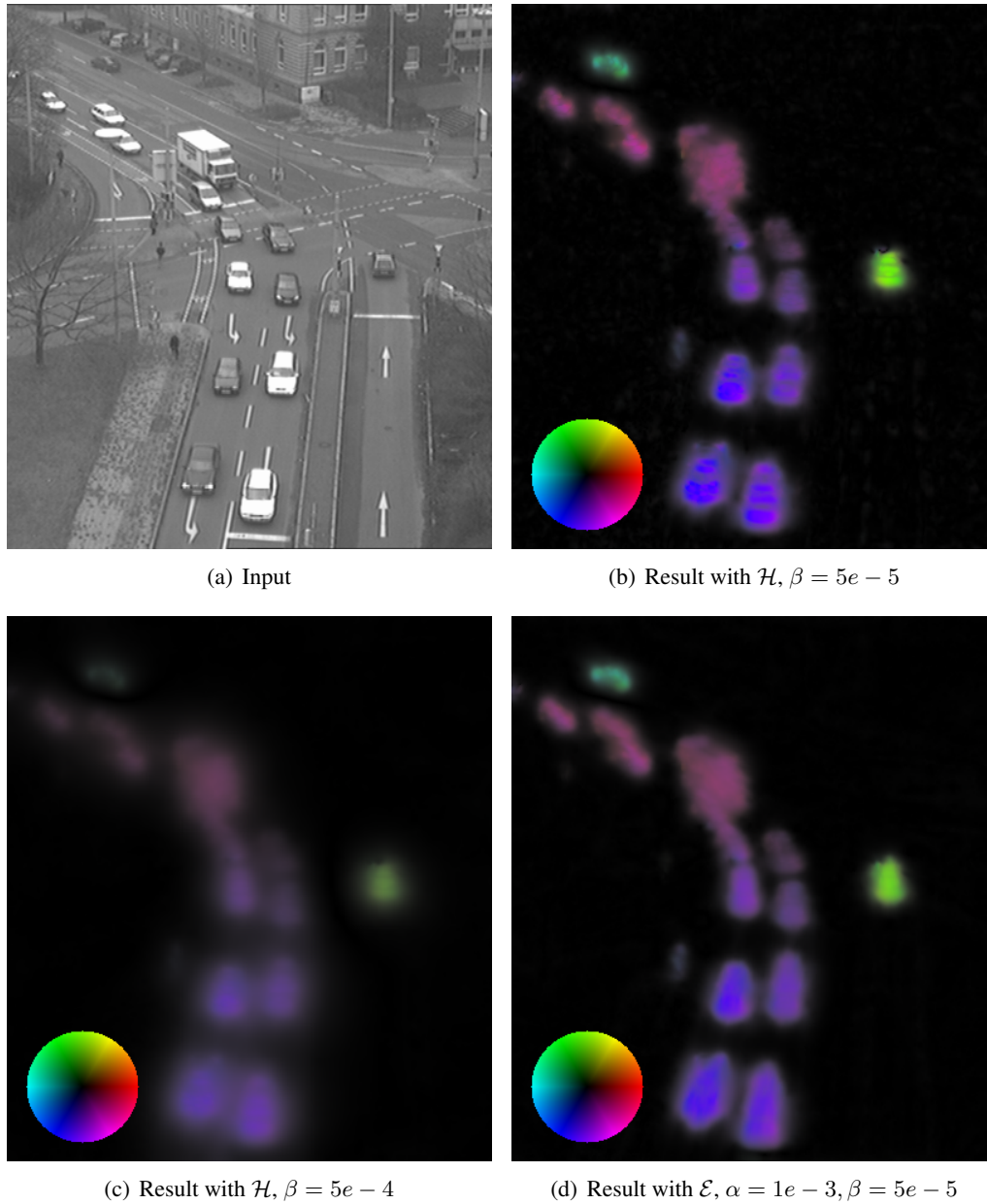


FIGURE 4.5: Comparison of isotropic and convective regularization.

acts on the vector field not only as a projection term but also as an edge-preserving anisotropic regularizer.

We tested the convective regularization term by incorporating it into a reference optical flow model and comparing the results with and without the new term. In order to make the changes as apparent as possible and to avoid potential side effects we tried to keep the complexity of the reference model at a minimum. Therefore, the resulting functional (4.2.9) should mainly be viewed as a prototype of an optical flow model with convective regularization which can be improved upon by future research.

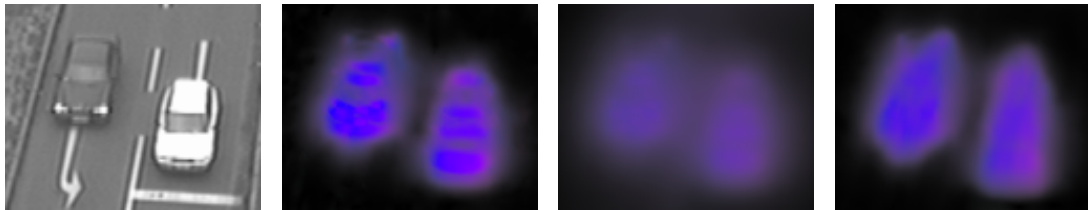


FIGURE 4.6: Cutout from Figure 4.5. The use of convective regularization allows to obtain nearly-constant optical flow field inside the objects without excessively enlarging the support.

**Acknowledgements.** This work has been supported by the Austrian Science Fund (FWF) within the national research network Geometry + Simulation (project S11704, Variational Methods for Imaging on Manifolds). Our finite element implementation was carried out in the Quocmesh library,<sup>1</sup> AG Rumpf, Institute for Numerical Simulation, Universität Bonn. For our experiments, we have used footage from the datasets of Lund University<sup>2</sup> (sequence “Conflicts-20100628-1344, camera 1”) and Universität Karlsruhe<sup>3</sup> (sequences “taxi” and “dt\_passat\_part2”).

## References

- [Alv+93] L. Alvarez, F. Guichard, P.-L. Lions, and J.-M. Morel. “Axioms and fundamental equations of image processing”. *Arch. Ration. Mech. Anal.* 123.3 (1993), pp. 199–257.
- [AMK13] F. Amat, E. W. Myers, and P. J. Keller. “Fast and robust optical flow for time-lapse microscopy using super-voxels”. *Bioinformatics* 29.3 (2013), pp. 373–380.
- [CCBT03] J.P. Cocquerez, L. Chanas, and J. Blanc-Talon. “Simultaneous Inpainting and Motion Estimation of Highly Degraded Video-Sequences”. In: *Image Analysis*. Ed. by J. Bigun and T. Gustavsson. Vol. 2749. Lecture Notes in Computer Science. Springer Berlin Heidelberg, 2003, pp. 685–692.
- [CM95] K. Chaudhury and R. Mehrotra. “A trajectory-based computational model for optical flow estimation”. *IEEE Trans. on Robot. Autom.* 11.5 (1995), pp. 733–741.
- [Dac08] B. Dacorogna. *Direct methods in the calculus of variations*. 2nd ed. Vol. 78. Applied Mathematical Sciences. New York: Springer, 2008. xii+619.
- [Eva10] L. C. Evans. *Partial Differential Equations*. Second. Vol. 19. Graduate Studies in Mathematics. Providence, RI: American Mathematical Society, 2010.
- [HS81] B. K. P. Horn and B. G. Schunck. “Determining optical flow”. *Artificial Intelligence* 17 (1981), pp. 185–203.

<sup>1</sup><http://numod.ins.uni-bonn.de/software/quocmesh/>

<sup>2</sup>[http://www.tft.lth.se/video/co\\_operation/data\\_exchange/](http://www.tft.lth.se/video/co_operation/data_exchange/)

<sup>3</sup>[ftp://ftp.ira.uka.de/pub/vid-text/image\\_sequences/](ftp://ftp.ira.uka.de/pub/vid-text/image_sequences/)

- [LL01] E. H. Lieb and M. Loss. *Analysis*. Second. Vol. 14. Graduate Studies in Mathematics. American Mathematical Society, 2001, pp. xxii+346.
- [LV98] S.-H. Lai and B.C. Vemuri. “Reliable and Efficient Computation of Optical Flow”. *Int. J. Comput. Vision* 29.2 (1998), pp. 87–105.
- [Nag83] H.-H. Nagel. “Constraints for the estimation of displacement vector fields from image sequences”. In: *Proceedings of the Eighth International Joint Conference on Artificial Intelligence*. IJCAI 83. Karlsruhe, Germany, 1983, pp. 945–951.
- [Nag90] H.-H. Nagel. “Extending the ‘Oriented Smoothness Constraint’ into the Temporal Domain and the Estimation of Derivatives of Optical Flow”. In: *Proceedings of the First European Conference on Computer Vision*. ECCV 90. Antibes, France: Springer-Verlag New York, Inc., 1990, pp. 139–148.
- [Pre+08] T. Preusser, M. Droske, C.S. Garbe, A. Telea, and M. Rumpf. “A Phase Field Method for Joint Denoising, Edge Detection, and Motion Estimation in Image Sequence Processing”. *SIAM J. Appl. Math.* 68.3 (2008), pp. 599–618.
- [QV08] A. Quarteroni and A. Valli. *Numerical Approximation of Partial Differential Equations*. Vol. 23. Springer Series in Computational Mathematics. Berlin: Springer Verlag, 2008.
- [Sch+13] B. Schmid, G. Shah, N. Scherf, M. Weber, K. Thierbach, C. Campos Pérez, I. Roeder, P. Aanstad, and J. Huisken. “High-speed panoramic light-sheet microscopy reveals global endodermal cell dynamics”. *Nat. Commun.* 4 (2013), p. 2207.
- [Sch91] Ch. Schnörr. “Determining optical flow for irregular domains by minimizing quadratic functionals of a certain class”. *Int. J. Comput. Vision* 6 (1991), pp. 25–38.
- [SS07] A. Salgado and J. Sánchez. “Temporal Constraints in Large Optical Flow Estimation”. In: *Computer Aided Systems Theory – EUROCAST 2007*. Ed. by R. Moreno-Díaz, F. Pichler, and A. Quesada-Arencibia. Vol. 4739. Lecture Notes in Computer Science. Springer Berlin Heidelberg, 2007, pp. 709–716.
- [Vol+11] S. Volz, A. Bruhn, L. Valgaerts, and H. Zimmer. “Modeling temporal coherence for optical flow”. In: *IEEE International Conference on Computer Vision (ICCV)*. Nov. 2011, pp. 1116–1123.
- [WS01a] J. Weickert and Ch. Schnörr. “A theoretical framework for convex regularizers in PDE-based computation of image motion”. *Int. J. Comput. Vision* 45.3 (2001), pp. 245–264.
- [WS01b] J. Weickert and Ch. Schnörr. “Variational optic flow computation with a spatio-temporal smoothness constraint”. *J. Math. Imaging Vision* 14 (3 2001), pp. 245–255.
- [ZBW11] H. Zimmer, A. Bruhn, and J. Weickert. “Optic flow in harmony”. *Int. J. Comput. Vision* 93.3 (2011), pp. 368–388.

# A

## First Variation of Level Set Shell Energies

For completeness, we include the largely elementary but sometimes involved calculations of the first variations of the volume, membrane and shell terms in Chapters 2 and 3, expressed in forms amenable to numerical implementation. Clearly, it is enough to compute the derivatives of the combined densities with respect to the deformation and derivative arguments ( $\phi$  and  $\mathcal{D}\phi$ , respectively) to be inserted in the Euler-Lagrange equation. In what follows we adopt the notation of Chapter 3.

We make use of the Frobenius inner product, defined for square matrices  $A, B \in \mathbb{R}^{n,n}$  by

$$A : B := \text{tr}(A^T B) = \text{tr}(AB^T),$$

and the following elementary formulas, which rely on the invariance of the trace under cyclic permutations of products

$$A : BCD = \text{tr}(A^T BCD) = \text{tr}(DA^T BC) = B^T AD^T : C, \quad (\text{A.0.1})$$

$$A : BCD = \text{tr}(A^T BCD) = \text{tr}(CDA^T B) = AD^T C^T : B, \quad (\text{A.0.2})$$

$$A : BC = \text{tr}(A^T BC) = \text{tr}(CA^T B) = AC^T : B, \quad (\text{A.0.3})$$

$$A : (v \otimes w) = \text{tr}(A^T vw^T) = \sum_{ij} A_{ij} v_i w_j = A_{ij} w_j v_i = (Aw) \cdot v. \quad (\text{A.0.4})$$

where  $A, B, C, D \in \mathbb{R}^{n \times n}$  and  $v, w \in \mathbb{R}^n$ .

Further, we will also make use of Jacobi's formula for the derivative of the determinant of a function  $A : \mathbb{R} \rightarrow \mathbb{R}^{n \times n}$ ,

$$\frac{d}{dt} \det(A(t)) = \text{tr} \left( \text{Adj } A(t) \frac{dA(t)}{dt} \right),$$

where  $\text{Adj}$  denotes the adjoint matrix. Considering the function  $\det : \mathbb{R}^{n \times n} \rightarrow \mathbb{R}$ , the above may also be expressed as

$$D \det(B) : C = \text{tr}(\text{Adj } BC) = \text{tr}(\text{Cof } B^T C), \quad (\text{A.0.5})$$

where  $B, C \in \mathbb{R}^{n \times n}$ . Therefore, we have  $D \det(B) = \text{Cof } B$ , where  $D \det$  denotes the gradient of the function  $\det$ , written as a square matrix.

For the Frobenius norm  $|\cdot|$ , and  $p > 0$ , we recall

$$\begin{aligned} D(|\cdot|^p)(B) : C &= D((|\cdot|^2)^{\frac{p}{2}})(B) : C = \frac{p}{2} |B|^{p-2} D(|\cdot|^2)(B) : C \\ &= \frac{p}{2} |B|^{p-2} \text{tr}(B^T C + C^T B) = p |B|^{p-2} B : C, \end{aligned} \quad (\text{A.0.6})$$

where  $B \neq 0$  is assumed if  $p < 1$ .

And finally, for powers of the Frobenius norm of the cofactor matrix we get

$$D(|\text{Cof} \cdot|^q)(B) : C = q|\text{Cof} B|^{q-2} Z(B) : C, \quad (\text{A.0.7})$$

where the entries  $Z(B)_{ij}$  of the matrix  $Z(B) \in \mathbb{R}^{3 \times 3}$  are given by

$$\begin{aligned} Z(B)_{11} &= B_{22} + B_{33} - B_{32} - B_{23}, \\ Z(B)_{12} &= B_{31} + B_{23} - B_{33} - B_{21}, \\ Z(B)_{13} &= B_{32} + B_{21} - B_{31} - B_{22}, \\ Z(B)_{21} &= B_{32} + B_{13} - B_{33} - B_{12}, \\ Z(B)_{22} &= B_{33} + B_{11} - B_{31} - B_{13}, \\ Z(B)_{23} &= B_{31} + B_{12} - B_{32} - B_{11}, \\ Z(B)_{31} &= B_{23} + B_{12} - B_{22} - B_{13}, \\ Z(B)_{32} &= B_{21} + B_{13} - B_{11} - B_{23}, \\ Z(B)_{33} &= B_{22} + B_{11} - B_{21} - B_{12}. \end{aligned}$$

From (A.0.6), (A.0.5), and (A.0.7) the first variation of the volume terms can be computed easily.

## A.1 Functionals of Chapter 2

### A.1.1 Membrane energy

Let us now compute the first variation of the tangential membrane energy term. We have

$$\begin{aligned} \partial_{\mathcal{D}\phi}(W_m \circ C_1)(\phi) &= \frac{\partial W_m}{\partial a} \partial_{\mathcal{D}\phi} \left( \text{tr}(\mathbf{P}_1 \mathcal{D}\phi^T \mathcal{D}\phi \mathbf{P}_1) \right) \\ &\quad + \frac{\partial W_m}{\partial d} \partial_{\mathcal{D}\phi} \left( \det(\mathbf{P}_1 \mathcal{D}\phi^T \mathcal{D}\phi \mathbf{P}_1 + \mathbf{n}_1 \otimes \mathbf{n}_1) \right). \end{aligned}$$

For the first term we compute, for arbitrary  $V \in \mathbb{R}^{n \times n}$ ,

$$\begin{aligned} \partial_{\mathcal{D}\phi} \text{tr} \left( \mathbf{P}_1 \mathcal{D}\phi^T \mathcal{D}\phi \mathbf{P}_1 \right) : V &= \text{tr} \left( \mathbf{P}_1 V^T \mathcal{D}\phi \mathbf{P}_1 + \mathbf{P}_1 \mathcal{D}\phi^T V \mathbf{P}_1 \right) \\ &= 2 \text{tr} \left( \mathbf{P}_1 \mathcal{D}\phi^T V \mathbf{P}_1 \right) = 2 \text{tr} \left( \mathcal{D}\phi \mathbf{P}_1 \mathbf{P}_1 V^T \right) \\ &= 2 \text{tr} \left( \mathcal{D}\phi \mathbf{P}_1 V^T \right) = 2(\mathcal{D}\phi \mathbf{P}_1) : V, \end{aligned}$$

where we have used the symmetry of  $\mathbf{P}_1$  and the fact that it is a projection ( $\mathbf{P}_1^2 = \mathbf{P}_1$ ). For the second term, we have

$$\begin{aligned} \partial_{\mathcal{D}\phi} \det(\mathbf{P}_1 \mathcal{D}\phi^T \mathcal{D}\phi \mathbf{P}_1 + \mathbf{n}_1 \otimes \mathbf{n}_1) : V &= \text{Cof}(\mathbf{P}_1 \mathcal{D}\phi^T \mathcal{D}\phi \mathbf{P}_1 + \mathbf{n}_1 \otimes \mathbf{n}_1) : (\mathbf{P}_1 \mathcal{D}\phi^T V \mathbf{P}_1 + \mathbf{P}_1 V^T \mathcal{D}\phi \mathbf{P}_1) \\ &= 2 \text{Cof}(\mathbf{P}_1 \mathcal{D}\phi^T \mathcal{D}\phi \mathbf{P}_1 + \mathbf{n}_1 \otimes \mathbf{n}_1) : (\mathbf{P}_1 \mathcal{D}\phi^T V \mathbf{P}_1) \end{aligned}$$

$$\begin{aligned}
&= 2 \mathbf{P}_1 \text{Cof} (\mathbf{P}_1 \mathcal{D}\phi^T \mathcal{D}\phi \mathbf{P}_1 + \mathbf{n}_1 \otimes \mathbf{n}_1) : (\mathbf{P}_1 \mathcal{D}\phi^T V) \\
&= 2 \mathcal{D}\phi \mathbf{P}_1 \text{Cof} (\mathbf{P}_1 \mathcal{D}\phi^T \mathcal{D}\phi \mathbf{P}_1 + \mathbf{n}_1 \otimes \mathbf{n}_1) \mathbf{P}_1 : V.
\end{aligned}$$

where we have used that the cofactor matrix of a symmetric matrix is again symmetric, the symmetry of  $\mathbf{P}_1$ , and (A.0.1).

### A.1.2 Bending energy

For the squared Frobenius norm of the relative shape operator defined through the tangential derivative  $\mathcal{D}_1\phi = \mathcal{D}\phi \mathbf{P}_1$ , denote

$$R(\phi, \mathcal{D}\phi) = \|\mathcal{D}_1\phi^T (\mathcal{S}_2 \circ \phi) \mathcal{D}_1\phi - \mathcal{S}_1\|^2,$$

we can compute separately the derivatives with respect to the  $\phi$  and  $\mathcal{D}\phi$  arguments, which are afterwards combined for the variation in the standard way.

For the derivative with respect to  $\phi$ , we can compute directly

$$\partial_{\phi_j} R(\phi, \mathcal{D}\phi) = 2 \operatorname{tr} \left( \left( \mathcal{D}_1\phi^T (\mathcal{S}_2 \circ \phi) \mathcal{D}_1\phi - \mathcal{S}_1 \right)^T \left( \mathcal{D}_1\phi^T (\partial_j \mathcal{S}_2 \circ \phi) \mathcal{D}_1\phi \right) \right),$$

where  $\partial_j \mathcal{S}_2$  denotes the matrix composed of the partial derivatives of each entry of  $\mathcal{S}_2$  with respect to  $x_j$ .

And with respect to  $\mathcal{D}\phi$  for any matrix  $V$ ,

$$\begin{aligned}
&\partial_{\mathcal{D}\phi} R(\phi, \mathcal{D}\phi) : V \\
&= 2 \left( \mathbf{P}_1 \mathcal{D}\phi^T (\mathcal{S}_2 \circ \phi) \mathcal{D}\phi \mathbf{P}_1 - \mathcal{S}_1 \right) : \left( \partial_{\mathcal{D}\phi} \left( \mathbf{P}_1 \mathcal{D}\phi^T (\mathcal{S}_2 \circ \phi) \mathcal{D}\phi \mathbf{P}_1 \right) \cdot V \right) \\
&= 2 \left( \mathbf{P}_1 V^T (\mathcal{S}_2 \circ \phi) \mathcal{D}\phi \mathbf{P}_1 + \mathbf{P}_1 \mathcal{D}\phi^T (\mathcal{S}_2 \circ \phi) V \mathbf{P}_1 \right) : \left( \mathbf{P}_1 \mathcal{D}\phi^T (\mathcal{S}_2 \circ \phi) \mathcal{D}\phi \mathbf{P}_1 - \mathcal{S}_1 \right) \\
&= 4 \left( \mathbf{P}_1 \mathcal{D}\phi^T (\mathcal{S}_2 \circ \phi) V \mathbf{P}_1 \right) : \left( \mathbf{P}_1 \mathcal{D}\phi^T (\mathcal{S}_2 \circ \phi) \mathcal{D}\phi \mathbf{P}_1 - \mathcal{S}_1 \right) \\
&= 4V : \left( (\mathcal{S}_2 \circ \phi)^T \mathcal{D}\phi \mathbf{P}_1 \left( \mathbf{P}_1 \mathcal{D}\phi^T (\mathcal{S}_2 \circ \phi) \mathcal{D}\phi \mathbf{P}_1 - \mathcal{S}_1 \right) \mathbf{P}_1 \right),
\end{aligned}$$

where we have used the symmetry of  $\mathbf{P}_1$  and  $\mathcal{D}_1\phi^T (\mathcal{S}_2 \circ \phi) \mathcal{D}_1\phi - \mathcal{S}_1$ , and the relation between inner product and transposes.

## A.2 Functionals of Chapter 3

### A.2.1 Membrane energy

We need to deal with the extended tangential derivative

$$\mathcal{D}_{\text{tg}}\phi + (\mathbf{n}_2 \circ \phi) \otimes \mathbf{n}_1 = (\mathbf{P}_2 \circ \phi) \mathcal{D}\phi \mathbf{P}_1 + (\nabla \mathbf{d}_2 \circ \phi) \otimes \nabla \mathbf{d}_1.$$

considered as a function of  $\phi$  and  $\mathcal{D}\phi$ , that is  $\mathbb{R}^d \times \mathbb{R}^{d \times d} \mapsto \mathbb{R}^{d \times d}$ , so the full derivatives have three and four indices.

Defining

$$\begin{aligned}\square &:= (\mathbf{P}_2 \circ \phi) \mathcal{D}\phi \mathbf{P}_1 + (\nabla \mathbf{d}_2 \circ \phi) \otimes \nabla \mathbf{d}_1 \text{ and} \\ F(\phi, \mathcal{D}\phi) &:= W(\square) = W((\mathbf{P}_2 \circ \phi) \mathcal{D}\phi \mathbf{P}_1 + \nabla(\mathbf{d}_2 \circ \phi) \otimes \nabla \mathbf{d}_1),\end{aligned}$$

we get for the derivative with respect to the second argument

$$\begin{aligned}\partial_{\mathcal{D}\phi} F(\phi, \mathcal{D}\phi) : V &= DW(\square) : ((\mathbf{P}_2 \circ \phi) V \mathbf{P}_1) = DW(\square) : ((\mathbf{P}_2 \circ \phi) V \mathbf{P}_1) \\ &= ((\mathbf{P}_2 \circ \phi) DW(\square) \mathbf{P}_1) : V,\end{aligned}$$

where we have used the symmetry of the  $\mathbf{P}_i$  and (A.0.1). Here,  $DW : \mathbb{R}^{n \times n} \rightarrow \mathbb{R}^{n \times n}$  is the derivative of the density  $W$ , which is easily computed using the remarks at the beginning of this appendix.

For the displacement argument, we fix  $v \in \mathbb{R}^n$  and split the computation as

$$\partial_\phi F(\phi, \mathcal{D}\phi) \cdot v = I + II,$$

of which

$$\begin{aligned}I &:= DW(\square) : (\partial_\phi((\nabla \mathbf{d}_2 \circ \phi) \otimes \mathbf{n}_1)[v]) = DW(\square) : (((\mathcal{D}^2 \mathbf{d}_2 \circ \phi)v) \otimes \nabla \mathbf{d}_1) \\ &= (DW(\square) \nabla \mathbf{d}_1) \cdot ((\mathcal{D}^2 \mathbf{d}_2 \circ \phi)v) = ((\mathcal{D}^2 \mathbf{d}_2 \circ \phi)^T DW(\square) \nabla \mathbf{d}_1) \cdot v \\ &= ((\mathcal{D}^2 \mathbf{d}_2 \circ \phi) DW(\square) \nabla \mathbf{d}_1) \cdot v,\end{aligned} \tag{A.2.1}$$

using (A.0.4) and symmetry of the Hessian. For the other term, we have

$$\begin{aligned}II &:= DW(\square) : (\partial_\phi(\mathbf{P}_2 \circ \phi)[v] \mathcal{D}\phi \mathbf{P}_1) \\ &= (DW(\square) \mathbf{P}_1 \mathcal{D}\phi^T) : \partial_\phi(\mathbf{P}_2 \circ \phi)[v],\end{aligned} \tag{A.2.2}$$

from which we now compute the matrix  $\partial_\phi(\mathbf{P}_2 \circ \phi)[v]$ . We obtain

$$\partial_\phi(\mathbf{P}_2 \circ \phi)[v] = ((\mathcal{D}^2 \mathbf{d}_2 \circ \phi)v) \nabla(\mathbf{d}_2 \circ \phi)^T + (\nabla \mathbf{d}_2 \circ \phi)((\mathcal{D}^2 \mathbf{d}_2 \circ \phi)v)^T, \tag{A.2.3}$$

and therefore, for any  $M \in \mathbb{R}^{n \times n}$  and using (A.0.4) we have

$$\begin{aligned}M : (\partial_\phi(\mathbf{P}_2 \circ \phi)[v]) &= (M(\nabla \mathbf{d}_2 \circ \phi)) \cdot (\mathcal{D}^2 \mathbf{d}_2 \circ \phi)v + (M(\mathcal{D}^2 \mathbf{d}_2 \circ \phi)v) \cdot (\nabla \mathbf{d}_2 \circ \phi) \\ &= (\nabla \mathbf{d}_2 \circ \phi)^T M^T (\mathcal{D}^2 \mathbf{d}_2 \circ \phi)v + (\nabla \mathbf{d}_2 \circ \phi)^T M (\mathcal{D}^2 \mathbf{d}_2 \circ \phi)v \\ &= (\nabla \mathbf{d}_2 \circ \phi)^T (M + M^T) (\mathcal{D}^2 \mathbf{d}_2 \circ \phi)v \\ &= ((\mathcal{D}^2 \mathbf{d}_2 \circ \phi)(M + M^T)(\nabla \mathbf{d}_2 \circ \phi)) \cdot v.\end{aligned} \tag{A.2.4}$$

Setting  $M = DW(\square) \mathbf{P}_1 \mathcal{D}\phi^T$  we finally get

$$II = ((\mathcal{D}^2 \mathbf{d}_2 \circ \phi)(DW(\square) \mathbf{P}_1 \mathcal{D}\phi^T + \mathcal{D}\phi^T \mathbf{P}_1 DW(\square)^T)(\nabla \mathbf{d}_2 \circ \phi)) \cdot v. \tag{A.2.5}$$



### A.2.2 Bending energy

As before, define

$$\diamond := (\mathbf{P}_2 \circ \phi)(\mathcal{C}(\mathcal{S}_2^{ext})^{\frac{1}{2}} \circ \phi)(\mathbf{P}_2 \circ \phi) \mathcal{D}\phi \mathbf{P}_1 \mathcal{C}(\mathcal{S}_1^{ext})^{-\frac{1}{2}} \mathbf{P}_1 + (\nabla \mathbf{d}_2 \circ \phi) \otimes \nabla \mathbf{d}_1 \text{ and} \\ G(\phi, \mathcal{D}\phi) := W(\diamond).$$

The derivative with respect to the Jacobian variable is again simple to compute,

$$\partial_{\mathcal{D}\phi} G(\phi, \mathcal{D}\phi) : V = DW(\diamond) : ((\mathbf{P}_2 \circ \phi)(\mathcal{C}(\mathcal{S}_2^{ext})^{\frac{1}{2}} (\mathbf{P}_2 \circ \phi) V \mathbf{P}_1 \mathcal{C}(\mathcal{S}_1^{ext})^{-\frac{1}{2}} \mathbf{P}_1) \\ = ((\mathbf{P}_2 \circ \phi)(\mathcal{C}(\mathcal{S}_2^{ext})^{\frac{1}{2}} (\mathbf{P}_2 \circ \phi) DW(\diamond) \mathbf{P}_1 \mathcal{C}(\mathcal{S}_1^{ext})^{-\frac{1}{2}} \mathbf{P}_1) : V,$$

and we split the displacement derivative in four terms,

$$\partial_{\phi} G(\phi, \mathcal{D}\phi) \cdot v = I + II.i + II.o + III.$$

Of these,

$$I := DW(\diamond) : (\partial_{\phi}((\nabla \mathbf{d}_2 \circ \phi) \otimes \mathbf{n}_1)[v]) \\ = ((\mathcal{D}^2 \mathbf{d}_2 \circ \phi) DW(\diamond) \nabla \mathbf{d}_1) \cdot v,$$

exactly as in (A.2.1). Next,

$$II.i := DW(\diamond) : ((\mathbf{P}_2 \circ \phi)(\mathcal{C}(\mathcal{S}_2^{ext})^{\frac{1}{2}} \circ \phi) \partial_{\phi}(\mathbf{P}_2 \circ \phi)[v] \mathcal{D}\phi \mathbf{P}_1 \mathcal{C}(\mathcal{S}_1^{ext})^{-\frac{1}{2}} \mathbf{P}_1),$$

for which, setting

$$M = (\mathcal{C}(\mathcal{S}_2^{ext})^{\frac{1}{2}} \circ \phi)(\mathbf{P}_2 \circ \phi) DW(\diamond) \mathbf{P}_1 (\mathcal{S}_1^{ext})^{-\frac{1}{2}} \mathbf{P}_1 \mathcal{D}\phi^T$$

in (A.2.3), and analogously to (A.2.5) we have

$$II.i = ((\mathcal{D}^2 \mathbf{d}_2 \circ \phi)(M + M^T)(\nabla \mathbf{d}_2 \circ \phi)) \cdot v.$$

For the third term,

$$II.o := DW(\diamond) : (\partial_{\phi}(\mathbf{P}_2 \circ \phi)[v](\mathcal{C}(\mathcal{S}_2^{ext})^{\frac{1}{2}} \circ \phi)(\mathbf{P}_2 \circ \phi) \mathcal{D}\phi \mathbf{P}_1 \mathcal{C}(\mathcal{S}_1^{ext})^{-\frac{1}{2}} \mathbf{P}_1) \\ = (DW(\diamond) \mathbf{P}_1 \mathcal{C}(\mathcal{S}_1^{ext})^{-\frac{1}{2}} \mathbf{P}_1 \mathcal{D}\phi^T (\mathbf{P}_2 \circ \phi)(\mathcal{C}(\mathcal{S}_2^{ext})^{\frac{1}{2}} \circ \phi)) : \partial_{\phi}(\mathbf{P}_2 \circ \phi)[v],$$

we again get the above expression, now with

$$M = DW(\diamond) \mathbf{P}_1 \mathcal{C}(\mathcal{S}_1^{ext})^{-\frac{1}{2}} \mathbf{P}_1 \mathcal{D}\phi^T (\mathbf{P}_2 \circ \phi)(\mathcal{C}(\mathcal{S}_2^{ext})^{\frac{1}{2}} \circ \phi).$$

The last term appears due to the dependency of  $(\mathcal{C}(\mathcal{S}_2^{ext})^{\frac{1}{2}} \circ \phi)$  on  $\phi$  and reduces to

$$III := DW(\diamond) : ((\mathbf{P}_2 \circ \phi) \partial_{\phi}(\mathcal{C}(\mathcal{S}_2^{ext})^{\frac{1}{2}} \circ \phi)[v](\mathbf{P}_2 \circ \phi) \mathcal{D}\phi \mathbf{P}_1 \mathcal{C}(\mathcal{S}_1^{ext})^{-\frac{1}{2}} \mathbf{P}_1) \\ = \sum_j \text{tr}((\mathbf{P}_2 \circ \phi) \mathcal{D}\phi \mathbf{P}_1 \mathcal{C}(\mathcal{S}_1^{ext})^{-\frac{1}{2}} \mathbf{P}_1 DW(\diamond) (\mathbf{P}_2 \circ \phi)(\partial_j(\mathcal{C}(\mathcal{S}_2^{ext})^{\frac{1}{2}} \circ \phi)) v_j).$$



## Deutsche Kurzfassung

Die Registrierung von zwei oder mehreren Bildern ähnlicher Objekte ist von großer Bedeutung in verschiedenen Bereichen der Bildverarbeitung (z.B. bei medizinischen oder biologischen Anwendungen). Hier werden zwei derartige Probleme behandelt, zuerst als kontinuierliche Variationsmodelle welche dann für die numerische Behandlung diskretisiert werden. Eine Gemeinsamkeit der hier vorgestellten Modelle ist die Verwendung von nicht-konvexer Regularisierung, zusätzlich zur bereits vorhandenen Nicht-Konvexität der Registrierungsprobleme.

Das erste Problem ist Abgleichung von Oberflächen. Hier sind die Daten zwei verschiedene Oberflächen. In diesem Zusammenhang behandeln wir Oberflächen, welche in einer Rechendomäne durch eine vorzeichenbehaftete Distanzfunktion dargestellt werden. Unser Arbeit basiert auf Schalen-Energien welche Expansion, Kompression und Biegung der ersten Oberfläche penalisieren. Diese werden durch Level-Set-Darstellung und die Geometrie der zweiten Oberfläche vereinfacht. Für dieses Problem werden zwei Modelle vorgeschlagen. Das Erste ist ein direkter Zugang welcher die Geometrie direkt repräsentiert. Die zweite Formulierung ermöglicht es, schwache Unterhalbstetigkeit und die Existenz von Minimierern zu beweisen. Numerisch kann sie effizient auf adaptiven Rastern implementiert werden.

Das zweite Problem ist die Schätzung des optischen Flusses einer Sequenz von Bildern. Hier schlagen wir eine neuartige Regularisierung entlang der Trajektorien des Flusses vor. Diese penalisiert konvektive Beschleunigung der entstehenden Vektorfelder anstelle der Zeitableitung des Eulerschen Geschwindigkeitsfeldes. Das entstehende Problem kann auf semi-implizite Art durch eine Abfolge linearer Probleme approximiert werden. Verglichen mit der Verwendung der Zeitableitung, zeigen unsere numerischen Ergebnisse eine deutliche Verbesserung.



# C

---

## Curriculum Vitae

### Current Position

- 12.2012-10.2015 PhD student in Mathematics. Computational Science Center, University of Vienna.
  - Advisor: Otmar Scherzer. Co-Advisor: Martin Rumpf.
  - Projektmitarbeiter within NFN S117 ‘Geometry + Simulation’ of the FWF.
  - Associated DK student in ‘Doctoral Program Dissipation and Dispersion in Nonlinear PDEs’.

### Education

- M.Sc. Mathematics, Complutense University of Madrid, 09.2009-09.2010.
  - Thesis: Morse theory from a modern standpoint.
  - Advisor: Vicente Muñoz, Geometry and Topology Department, UCM.
- B.Sc. Mathematics (5-year ‘licenciatura’), Complutense University of Madrid, 09.2005-06.2010.
  - Focus area: ‘Fundamental Mathematics’.
- Engineer (comparable to Diploma) in Telecommunication engineering, Polytechnic University of Madrid, 09.2003-09.2009.
  - Recognized by the Accreditation Board for Engineering and Technology (EAC/ABET) at M.Sc. level.
  - Focus area: Signal Processing (Image and Speech Processing).
  - Thesis: Design and implementation of a new version of a speech to sign language translation system (in Spanish).
  - Advisor: Rubén San-Segundo Hernández. Department of Electronic Engineering, UPM.
  - Universia Foundation Award (ex-aequo) 2009 for best M.Sc. Thesis contributing to accessibility and integration of people with disabilities into the workforce.

## Publications

### Journal Papers

- J. A. Iglesias, A. M. Bruckstein. On the Gamma-convergence of some polygonal curvature functionals. *Applicable Analysis*, 94(5):957-979, 2015.

### Preprints

- J. A. Iglesias, C. Kirisits. Convective regularization for optical flow. Submitted for publication, 2015. arXiv:1505.04938.
- J. A. Iglesias, M. Rumpf, O. Scherzer. Shape Aware Matching of Implicit Surfaces Based on Thin Shell Energies. Submitted for publication, 2015. arXiv:1509.06559.

### Refereed Conference Proceedings

- J. A. Iglesias, B. Berkels, M. Rumpf, O. Scherzer. A Thin Shell Approach to the Registration of Implicit Surfaces. In *Proceedings of the 18th International Workshop on Vision, Modeling and Visualization (VMV 2013)*, pp. 89-96, Eurographics Association, 2013.
- J. A. Iglesias, R. Kimmel. Schrödinger Diffusion for Shape Analysis with Texture. *Fifth Workshop on Non-Rigid Shape Analysis and Deformable Image Alignment (NORDIA'12)*. In *ECCV 2012. Workshops and Demonstrations*, Lecture Notes in Computer Science 7583, pp. 123-132, Springer, 2012.

### Technical reports

- C. Castellanos, J. A. Iglesias, X. Liu, A. Martín, A. Thomas (Supervisor: P. Athavale) Spatial Adaptivity and Parameter Selection in TV Denoising, *Summer Research School on the Mathematics of Medical Imaging, Fields Institute, July 2012*.

### Past Employment

- Marie Curie Early Stage Researcher, Initial Training Network 'Fronts and Interfaces in Science and Technology' (FIRST). Technion-Israel Institute of Technology, 12.2010-11.2012.
  - Research on variational and geometric approaches for computer vision problems.
- Research Assistant, Department of Electronic Engineering, UPM, 3.2008-1.2009.
  - Took part in the development (in C/C++) of a speech to sign language translation system.

### Attendance to Workshops and Summer Schools

- RICAM Special Semester on New Trends in Calculus of Variations: Workshops 'Shape and topological optimization' and 'Variational methods in imaging'. October-December 2014, Linz.
- RICAM Special Semester on New Trends in Calculus of Variations: Imaging school. October 22-24, 2014, Linz.
- Workshop on Microlocal Methods in Medical Imaging. August 13-17, 2012, Fields Institute, Toronto.
- Summer Research School on the Mathematics of Medical Imaging. July 3-31, 2012, Fields Institute, Toronto.
- Thematic program on Variational Methods and Compressive Sensing in Imaging. Part of the Thematic Period in Inverse Problems and Imaging. April 30-May 31, 2012, Fields Institute, Toronto.
- Getting Started with PDE. Summer Workshop for Graduate Students. September 18-22, 2011, Technion, Haifa.

### Research Visits

- Institute for Numerical Simulation, Universität Bonn. February 4-March 2, 2013. July 21-August 1, 2013, December 9-13, 2013, November 10-14, 2014.  
Worked with Prof. M. Rumpf on the formulation and numerical solution of shell models for implicit surface matching.

### Talks

- A lower semicontinuous model for the matching of implicit shell surfaces. Workshop on Riemannian geometry in shape analysis and computational anatomy. February 20, 2015. Erwin Schrödinger Institute, Vienna.
- A Level Set Method for the Matching of Implicit Surfaces. 6th International Conference on Computational Methods in Applied Mathematics (CMAM-6). September 30, 2014. St. Wolfgang, Austria.
- A Thin Shell Approach to the Registration of Implicit Surfaces. 18th International Workshop on Vision, Modeling and Visualization (VMV 2013). September 12, 2013. Lugano, Switzerland.
- Schrödinger Diffusion for Shape Analysis with Texture. Fifth Workshop on Non-Rigid Shape Analysis and Deformable Image Alignment (NORDIA'12). October 7, 2012. Firenze, Italy (in conjunction with ECCV 2012).
- Diffusion with Schrödinger Operators for Shape Analysis With Texture. FIRST Workshop. September 11, 2012. Jerusalem, Israel.

- Morse Theory from a Modern Standpoint. Workshop of Young Researchers in Mathematics. September 23, 2010. Complutense University of Madrid, Spain.

### **Posters**

- A shell model for matching implicit surfaces. RICAM Special Semester Workshop 'Variational methods in imaging'. October 27-31, 2014. Linz, Austria.
- On the Gamma-Convergence of some Polygonal Curvature Functionals. FIRST Workshop. September 11-12, 2012. Jerusalem, Israel.

### **Reviewing**

- Advances in Computational Mathematics (2015), Innovations for Shape Analysis (Springer Mathematics and Visualization series) (2012).

### **Languages**

- Spanish: Mother tongue.
- English: Advanced (TOEFL 101, 09.2010).
- German: Intermediate (CEFR B2/2, 06.2015).

### **Other Skills**

- Programming: C++ (templates, STL and Boost libraries, FEM simulations), MATLAB, Java.
- Other scientific software: LaTeX, Maple.